International Committee for Future Accelerators

Sponsored by the Particles and Fields Commission of IUPAP

Beam Dynamics Newsletter

No. 29

Editors in Chief:
W. Chou and J.M. Jowett

Editors:
C. Biscari, S. Chattopadhyay, S. Ivanov,
A.M. Lombardi, H. Mais, J. Wei, and C. Zhang

December 2002

Contents

1 Foreword

1.1 From the Chairman

John Jowett, CERN

John.Jowett@cern.ch

This issue of the ICFA Beam Dynamics Newsletter has been edited by a new member of the editorial team, Dr Alessandra Lombardi, who joined the Beam Dynamics Panel earlier this year. She has chosen the special theme of Neutrino Factories, one of the brightest hopes for extending the reach of particle accelerators into regions of unexplored physics beyond those that will be opened up by the LHC and, we hope, a linear collider.

1.1.1 ICFA Seminar

The ICFA Seminar on Future Perspectives in High Energy Physics is an event held every three years. The most recent one, on 8-11 October 2002 at CERN, was a prime occasion for reviewing the current status and most of the known options for the future of particle physics. There were talks on everything from the current status of fundamental theory to the problems of "outreach" to the general public. Between these lay concise reviews of the activities of the world's major accelerator labs, the status of the various linear collider studies, neutrino sources, e^+e^- factories and hadron colliders.

The report from the International Linear Collider Technical Review Committee, commissioned by ICFA in early 2001 was an eagerly awaited item. Greg Loew, chairman of the ILC-TRC, gave a preview of the final report that should be published early next year. One conclusion was that, around the end of 2003 when some additional R&D is complete, all the *technical* elements required to make the choice among the competing linear collider proposals will be available. Considerations of cost, site, etc. can then be folded into the discussion. Meanwhile the International Steering Group for the Promotion of Linear Colliders is actively preparing the political ground for what we hope will be the next major particle physics project.

These talks are of interest to our whole community, not only those able to attend the seminar. Most of the transparencies can be found at

http://dsu.web.cern.ch/dsu/of/Icfaprog1.html

1.1.2 ICFA Advanced Beam Dynamics Workshops

At its meeting at CERN on 10 October, ICFA approved the 30th ICFA Advanced Beam Dynamics Workshop: Beam Dynamics Issues for High Luminosity e+e- Factories, to be held at SLAC. Tentative dates are 13-17 October, 2003. This will be a continuation of

the series of workshops held in Frascati in 1997, KEK in 1999, and Cornell in 2001. Further information on this workshop will be available from the Panel's home page

http://wwwslap.cern.ch/icfa

in due course.

Since the first workshop in this series back in 1987, a wealth of valuable information on many advanced topics in beam dynamics has accumulated in their proceedings. Many of these are now accessible on the Web from the Panel's home page. Others are available from various publishers. In some cases the workshop Web sites give access to the original transparencies of the presentations.

Two recent additions to the corpus are the proceedings of the Proceedings of the 18th Advanced ICFA Beam Dynamics Workshop, Quantum Aspects of Beam Physics (World Scientific, Singapore) and those of the 20th ICFA Advanced Beam Dynamics Workshop on High Intensity and High Brightness Hadron Beams (American Insitiute of Physics).

Our community is indebted to the authors and editors of these many volumes.

1.1.3 Beam Dynamics Panel Working Groups

There has been considerable interest recently in the idea of operating particle accelerators remotely, whether as a step towards the implementation of a Global Accelerator Network or simply as a way of conducting experiments in accelerator physics on an existing machine. Following an initial tentative proposal to ICFA, discussions are presently under way about the form and mission of a possible working group within the ICFA Beam Dynamics Panel. The Panel member coordinating the discussion is Dr David Rice (dhr1@cornell.edu). The intention is to formulate a proposal for the ICFA meeting in February 2003.

1.2 From the Editor

Alessandra Lombardi, CERN

alessandra.lombardi@cern.ch

This issue of the beam dynamics newsletter has a special topic: Neutrino Factories. The general scheme of a neutrino factory is the following: a high power proton beam (of few MW) is sent on a (mercury) target; the forward going pions are collected and decay into muons. The pions/muons energy distribution is peaked around 200 MeV almost independently of the primary beam energy. Muons are further manipulated (phase rotation and ionization cooling) before being accelerated to energies of several tens of GeV and stored in a ring where they decay into neutrinos. The possibility of selecting at the source positive or negative muons allows for a beam containing only one flavour neutrino at the time; a condition which is necessary for observing CP

violation. Each stage of the neutrino factory (high power proton beam generation, pion production and collection, muon manipulation and acceleration) is technologically challenging and must be optimized very carefully in order to overcome the low proton-to-pion conversion (of the order of 1%). Studies and experimental activities are going on in Japan, Europe and in the Unite States. Neutrino factories activities bring together accelerator and particle physicists, as the interplay between these two disciplines is very strong at almost every stage of the machine. This synergy is reflected in the collection of articles in this newsletter. After an introduction on the physics motivation, a description of the KEK activities and a report on FFAG acceleration comes a collection of articles describing ionization cooling from three points of view (beam dynamics, experimental and analytical). The section is closed by a description of the experiment HARP which will provide an important input to the neutrino factory design by measuring, amongst others, the spectrum of the pions produced by a proton beam of varying energy on different target material.

The activity section contains the important results at the TWAC facility at ITEP where some 10^{10} C^{6+} ions have been successfully accumulated and several reports from workshop and conferences.

The final section recalls the upcoming ICFA beam dynamics workshops (the 28^{th} , 29^{th} and 30^{th} and the 12^{th} mini-workshop) and other workshops related to cooling (COOL03) and neutrinos (Nufact03). Finally in appendix there are two tables : the first listing the simulation codes used for slow extraction design and analysis and the second with the status of instrumentation for existing and planned machines around the world. They were compiled at the 10^{th} and 11^{th} ICFA mini workshop, respectively.

Notwithstanding the protests of several authors this document has been entirely written using Microsoft Word. I would like to take this occasion to thank all the contributors for their patience and understanding.

2 Letters to the Editors

2.1 From Steve Geer

Steve Geer, FNAL

sgeer@fnal.gov,

Dear Editors,

For those of us interested in the future of particle physics, we are living in both exciting and troubling times. Exciting because we expect the LHC and a Linear Collider (if built) to teach us about physics beyond the Standard Model. Troubling because investment in accelerator R&D seems inadequate to prepare for the facilities we will need beyond or in addition to these next machines.

Over the last five years the Neutrino Factory and Muon Collider Collaboration (normally referred to as the Muon Collaboration or MC) has been exploring the possibilities for neutrino factories and Muon Colliders. Neutrino Factories would provide intense beams of muon- and electron-neutrinos that are ideally suited to probe and exploit neutrino oscillations. Muon Colliders offer the dream of very high energy, but reasonably sized, lepton colliders. The ideas and prospects for Neutrino Factories and Muon Colliders are sufficiently exciting that many particle and accelerator physicists are working on them. However, no single US laboratory has chosen this work as a primary activity. As a result, a new way of pursuing accelerator R&D in a multi-institution collaboration has evolved. The MC is a grass roots collaboration, consisting of about 130 accelerator- and particle-physicists from laboratories and Universities. Although mostly a US collaboration, there is also a healthy component from Europe and Japan. Funding comes directly to the collaboration from the US funding agencies, and is then distributed to the institutions within the MC after an internal technical review. University physicists are attracted to the MC not only because of the seductive dream of Neutrino Factories and Muon Colliders, but also because of the intellectual challenges and the possibility of inventing something new that makes a significant impact on the future of our field. Particle physicists that have no previous accelerator R&D experience are attracted to the MC because, in addition to learning new things, they find that they can quickly make significant contributions within the stimulating environment of a "small" collaboration.

This new way of doing business appears to be succeeding, bringing together accelerator- and particle-physicists to pursue the design, simulation, and hardware studies required to develop very intense cold muon sources. These design and simulation activities have been extensive, and have been carried out in collaboration with those engaged in studies going on in Europe and Japan. New simulation tools have been developed and used to design realistic schemes for the phase rotation, cooling, and acceleration of the muon beams required for Neutrino Factories and Muon Colliders. The MC and our collaborators are necessarily confronting many challenging beam dynamics problems, and we are finding that particle physicists are making valuable contributions that complement the work of more experienced accelerator physicists. Therefore, the way the MC works is perhaps worthy of note.

In summary, besides the R&D that is being successfully performed, the MC is itself an experiment that we feel is succeeding. It has demonstrated that it is possible to (i) build a grass-roots accelerator R&D activity that draws together many particle and accelerator physicists from many institutions, (ii) receive funds directly from the agencies and distribute it within the collaboration in an effective way, and (iii) deliver a productive R&D program (the most recent external technical review of the MC activities resulted in a very positive report).

If we believe that to keep particle physics healthy it is desirable that a greater fraction of our community is engaged in accelerator R&D, then the example of the MC provides food for thought.

To find out more about the Muon Collaboration:

http://www.cap.bnl.gov/mumu/

Steve Geer
(MC cospokesperson)

2.2 Situation of Neutrino Factory R&D at CERN and in Europe

Helmut Haseroth, CERN

Helmut.Haseroth@cern.ch,

CERN created a Neutrino Factory Working Group some three years ago with the intention of having two possible options for CERN after LHC: CLIC and a Neutrino Factory. A neutrino Factory is composed of a proton driver (several MW of beam power), a target, where the impinging protons produce pions, a device where the pions are collected to produce by their decay a muon beam and a subsequent section where the muons are converted into a "useful" beam by cutting the emittance and/or by "cooling" techniques. Subsequent acceleration and injection into a storage ring where the muon decay produces highly directional neutrino beams are necessary ingredients.

A substantial amount of manpower and material was invested in this project by CERN together with considerable help received from different institutes in Europe. Many of the results were achieved in close collaboration with the American Muon Collaboration and with Japanese labs. Joint meetings (NuFact99, NuFact00, NuFact01 and NuFact02) fostered close collaboration and exchange of ideas. At CERN particular achievements or at least alternative scenarios were obtained with the proton driver (use of a 2.2 GeV linac), in the field of ionization cooling, the use of a horn to collect the pions and with target experiments using mercury.

The suddenly discovered financial "LHC crisis" put an unexpected end to this activity at CERN. CERN is now only expected to follow what is going on elsewhere without making contributions of its own. One FTE/year is what can be afforded. The only positive point in this sad scenario is the creation of the European Muon Coordination and Oversight Group (EMCOG) created in a joint effort by the lab directors of major European institutes (CEA, CERN, GSI, INFN, IN2P3, RAL) with the specific aim of launching a common effort in this domain, with priorities for the proton driver, including a "super beam", the target and horn part and also the "Muon Ionisation Cooling Experiment" (MICE). This group requested also the creation of a European Neutrino Factory Working Group, which is being built up at present. Requests for support will go to the European Union within the context of the FP6 programme.

It is hoped that with a joint European effort we can carry on working in this exciting domain and continue our collaboration with Japan and the US. New collaborators to join this stimulating endeavor are always welcome, even with a small percentage of their time.

3 Neutrino factories

3.1 Introduction to the Neutrino Factory

Simone Gilardoni, Université de Genève and CERN

simone.gilardoni@cern.ch,

The neutrino history is full of puzzle and surprises. Neutrinos were invented by Pauli to solve the puzzle of the electron spectrum emitted in beta decay, but his regret was the invention of a particle *that cannot be experimentally observed*. Nowadays, after 50 years of *experimental* neutrino physics, in spite of the Pauli's worries, the discovery of neutrino oscillation opened a new era for physics beyond the standard model.

3.1.1 Neutrino History

The official history of neutrinos started the 4 December 1930 when Pauli wrote this letter to a meeting in Tubingen [1]:

Dear Radioactive Ladies and Gentlemen,

As the bearer of these lines, to whom I graciously ask you to listen, will explain to you in more detail, how because of the "wrong" statistics of the N and Li6 nuclei and the continuous beta spectrum, I have hit upon a desperate remedy to save the "exchange theorem" of statistics and the law of conservation of energy. Namely, the possibility that there could exist in the nuclei electrically neutral particles, that I wish to call neutrons, which have spin 1/2 and obey the exclusion principle and which further differ from light quanta in that they do not travel with the velocity of light. The mass of the neutrons should be of the same order of magnitude as the electron mass and in any event not larger than 0.01 proton masses. The continuous beta spectrum would then become understandable by the assumption that in beta decay a neutron is emitted in addition to the electron such that the sum of the energies of the neutron and the electron is constant [...].

I agree that my remedy could seem incredible because one should have seen those neutrons very earlier if they really exist. But only the one who dare can win and the difficult situation, due to the continuous structure of the beta spectrum, is lighted by a remark of my honoured predecessor, Mr Debye, who told me recently in Bruxelles: "Oh, It's well better not to think to this at all, like new taxes". From now on, every solution to the issue must be discussed. Thus, dear radioactive people, look and judge. Unfortunately, I cannot appear in Tubingen personally since I am indispensable here in Zurich because of a ball on the night of 6/7 December.
With my best regards to you, and also to Mr Back.

Your humble servant, W. Pauli

The famous physicist was trying to solve one of the most puzzling problems of the époque, the continuous spectrum of the electron produced in beta decay. At that time only the alpha decay had found an explanation, since every element participating in the reaction is detected. Being a two-body decay ${}^{A}_{z}X \rightarrow {}^{A-4}_{Z-2}Y + \alpha$, the energy of the alpha emitted is more or less constant. However, in the beta decay, ${}^{A}_{z}X \rightarrow {}^{A}_{Z+1}X + e^{-} + \bar{\nu}_e$, the energy of the particle emitted and detected, the electron, has a continuous spectrum. This is impossible without admitting the presence of a third particle, which escapes from detection: the neutron invented by Pauli. Today the neutron is the particle discovered by Chadwick in 1932 and it is the partner of the proton as constituent of the nucleus, while E. Fermi introduced the name of neutrino for the Pauli's particle. The first (anti)neutrino was detected by F. Reines and C.L. Cowan in 1956 using as source the Savannah River nuclear reactor [2]. The exciting history of this particle had started.

3.1.1.1 *The solar neutrino puzzle*

The second puzzle in neutrino physics came just few years after the detection of the first neutrinos. R. Davies realised in the late 60's in the Homestake mine the first experiment [3] to measure the neutrino flux coming from the sun. The different fusion reactions happening in the sun produce only ν_e with an energy spectrum shown in Figure 3.1.1 (left). The typical ν_e flux reaching the earth equals $10^8 \nu_e/s/m^2$.

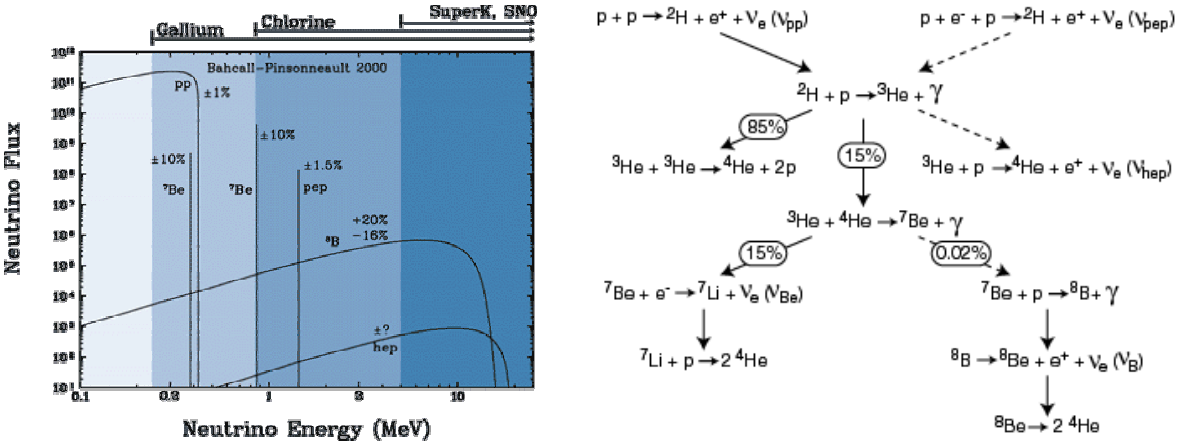

Figure 3.1.1 : The different fusion reactions (right) produce the neutrino spectrum on the left [4]

The experiment proposed and run by Davies is able to detect only ν_e by inverse beta decay reaction, $\nu_e + {}^{37}Cl \rightarrow {}^{37}Ar + e^{-}$, in a pool of $400m^3$ of C_2Cl_4. Then the number of Ar nuclei produced gives the electron neutrino flux. However after 30 years of data taking the result is surprising: the ν_e detected are only half the number predicted by the Standard Solar Model (SSM)[4]. The possibility that either the SSM calculation or the experimental results could be wrong can be easily ruled out. In fact the SSM prediction on the power emitted from the sun and the vibration modes of the solar surface are in perfect agreement with experimental observation and the power in the visible light is produced by the same fusion processes that generate neutrinos.

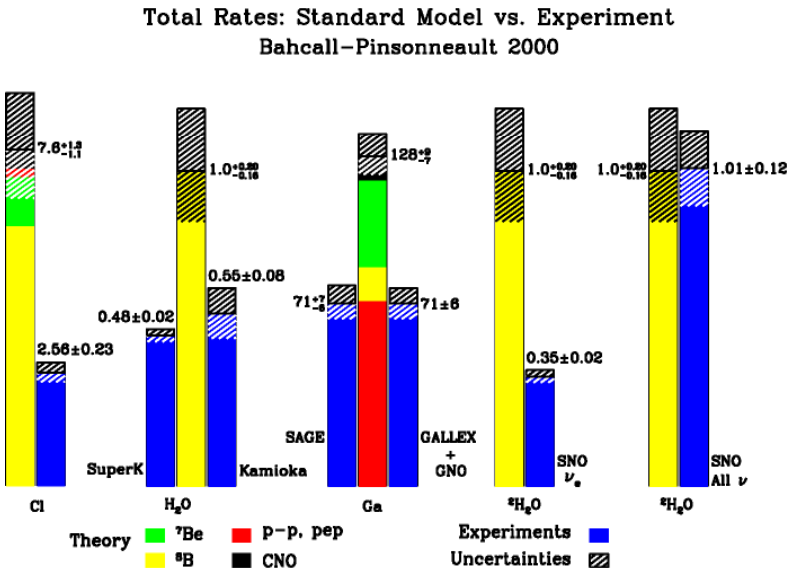

Figure 3.1.2 : Solar Neutrino fluxes in SNU (Solar Neutrino Unit) of different experiments compared to the SSM prediction [4].

Moreover more than one experiment measured or is measuring the lack of neutrinos using different techniques (Homestake, Gallex Sage and GNO the inverse beta decay and Kamiokande and Super-Kamiokande are water Cerenkov detector, see Figure 3.1.2).

The only possible explanation is that ν_e transforms into a neutrino of a different flavour , not detectable by an inverse beta decay detector.

The final solution has been found in 2002 by the Canadian experiment SNO. SNO is a heavy water Cerenkov detector (D_2O)[5], which allows three different neutrino interactions involving all neutrino flavours. The three possible interactions are :

- Elastic Scattering (ES). The neutrino of any flavour can scatter on an electron that produces Cherenkov light.
- Charged Current (CC) interaction. The electron neutrino interacts with the one quark in the Deuterium neutron and produces a proton causing the dissociation of the nucleus. Again the electron produced in the weak interaction is detected via Cerenkov light.
- Neutral Current (NC) interaction. The neutrino of any flavour can interact with a quark of the neutron or the proton of the Deuterium dissociating the nucleus. The free neutron then is captured by a nucleus and the emitted photon is detected.

The presence in the ν_e solar flux of non ν_e neutrinos can be identified by comparing the neutrino flux extracted from the CC events, Φ_{CC}, and the ES events, Φ_{ES}, or the CC events and the NC events, Φ_{NC}. If the rate between the fluxes Φ_{CC} and Φ_{ES} is smaller than one and the rate between Φ_{CC} and Φ_{NC} is also smaller than one there are non electron neutrinos in the solar flux. The results [6] of the following lines

$$\Phi_{SNO}^{ES}(\nu_x) = \Phi_e + \varepsilon\Phi_{\mu\tau} = 2.39 \pm_{0.23}^{0.24} (stat) \pm_{0.14}^{0.16} (sys) \times 10^6 cm^{-2} s^{-1}$$
$$\Phi_{SNO}^{NC}(\nu_x) = \Phi_e + \Phi_{\mu\tau} = 5.09 \pm_{0.43}^{0.44} (stat) \pm_{0.43}^{0.46} (sys) \times 10^6 cm^{-2} s^{-1}$$
$$\Phi_{SNO}^{CC}(\nu_e) = \Phi_e = 1.76 \pm_{0.05}^{0.06} (stat.) \pm_{0.12}^{0.11} (sys.) \times 10^6 cm^{-2} s^{-1}$$

confirm the suspects: solar neutrinos oscillate.

3.1.1.2 *Atmospheric neutrinos*

After the sun, the other main natural source of neutrinos is the earth atmosphere.

Particles from the cosmic background impinge on the high atmosphere and produce a huge number of secondaries. In particular, pions of both sign decays in flight via $\pi^+ \rightarrow \mu^+ + \nu_\mu$ ($\pi^- \rightarrow \mu^- + \bar{\nu}_\mu$). The muon again will decay to $\mu^+ \rightarrow e^+ + \nu_e + \bar{\nu}_\mu$ ($\mu^- \rightarrow e^- + \bar{\nu}_e + \nu_\mu$). The typical energies of atmospheric neutrinos range from some hundred MeV to few GeV.

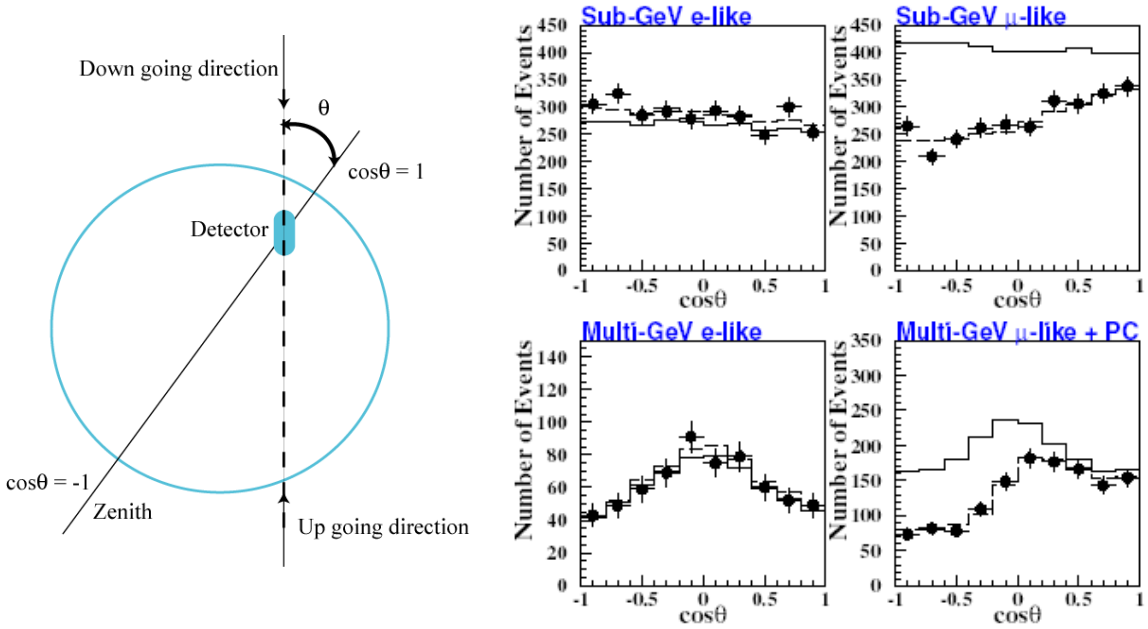

Figure 3.1.3 : Results of SuperKamiokande for the atmospheric neutrino flux compared to the non-oscillation hypothesis. [7]

Super-Kamiokande [8] is a water Cerenkov detector located in Japan, which observes both neutrino flavours coming from the atmosphere up to the detector and the opposite site of the earth. The experiment counts ν_e and ν_μ in bin of cosinus of the azimutal angle θ (cos θ =1 for the neutrinos coming from the top and cos θ =-1 from the bottom, see Figure 3.1.3, left) and compares the number of down going neutrinos with the up going ones. The result is quite striking: the ν_μ coming from the bottom, hence traversing the earth diameter, are nearly half of the ones coming from the top. At a first glance the easiest explication would sound like: neutrinos have interacted with the earth. But there are two caveats: the first is that from Figure 3.1.3 the asymmetry

doesn't appear for ν_e, and the second is that the earth is practically transparent for neutrinos of less than few GeV energy. The conclusion is that atmospheric ν_μ transform into another neutrino flavour, which is not ν_e.

3.1.1.3 *Neutrino Oscillation*

From the experimental results of SNO and Super-Kamiokande it is proven that during their flight neutrinos of one flavour transform in neutrinos of another flavour. The first implication is already quite impressive: this process is allowed only if neutrinos have a non-zero mass, while in the Standard Model they have strictly zero mass.

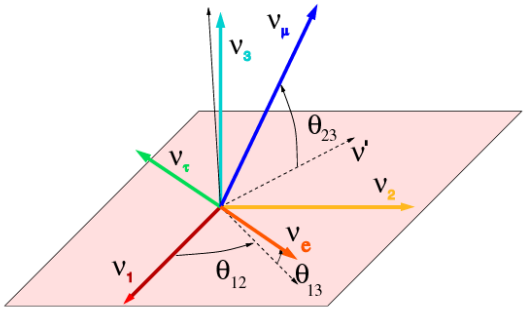

Figure 3.1.4 : The mass eigenstate vectors don't coincide with the flavour eigenvectors.

The flavour changing process of neutrino oscillation is possible if the neutrino mass states, which describe the propagation in space, are different from the flavour states, which describe the weak interaction of neutrinos in the standard model (see Figure 3.1.4) [9]. Let's assume that at time t_0 a neutrino is produced by weak interaction in a given flavour state ν_α (α=e,μ,τ), that is a given mix of mass states ν_i (i=1,2,3), together with its lepton partner α[1]. As the neutrino propagates, each individual mass state of mass m_i(i=1,2,3) will propagate according to the Schrödinger equation. At a distance L, where the detector is placed, or at time $t>t_0$, the mixing between the mass states could be different from the original and so the neutrino flavour. Then the experiment will try to identify the neutrino flavour via the flavour of the lepton produced by weak interaction. The process of flavour transformation could be described in the following way. Since the leptons are three (e, μ, τ), also the neutrino flavours are three (ν_e, ν_μ,ν_τ) and so the neutrino mass states (ν_1,ν_2,ν_3). The mass states ν_i and the flavour states ν_α are related via a 3x3 mixing matrix U:

$$U = \begin{pmatrix} c_{13}c_{12} & c_{13}s_{12} & s_{13}e^{-i\delta} \\ -c_{23}s_{12} - s_{13}s_{23}c_{12}e^{i\delta} & c_{23}c_{12} - s_{13}s_{23}s_{12}e^{i\delta} & c_{13}s_{23} \\ s_{23}s_{12} - s_{13}c_{23}c_{12}e^{i\delta} & -s_{23}c_{12} - s_{13}c_{23}s_{12}e^{i\delta} & c_{13}c_{23} \end{pmatrix}$$

[1]The identification of the neutrino flavour is possible only stating the associated lepton flavour.

with $c_{ij}=\cos\theta_{ij}$, $s_{ij}=\sin\theta_{ij}$ and δ the CP violating phase. With some quantum mechanics calculations, it can be shown that, for example, the probability for a ν_e of energy E_ν to transform into a ν_μ after the distance L equals:

$$P(\nu_e \to \nu_\mu) = \sin^2 2\theta_{13} \sin^2 \theta_{23} \sin^2\left(\frac{\Delta m^2_{23} L}{4E_\nu}\right)$$

where $\Delta m_{23}^2 = m_2^2 - m_3^2$ is the difference between the square of the masses of the two mass eigenstates 2 and 3.

There is a total of six parameters in the oscillation theory: three mixing angles, two mass splittings and a CP violating phase.

For a given mixing angle, an experiment will be able to probe the Δm^2 values of the order of the inverse of L/E. Table 3.1.1 shows the typical Δm^2 values:

Table 3.3.1

Neutrino Source	L(km)	E(GeV)	L(km)/E(GeV)	Δm^2	Experiment
Solar	10^8	10^{-3}	10^{11}	10^{-11}	SNO
Atmospheric	10^4	1	10^4	10^{-4}	Super-Kamiokande
Accelerator (Short baseline)	10^2	1	10^2	10^{-2}	K2K
Reactor	1	10^{-3}	10^3	10^{-3}	Chooz, Kamland
Accelerator (Long baseline)	10^3	10	10^2	10^{-2}	Neutrino Factory

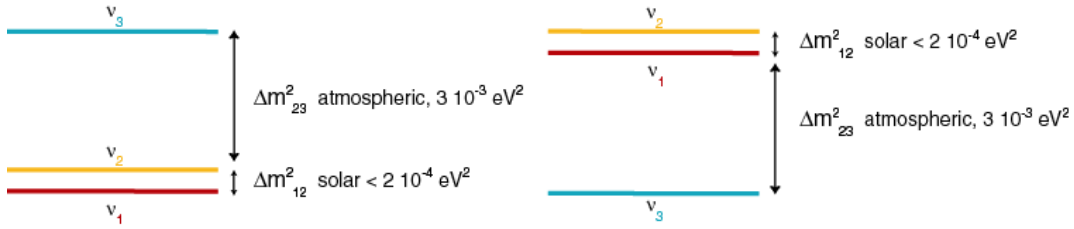

Figure 3.1.5 : The two possible scenarios for the atmospheric mass splitting

There are two regimes for the Δm^2 splitting, a small one that dominates the solar neutrinos, Δm_{12}^2, and a large one, which governs the atmospheric neutrinos, Δm_{23}^2. Two different pictures are possible for the sign of the mass splitting Δm_{23}^2 (see Figure 3.1.5): the third mass state is heavier than the other two (hierarchical spectrum) and the Δm_{23}^2 is negative, or the inverse situation, where m_3 is the lightest (degenerate spectrum).

3.1.1.4 *State of the art*

The mixing matrix U can be split into three matrices:

$$\begin{pmatrix} \nu_e \\ \nu_\mu \\ \nu_\tau \end{pmatrix} = \begin{pmatrix} 1 & 0 & 0 \\ 0 & c_{23} & s_{23} \\ 0 & -s_{23} & c_{23} \end{pmatrix} \begin{pmatrix} c_{13} & 0 & s_{13}e^{-i\delta} \\ 0 & 1 & 0 \\ -s_{13}e^{-i\delta} & 0 & c_{13} \end{pmatrix} \begin{pmatrix} c_{12} & s_{12} & 0 \\ -s_{12} & c_{12} & 0 \\ 0 & 0 & 1 \end{pmatrix} \begin{pmatrix} \nu_1 \\ \nu_2 \\ \nu_3 \end{pmatrix}$$

The neutrino oscillation experimental picture can be summarised in the following points:

- The first matrix drives the atmospheric neutrinos measured by Super-Kamiokande. ν_μ oscillate into ν_τ and not into ν_e. The mixing angles θ_{23} is large ($\approx 45°$) and $\Delta m_{23}^2 \approx 3\ 10^{-3}\ eV^2$
- The third matrix drives the solar neutrinos measured by SNO. ν_e oscillate into ν_x (x=μ or τ), the angle θ_{12} is large (LMA, Large Mixing Angle solution is the preferred) and Δm_{12}^2 is around $5\ 10^{-5}\ eV^2$
- The non-diagonal part, the central matrix, is small, since θ_{13} is not larger than 13° as measured by CHOOZ. However this value is only an upper limit, and the lower limit could be zero.

The present knowledge of neutrino oscillation allows filling most of the mixing matrix elements, namely [10]:

$$|U| = \begin{pmatrix} 0.73-0.89 & 0.45-0.66 & <0.24 \\ 0.23-0.66 & 0.24-0.75 & 0.52-0.87 \\ 0.06-0.57 & 0.40-0.82 & 0.48-0.85 \end{pmatrix}$$

with no indication of the value of the δ violating phase. What is still missing is a precise value for $\sin\theta_{13}$, which is the smallest element of the U matrix, the sign of Δm_{23}^2 and the CP violating phase.

3.1.2 Why a neutrino factory?

A number of experiments in the next ten years will try to see the oscillation $\nu_\mu \rightarrow \nu_e$, which has not been observed yet, and to measure θ_{13}. Figure 3.1.6 [11] shows the sensitivity to θ_{13} for different experiments. Why is this number so important for the theory? In the mixing matrix $\sin\theta_{13}$ multiplies the term containing the CP violating phase. If it is too small or zero, there is no hope to observe CP violation in the leptonic sector. The CP violation is the causes of the asymmetry in the universe between matter and antimatter, because particles and antiparticle don't behave in the same way, and CP violation in the hadronic sector is not enough to explain this asymmetry. The leptonic CP violation could be the solution of the problem, but it can be discovered only if $\sin\theta_{13}$ is non-zero or not too small: δ is the final "Holy Grail" for all the future neutrino experiments.

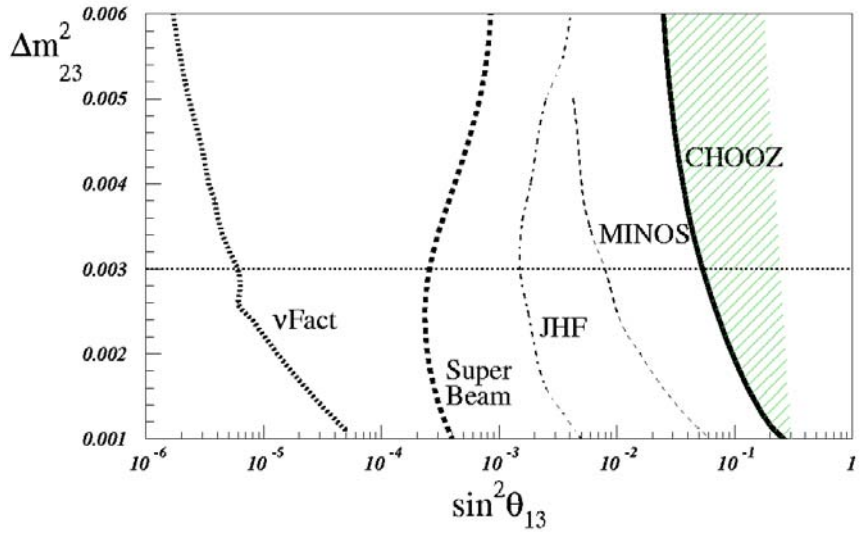

Figure 3.1.6 : Sensitivity to $\sin\theta_{13}$ for different future neutrino beam facilities.

If non zero, the leptonic CP violation can be observed in an appearance[2] experiment where, at different time, the two probabilities, $P(\nu_e \to \nu_\mu)$, $P(\bar{\nu}_e \to \bar{\nu}_\mu)$ are measured. The quantity A_{CP} (asymmetry) :

$$A_{CP} = \frac{P(\nu_e \to \nu_\mu) - P(\bar{\nu}_e \to \bar{\nu}_\mu)}{P(\nu_e \to \nu_\mu) + P(\bar{\nu}_e \to \bar{\nu}_\mu)} \propto \frac{\sin\delta \, \sin(\Delta m^2_{12} L/4E) \sin\theta_{12}}{\sin\theta_{13} + Solar\ terms}$$

will give the access to the CP violating phase. A_{CP} can be large if LMA[3] is the solution for the solar neutrinos, as seems to be case from SNO; and if $\sin\theta_{13}$ is small, but not too much otherwise the oscillation probabilities become too small and the statistic error becomes too large.

It is of fundamental importance to produce ν_e and anti-ν_e at high energy under the same controlled conditions and this is possible only in an artificial source that can accelerate alternatively positive and negative muons: a Neutrino Factory (N.F.).

Let suppose that the N.F. accelerate and stores μ^-. They will decay via $\mu^- \to e^- + \bar{\nu}_e + \nu_\mu$. If $\bar{\nu}_e$ oscillate into $\bar{\nu}_\mu$, the CC interaction of $\bar{\nu}_\mu$ in the detector will create a μ^+, while the interaction of ν_μ from the N.F. beam will generate again a μ^-. The $\bar{\nu}_e$ oscillation signature is the detection of a "wrong sign muon", a muon of opposite charge of the one stored in the decay ring. The selection of the charge between wrong sign muons and the other charge is possible using a large magnetized detector [11]. This kind of signature is not possible in traditional neutrino beams produced by pion and kaon decay because the beam contains a large fraction of the two flavours with the two helicities at the same time.

[2] A disappearance experiment measures the survival probability, namely $P(\nu_e \to \nu_e)$, which is time reversal. Since CPT has to be conserved, $P(\nu_e \to \nu_e)$ conserves CP.

[3] At the time of writing the Kamland experiment has confirmed LMA.

3.1.3 The machine

The aim of a Neutrino Factory is the production of high energy, highly collimated (anti)electron and (anti)muon neutrino beams from muon decay $\mu^+ \to e^+ + \nu_e + \bar{\nu}_\mu$ ($\mu^- \to e^- + \bar{\nu}_e + \nu_\mu$). The goal is to achieve a neutrino flux of the order of 10^{21} muon per year (1 year = 10^7 seconds). The typical scheme of the factory is the following: a high power proton beam (4 MW) impinges on a mercury target to produce pions. Pions are focused by a magnetic lens (a horn) or captured by a 20 T solenoid and injected into a solenoidal decay channel. The resulting muons have a large energy spread (300%) and an enormous transverse emittance. Such kind of beam can not be injected directly into a traditional accelerator without intolerable losses. The first step is the reduction of the muon energy spread by phase rotation. Then ionisation cooling reduces the transverse phase space. The resulting beam is accelerated to several tens of GeV (20-50). The final step is to store the muons in a triangular decay ring, whose two longer sides are pointing to two detectors placed at different locations.

3.1.3.1 *Machine parameter choice*

The choice of the machine parameter will determine the physics reach of the neutrino experiment: the higher the energy and the flux, the higher the physics reach (Figure 3.1.7). CP violation can be seen only at energies higher than 20 GeV and fluxes higher than 10^{20} muon/year.

Another important parameter is the distance between the machine and the far detector, first because the detector should be placed far enough to have a large oscillation probability, second because the neutrino interaction with matter will discriminate the sign of Δm_{23}^2. Infact ν_e interact differently from the other neutrino flavours since ordinary matter is full of electrons, while there are no muons or taus. Hence an electron neutrino can interact with proton, neutrons and electrons via neutral current, as the other flavours, but it can interact also with the electrons via charged current. An analogy can be drawn with the propagation of polarised light in a medium that has a different refraction index for each polarisation component. A polarisation component corresponds to a neutrino flavour: light enters in a medium with a given polarisation and emerges with a different polarisation. For neutrinos when propagating in matter there is a different oscillation probability (MSW effect or matter effect) from the case of propagation in vacuum. The variation of the oscillation probability depends on the sign of Δm_{23}^2 and is different for neutrinos and antineutrinos. In Figure 3.1.7 it is presented as function of distance, the rate between oscillated antineutrinos and oscillated neutrinos. This rate changes with the distance and with the sign of Δm_{23}^2. So the best distance seems to be around 5000 km, where the splitting between the two signs is maximal.

Unfortunately, also CP violation has influence on this rate, and at 5000 km the matter effect cancels the asymmetry introduced by the CP violation, since the lines for δ=90º and δ=-90º crosses. Hence the chosen distance is between 2000 km and 4000 km because going to further distance will decrease the neutrino flux but also will require a

vertical muon storage ring. Considering for example the CERN site for the neutrino factory, the possible detector locations are shown in Figure 3.1.8.

In the next paragraphs the CERN reference scenario (Figure 3.1.9) will be described as as an example of N.F. machine design.

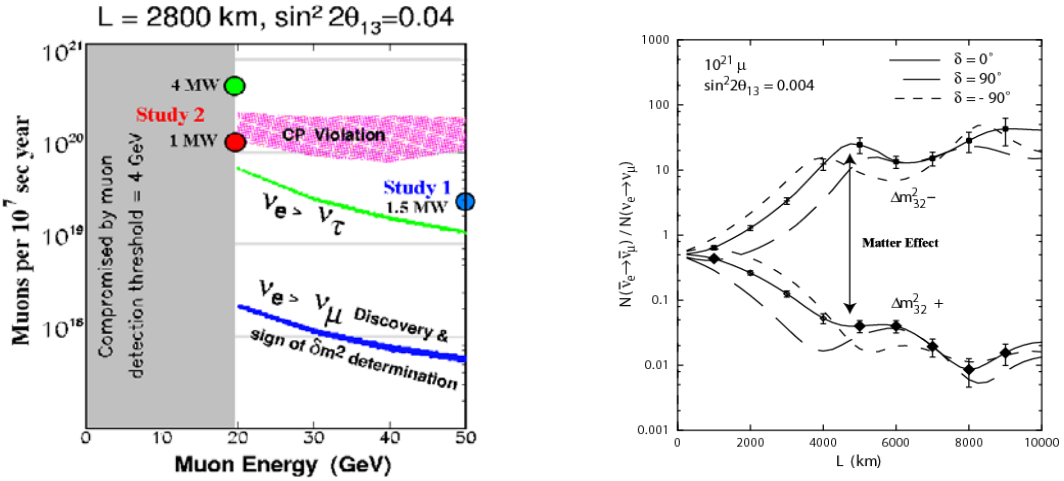

Figure 3.1.7 : Physics reach versus beam and energy intensity (left) [12] and baseline influence on the mass splitting recognition and CP measurements (right) [11]

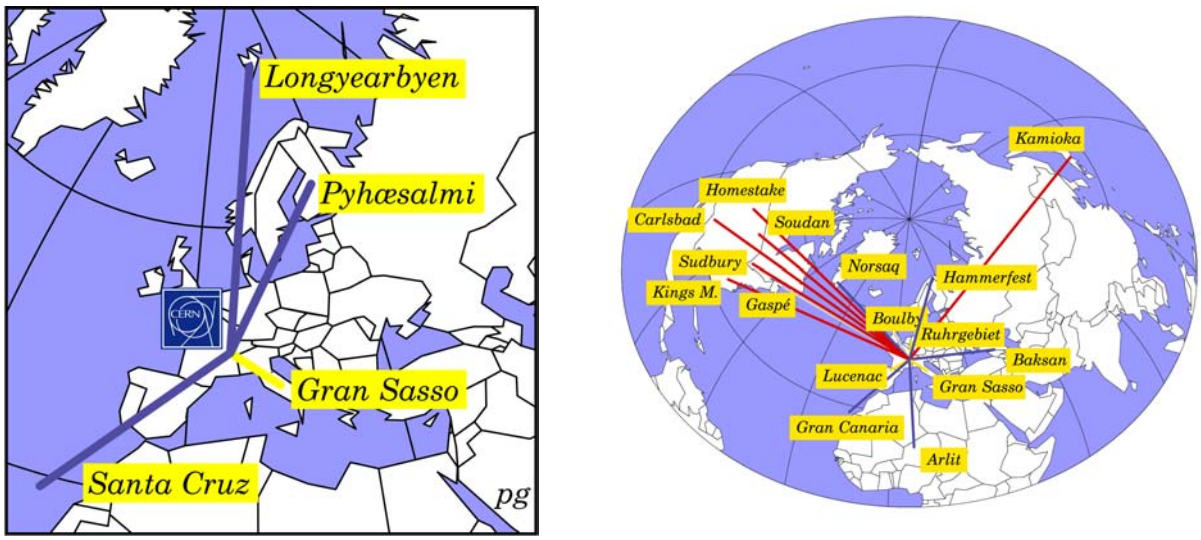

Figure 3.1.8 : Different detector locations are already identified in Europe around CERN, but also the entire world could be a nice playground

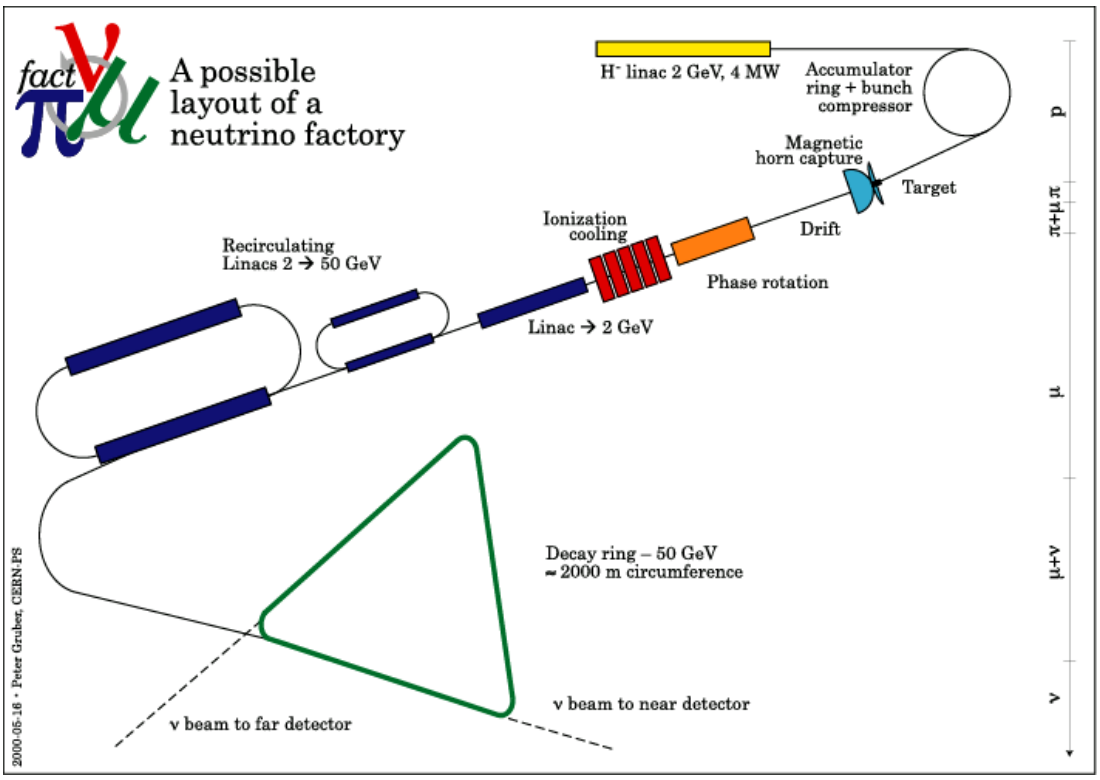

Figure 3.1.9 : Nufact accelerator complex layout. Not to scale.

3.1.3.2 *Proton Driver*

The first element of the N.F. is the proton driver. In the CERN scheme H^- ions are accelerated using a Superconducting Proton Linac (SPL) to 2.2 GeV[13]. The maximum proton beam power technically feasible is around 4 MW. This means 10^{23} protons per year at 2.2 GeV. The typical rate proton/muon conversion is around 1% and the flux of neutrinos from muon decay for the oscillation experiments is estimated around 10^{20} neutrinos per year. The SPL (see Figure 3.1.10) is composed of a room temperature low energy part (until 120 MeV), followed by a series of superconducting accelerating sections to reach 2.2 GeV. The SPL injects the stripped H^- into two rings, the first to accumulate protons and the second to compress them in time before the interaction with the target.

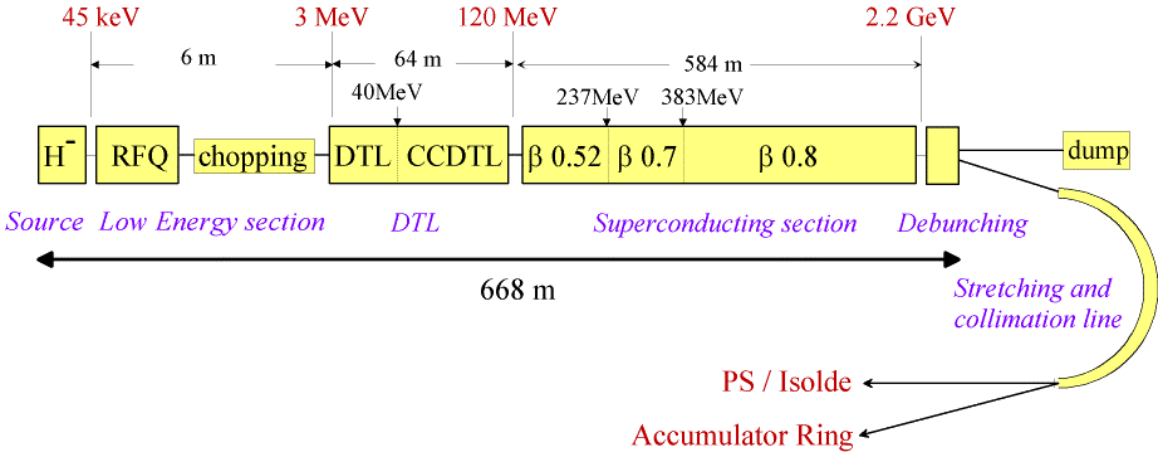

Figure 3.1.10 : Conceptual design of the SPL

3.1.3.3 *Target and capture*

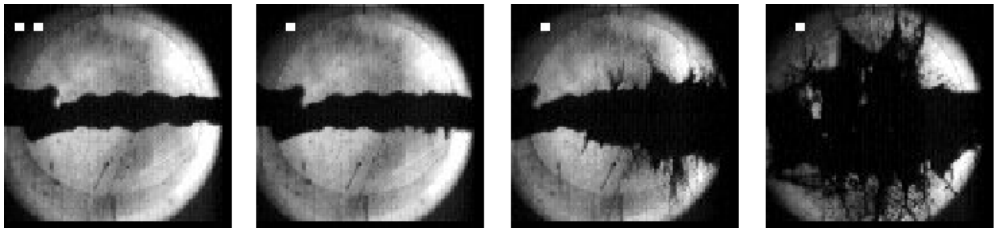

Figure 3.1.11 : Mercury Jet explosion due to proton impact. The time increases from left to right while protons are coming from the right part of the pictures

Protons impinge on a target to produce pions. The main challenge of such system is to sustain 4 MW and a high proton pulse repetition rate in a volume that cannot exceed the one of a pint of beer (L=30 cm and 1 cm radius) since a bigger target will decrease considerably the efficiency of the pion collection system. The baseline material chosen

is mercury because it has a high Z, which means high pion production per unit of length, it is liquid at room temperature and it can be easily replaced at every proton shot, while a solid one will not survive more than few proton pulses impacts. A number of experiments have been performed to measure the speed of the mercury explosion induced by the proton energy deposition [14] (see Figure 3.1.11). The speed required to exchange the target for every shoots is estimated around 20 m/s, and the transverse speed of the mercury drops generated by the explosion is around 30 m/s. The integration between target and the focusing system is still a design issue for the target station. Another major difficulty in evaluating the best target material comes from the large uncertainty on the pion production and interaction cross section for the range of energies between some hundred MeV and few GeV. The data taking of the Harp experiment [15] will provide new measurements of those quantities with an error of few percent and clarify which is the best material to be used for a given proton energy.

A magnetic lens called horn focuses pions produced in the target. A horn consists of two concentric conductors, which delimit a closed volume (see Figure 3.1.12). The current of 300 kA pulsed at 50 Hz running in the conductors generates in that volume a toroidal magnetic field whose intensity decreases proportionally to the distance from the horn axis. Pions entering in the magnetic volume are bent by the field and focused in the direction of the decay channel section. The sign of pion charge is selected by the current polarity, changing in this way the sign of the muons in the machine. The major limitation of the system comes from its short life-time, estimated around 6 weeks, mainly due to thermal and mechanical stresses induced by the high repetition rate [16].

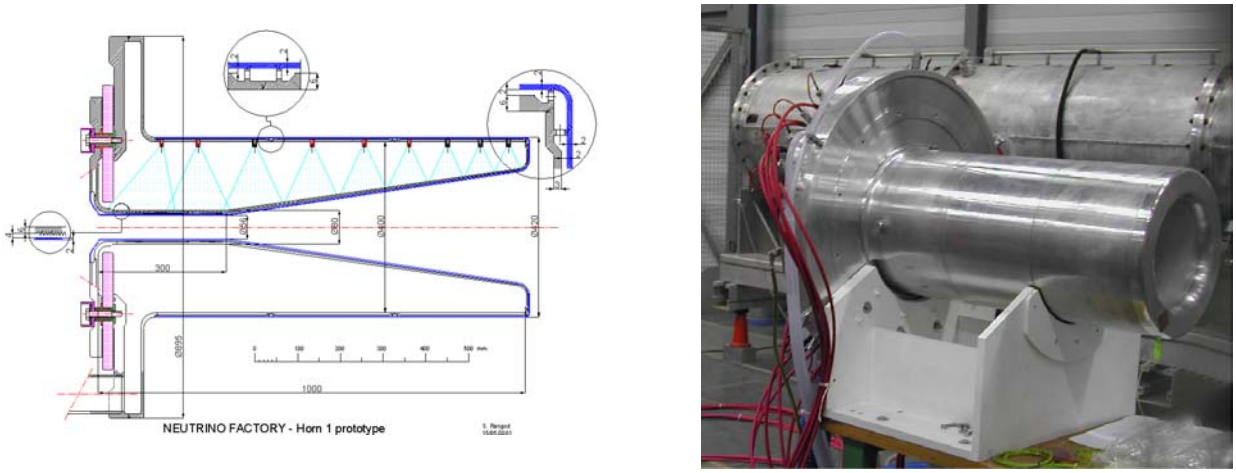

Figure 3.1.12 : Horn technical drawing (left) and the first prototype built and ready for test

3.1.3.4 *Decay Channel and phase rotation*

Pions injected into the solenoidal decay channel have a large energy spread which will be transmitted after the decay $\pi^+ \rightarrow \mu^+ + \nu_\mu$ ($\pi^- \rightarrow \mu^- + \overline{\nu}_\mu$) in the energy distribution of the muons. Moreover pions are not ultra-relativistic, since the average energy is around 200 MeV (see Figure 3.1.13,left), this means that to the energy spread corresponds a velocity spread. At the end of the decay channel muons at higher energy will arrive

before the less energetic ones. The building of the time-energy correlation could be used to reduce the energy spread with a series of RF.
The RFs phases are tuned to slow down the more energetic muons, which arrive earlier, and to accelerate the less energetic ones, which arrives later
The typical result after 30 RF cavities at 44 MHz, 2 MV/m can be seen in Figure 3.1.14: at the beginning of the channel pions have a banana distribution in the longitudinal phase space, and at the end of the channel muons are compressed around 200 MeV.

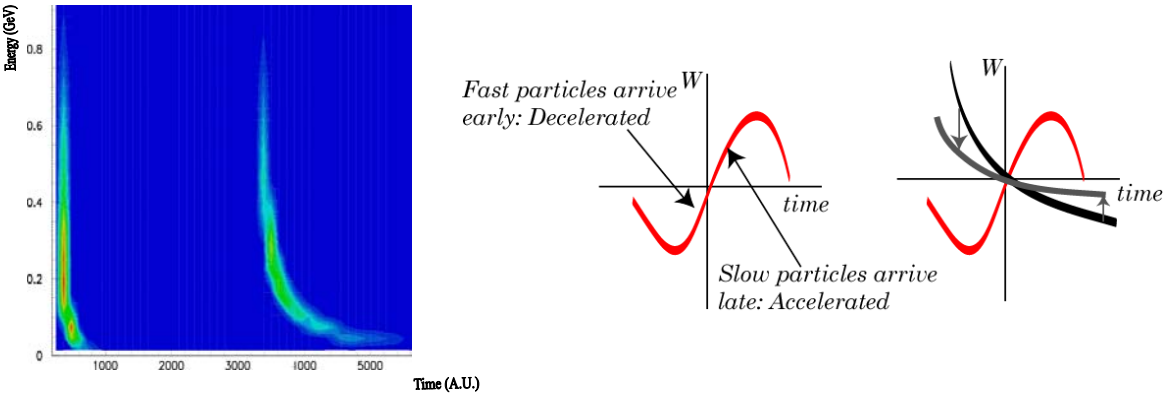

Figure 3.1.13 : Pion/Muon beam at the beginning and the end of the decay channel(left) and sketch of the phase rotation mechanism (right)

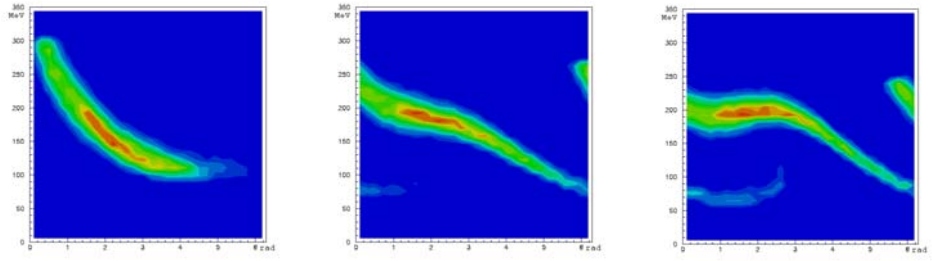

Figure 3.1.14 : Longitudinal phase plane during phase rotation

3.1.3.5 *Cooling*

After the phase rotation the transverse phase space dimensions (radius and angular divergence) are still too large to be accepted by a conventional accelerator: the beam has to be transversally cooled. Traditional techniques like stochastic cooling are too slow compared to the mean life-time of a muon (τ = 2,19 ms at rest), even for ultrarelativistic energies, so a faster process called ionisation cooling is used. Ionisation cooling involves three elements: solenoids, absorbers, RF cavities. The beam is confined by a series of solenoids and periodically focussed into an energy absorber of low Z material, like liquid hydrogen. Muons loose momentum in all direction passing through the material, while the RFs placed after the absorber restore only the longitudinal momentum, thus reducing the divergence of the beam . As first approximation the relative reduction of the tranverse phase space equals the relative energy losses in the absorber.

Liquid hydrogen is preferred for the absorber material to keep the beam heating due to multiple scattering as low as possible. Ionisation cooling was invented 20 years ago, but no experiment was ever tried in the past to demonstrate the feasibility of a part of a cooling machine. The MICE [17] experiment, proposed during this year, will test a section of the cooling channel of the N.F.. An International Collaboration has been already settled and a technical proposal will be submitted to RAL

3.1.3.6 *Acceleration and storage ring*

After the cooling section, muons are further accelerated by a conventional linac before being injected in a cascade of two recirculating linacs and accelerated to the final energy of 50 GeV. Then they feed a triangular storage ring. This shape is chosen to have two preferred decay directions pointing towards two experimental sites, one at short distance (≈700 km), and the other at far distance (≈ 3000 km).

References

[1] W. Pauli, "Zur älteren und neueren Geschichte des Neutrinos", in Collected Scientific Papers, ed. By R. Kronig and V. F. Weisskopf (Interscience, New York, 1964), volume 2, p.1313
[2] F. Reines et al., Science 124 (1956) 103
[3] R. Davis, Harmer and K.C. Hoffman, Phys. Rev. Lett. 21, 1205 (1968)
[4] J. Bahcall home page, http://www.sns.ias.edu/~jnb/
[5] SNO home page, http://www.sno.phy.queensu.ca/
[6] SNO collaboration, hep-ex/0211013v1
[7] Super-Kamiokande collaboration, hep-ex/0105023v1
[8] Super-Kamiokande home page, http://www-sk.icrr.u-tokyo.ac.jp/sk/
[9] As introduction Review, B. Kayser, hep-ph/0104147
[10] M.C. Gonzalez-Garcia , hep-ph/0210359
[11] Review of physics at the Neutrino Factory, M. Apollonio et al., hep-ph/0210192
[12] Feasibility Study-II of a Muon-Based Neutrino Source, ed., S.Ozaki, R.Palmer, M. Zisman, and J. Gallardo, BNL-52623 (2001)
[13] M. Vretenar (ed.), CERN 2000-012
[14] A. Fabich et al., J. Nucl. Mater. (2002) to be published
[15] G. Catanesi et al., CERN-SPSC 2002/019
[16] S. Gilardoni et al., Nufact02 proceedings, J. Phys. G (2002), to be published
[17] MICE LOI, http://hep04.phys.iit.edu/cooldemo/

3.2 Progress on FFAG Accelerators at KEK

Yoshiharu Mori , KEK

Yoshiharu.Mori@kek.jp

3.2.1 Introduction

A fixed-field alternating gradient(FFAG) accelerator seems to be very attractive, because the repetition rate of the accelerating cycle could be raised ten times or more

compared to that of the ordinary synchrotron. The idea of an FFAG accelerator was originally proposed by Ohkawa[1] in 1953, and later on Symon[2] and Kolomensky[3] have independently proposed this idea. Electron-beam machines demonstrating this principle have been successfully built in the MURA project, however, the only electron models were built and no proton accelerating FFAG has been built so far. The FFAG focusing is attractive for acceleration of high intensity beams and also short-lived particle beams such as muon beam because acceleration cycle could be increased. The magnetic field of FFAG is static, therefore, the acceleration time could be much shortened than that of ordinary synchrotron if an efficient high voltage RF accelerating system becomes available. Recently, a new type of high gradient RF cavity using high permeability magnetic alloy (MA) has been developed [5] and FFAG synchrotron becomes very promising.

In order to clarify the feasibility of rapid cycling FFAG synchrotron experimentally, proof-of-principle (POP) FFAG mod, which accelerates protons up to 1MeV with 1kHz repetition, has been developed at KEK and the first beam acceleration was successfully commissioned in June of 2000. The FFAG accelerator has large potentials. We have made several designs on high intensity proton accelerators with FFAG synchrotron for various applications such as spallation neutron source, proton driver for muon production and accelerator driven system (ADS) for energy breeder. Among them, short-lived particles such as muons can be accelerated with FFAG accelerators. The neutrino factory based on muon accelerator and muon storage ring has been proposed. In this, various R&D activities which have been carried out at KEK including the experimental results of proton acceleration in the FFAG POP proton model and also a neutrino factory based on FFAG accelerators will be presented.

3.2.2 Beam optics of scaling type of FFAG accelerator

In the scaling type of FFAG synchrotron, where the magnetic field is constant in time, the shape of the magnetic field should be such that the betatron tunes for both the horizontal and vertical planes should be constant for all closed orbit, and departing from all of the dangerous resonance lines. The condition above is called " zero-chromaticity".

$$\left.\frac{\partial}{\partial p}\left(\frac{K}{K_0}\right)\right|_{\vartheta=const.} = 0, \quad \left.\frac{\partial n}{\partial p}\right|_{\vartheta=const.} = 0. \qquad (1)$$

A magnetic field satisfying the scaling conditions described above must generally have the form ,

$$B(r,\theta) = B_i\left(\frac{r_i}{r}\right)^n F\left(\theta - \varsigma \ln\frac{r}{r_i}\right), \qquad (2)$$

$\frac{\pi}{N} = \theta_F - \theta_D$, N : sector number

geometrical field index : k

$$\frac{B}{B_0} = \left(\frac{r}{r_0}\right)^k$$

field index (seen by particle) : n

$$n = k\frac{1+\xi\cos\psi}{1+2\xi\cos\psi+\xi^2}$$

$\xi = \zeta - 1$, $\zeta = \frac{r_0}{\rho_{F,D}}$: circumference factor

$\alpha = \frac{1}{k+1}$: momentum compaction factor

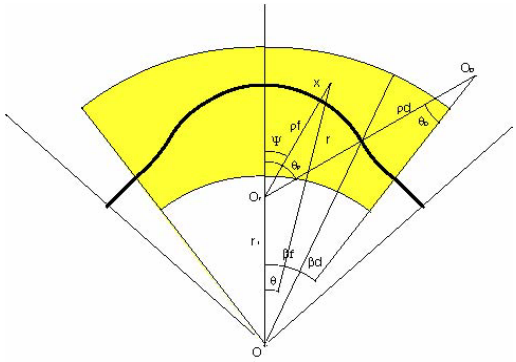

Figure.3.2.1 : Linearized orbit configuration of a triplet radial sector(DFD) type of FFAG.

This magnetic shape is called " radial sector". One the other hand, if behaves in a logarithmic manner, such as

$$\theta - \varsigma \ln\frac{r}{r_i} = const \quad , \qquad (3)$$

the orbits remain geometrically similar, but move around the beam center towards larger radii. This type is called " spiral sector".

The FFAG synchrotron is very attractive for accelerating intense proton beams as described above and several proposals have been submitted.[5][6] However, no practical proton-beam machine has been built so far. One of the most difficult technical issues to realize a high-repetition FFAG synchrotron is rf acceleration. The requested accelerating rf voltage per turn is

$$\Delta V = 2\pi(1+n)\left(\frac{dr}{dt}\right)p \quad . \qquad (4)$$

Here, is the orbit excursion rate. If we chose a radial sector type of ring configuration and each sector consists of a triplet focusing (DFD) lattice as shown in Figure 3.2.1, the linearized beam orbit parameters (beta function, dispersion) of the scaling type of FFAG ring can be estimated using an effective field index n with a circumference factor.

$$n = \pm\frac{(1+\xi\cos\psi)}{(1+2\xi\cos\psi+\xi^2)}, \qquad (5)$$

(+:focus, -:defocus)

where

$$\xi = \varsigma - 1 \quad . \qquad (6)$$

Here ζ is a so-called circumference factor and $\zeta=r_0/\rho$.

3.2.3 R&D activities of FFAG accelerators at KEK

3.2.3.1 *PoP FFAG proton model*

In order to clarify the availability of very rapid cycling in FFAG synchrotron, we have been developing a small POP (proof-of-principle) machine. The purposes of the POP machine are: (1) to prove the fast acceleration by FFAG synchrotron, and (2) to demonstrate the large acceptance of FFAG synchrotron. It should be noted that this POP machine is the world first proton FFAG accelerator. In this POP machine, the

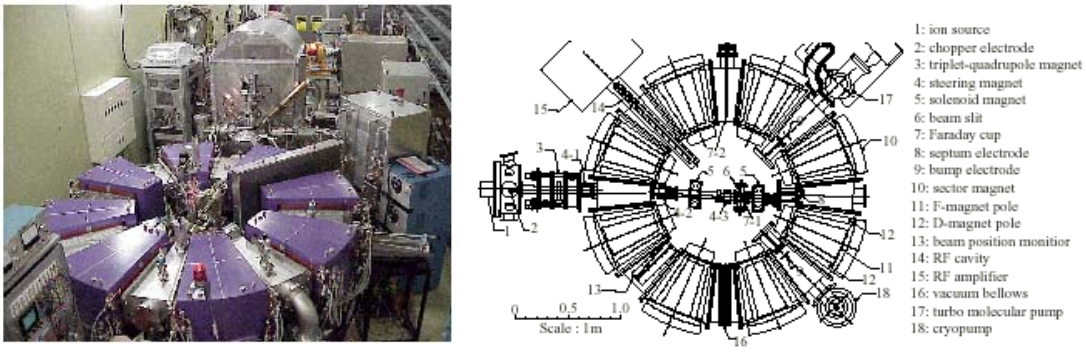

Figure 3.2.2 : Photograph and schematic layout of the POP FFAG machine.

maximum energy is limited to 0.5MeV because of radiation safety but the repetition rate of acceleration is 1kHz. The magnet configuration is a radial sector type and eight fold symmetry is chosen. Each sector consists of three dipole magnets which form a triplet focusing configuration DFD (defocus-focus-defocus). Field index (k) of each dipole magnet is k=2.5 and the maximum magnetic fields of the focusing and defocusing dipole magnets are 0.5 T and 0.2 T, respectively. The magnetic field configurations in three dimensional directions are calculated with OPERA-3D and their results are used for beam tracking simulation. The average beam radius changes from 0.81m to 1.14m according to the increase of beam energy from 50keV to 0.5MeV. The half gap heights of the magnet at the radius of 0.75m and 1.15m are 73mm and 25 mm, respectively. The schematic layout and the picture of the POP machine are shown in Figure 3.2.2.

The betatron tunes for horizontal and vertical directions are varied with field index and the product of the magnetic field and the effective magnet length (Bl-product). The design values of betatron tunes for horizontal and vertical directions are 2.25 and 1.25, respectively. The rf frequency changes from 0.61MHz to 1.38MHz. At the condition of the constant radial displacement as a function of time (dr/dt=const.), the rf voltage has to be increased from 1.3kV to 3kV. This rf voltage can be easily obtained by a magnetic alloy (MA) loaded rf cavity. [7]

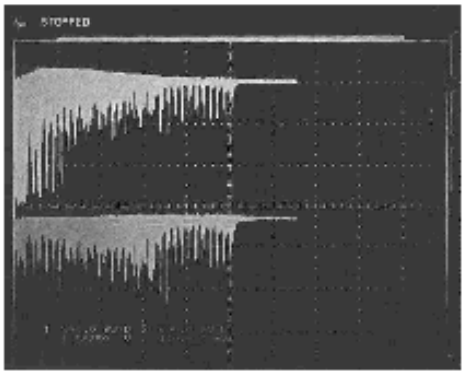

Figure 3.2.3 : Typical beam signal observed with the inner and outer electrodes of the beam position monitor during acceleration of a proton beam.

Intensive accelerator studies were carried out in order to make the characteristics of FFAG accelerator clear. The major items of the accelerator study are as follows.
*Demonstration f the fast acceleration,
*Betatron tune and synchrotron tune in various condition,
*Beam position in various energies, and
*Beam acceptance.

Beam acceleration [7]

Compared to ordinary synchrotron, the acceleration time of the FFAG synchrotron is not restricted by a ramping time of a pulsed magnet. Thus, the higher the acceleration field is, the quicker the acceleration is completed. It is one of the prominent merits of the FFAG synchrotron. To demonstrate this feature of FFAG accelerator is one of the strong motivation to develop the POP machine. In the case that a synchronous phase is set to be 20 degree, the rf voltage should be at least 1.3 kV during acceleration. We have developed a rf cavity using two rectangular FINEMET cores. The size of each core is 1.1 m (width) x 0.7 m (height) . The thickness of the core is 25 mm.A 55kW rf amplifier which consists of two tetrodes (Eimac 4CW25,000) was used. Figure 3.2.3 shows a typical beam signal observed by the inner and outer electrodes of the beam position monitor during acceleration of a proton beam. The beam has been successfully accelerated up to 500 keV within 1msec.

Tunes and beam position

Betatron tunes were measured in injection orbit at the various field configuration. Figure 3.2.4 shows the measured betatron tunes as a function of F/D ratio. The results were consistent with the results of the computer tracking simulation. The synchrotron tunes for various beam energies from 50keV to 500keV were also measured. The results shown in Figure 3.2.5a agreed well with the expected values. The beam positions were measured for different energies ranging from 100 keV to 400 keV. The results were summarized in Fig.3.2.5b. These are consistent with the simulation values within the systematic error.

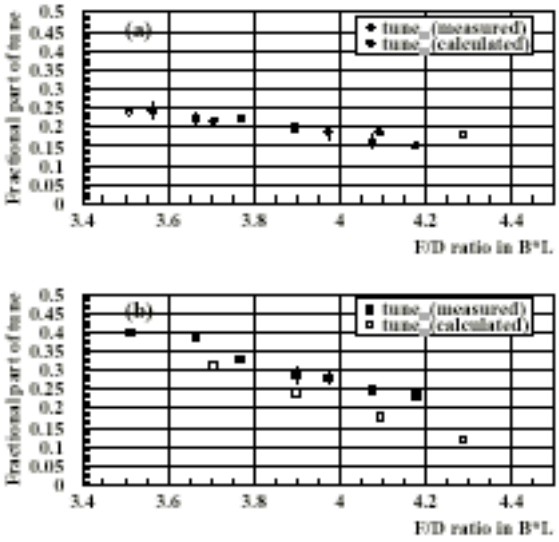

Figure 3.2.4 : Measured betatron tunes as a function of F/D ratio.

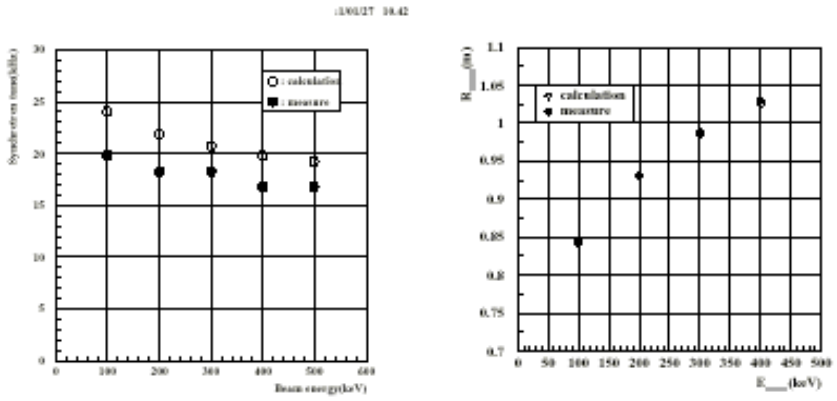

Figure.3.2.5a,b : Measured synchrotron tunes vs. beam energy and measured beam position vs. beam energy.

3.2.3.2 *150-MeV FFAG proton accelerator*

After the success of the POP FFAG commissioning, a new proposal to construct a larger size FFAG accelerator was approved in Japanese fiscal year (JFY) 2000. In this project, a FFAG synchrotron to accelerate protons up to 150 MeV will be constructed. The main parameters are summarized in Table 3.2.1. The schematic view of this 150-MeV FFAG accelerator is shown in Figure 3.2.6. Compared to POP FFAG, 150-MeV FFAG has three new features for R&D works: (1) yoke-free magnets, (2) beam extraction from the FFAG ring, and (3) high repetition operation. The yoke-free type of magnet is one of the key issues also for the future FFAG-based neutrino factory. This type of magnet allows an easy access of injection and extraction of the beams and also

gives a large flexibility for possible configuration of the beam apparatus. Thus, the demonstration of

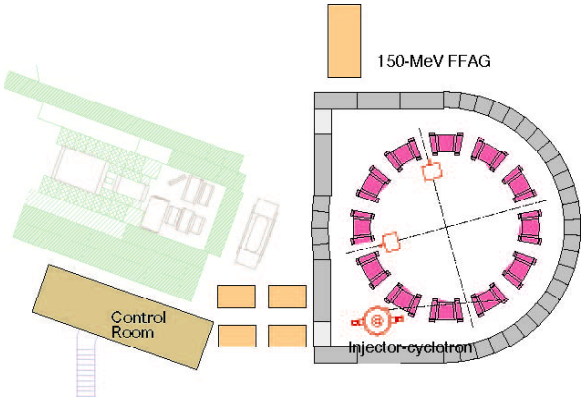

Figure 3.2.6 : Schematic view of the 150MeV FFAG

yoke-free type of magnet is useful. As the second item, it is now being considered to employ the following scheme. The beam in the FFAG ring is bend by a kicker magnet installed in the middle of the straight section. A typical field strength for 150-MeV FFAG is about 600 gauss.

Table 3.2.1:150MeV FFAG main parameters

No. of sectors	12
Field index(k -value)	7.5
Energy	12MeV - 150MeV
Repetition rate	250kHz
Max. Magnetic field	
Focus-mag.:	1.63 Tesla
Defocus-mag.:	0.13 Tesla
Closed orbit radius	4.4m -5.3m
Betatron tune	
Horizontal :	3.8
Vertical :	2.2
rf frequency	1.5 -4.6MHz

A decay time of the magnetic field is less than 150 ns. In the next straight section, a DC septum magnet is installed to give further horizontal kick to the beam. The required field strength is about 2 kgauss. Finally, the beam is extracted from the ring. As the third item, The capability of high-repetition operation has been already demonstrated at POP FFAG. The beam was accelerated within 1msec. In 150-MeV FFAG, repetition rate of 250 Hz is planned. A fast kicker with high repetition rate using IGBT switching device is under development. It is hoped that beam commissioning of the 150-MeV FFAG will start at the beginning of JFY 2002.

3.2.4 Summary

Recent progress on FFAG accelerators, which are development at KEK, is summarized. A proton accelerating FFAG model (POP-FFAG) has been developed at KEK and the beam was successfully accelerated in June of 2000. The FFAG accelerator has large potentials. Among them, short-lived particles such as muons can be accelerated with FFAG accelerators. The neutrino factory based on muon accelerator and muon storage ring has also been proposed.

Acknowledgment
The author would like to express his sincere appreciation to all the members of the FFAG project group at KEK.

References

[1] T.Ohkawa; Proc. of annual meeting of JPS (1953).
[2] K.R.Symon et al.;Phys. Rev. 103 (1956) 1837.
[3] A.A.Kolomensky et al.;ZhETF 33,298(1957).
[4] R.L.Kustom et al.;IEEE,NS-32,2672(1985).
[5] Y. Mori, Proc. of EPAC98, Stockholm, 1998, page 299.
[6] Y.Mori, Proc. of Thorium Fuel Cycle, Genshikaku Kenkyu, 43(1999)27.
[7] Y.Sato etal; Proc. of EPAC00, 2000, Wien.
[8] R.Palmer, D. Neuffer :1996, BNL-52503, FNAL Lab-conf.-96/092, LBNL-38946.
[9] N.Holtkamp : Neutrino Factory Design Report, 2000, FNAL.
[10] Nufact J Working Group ; “A Feasibility Study of A Neutrino Factory in Japan”, 2001, KEK.

3.3 FFAGs for Muon Acceleration

Scott Berg, BNL

jsberg@bnl.gov

Muons present unique challenges for acceleration. First of all, muons decay: this means that any acceleration must be rapid. A practical minimum is around 1 MV/m. This rules out traditional synchrotron designs, which contain a relatively small amount of RF per turn. One could have more RF per turn in a synchrotron, but then one runs into the challenge of ramping the magnetic fields sufficiently rapidly [1]. One could accelerate very rapidly in a linac, but that becomes very expensive: one would like to pass through the accelerating structures many times to reduce RF costs.

To be able to pass through the same linac many times without having to ramp magnets, previous studies have used a multiple-arc recirculating accelerator [2—3]. These too have their challenges. One must design a switchyard that puts the beam into a different arc corresponding to the beam’s energy on that pass. The number of passes through the switchyard is limited by the fact that the highest energy in the beam from one pass must not exceed the lowest energy in the beam at the next pass. With the

relatively large energy spreads in our beam, this is a nontrivial restriction. The finite transverse beam size and the necessity of extra space for the magnet coils, cryostats, and other hardware makes this even more restrictive. Furthermore, one has some emittance growth at each matching section from a linac to an arc. Finally, at some point the system cost begins to increase as one makes more turns, because the cost of additional arcs exceeds the cost reduction due to the reduced RF requirement.

An FFAG (**F**ixed **F**ield **A**lternating **G**radient) accelerator is one way to try to address some of these concerns. The idea behind an FFAG is to create a strong-focusing arc lattice with an extremely large energy acceptance (a factor of 2 to 3 in this article). If one can accomplish this, then one avoids the difficulties of the multiple-arc recirculating accelerator. There is no need for a switchyard, so energy overlap from one turn to the next is irrelevant. The matching problem can be avoided if the RF is distributed around the ring, and thus the beam sees an adiabatically changing lattice. Reducing the RF by going to more turns does not require than an additional arc be built. One can therefore hope that an FFAG can provide a cost-effective alternative for accelerating muons.

This article describes the current understanding of how FFAGs can be used for muon acceleration. It presents the work of many individuals and groups which will be listed in the references. In particular, there was recently a workshop on FFAGs for Muon Acceleration at Berkeley, from October 28 through November 8, 2002 (see http://www.cap.bnl.gov/mumu/conf/ffag-021028/), where much progress was made in this area. This article will focus on acceleration to 20 GeV, which was the primary focus of the workshop. Many of the considerations are the same for higher or lower energies, but the dominant problems often change as the energy regime changes.

3.3.1 Technical Constraints

The design of an arc that transports a factor of 2 or 3 in energy is a challenge. First one must deal with the issue of avoiding linear resonances over the entire energy range. One is making relatively few passes through the ring (typically 20 or fewer), so having a tune for the entire ring near a half integer or an integer is not of great concern, since such resonances are generally weak over that time scale. However, one must be concerned with linear resonances over the scale of a single cell, which will lead to catastrophic beam loss. There are three ways that are used to avoid linear resonances over such a large energy range:

Make a “scaling FFAG,” which has a constant tune over its entire energy range [4]. This is what people have historically referred to as an FFAG.

Keep the tune for a single cell below a half integer at the lowest energy, and the tune will then decrease as the energy increases [5].

Add sextupoles to set the chromaticity to zero in both planes, minimizing the tune variation over the energy range [6].

Once this basic constraint for transverse dynamics has been satisfied, one considers longitudinal dynamics. A lattice with such a large energy range naturally has a time-of-flight that varies significantly with energy over that energy range. While it is possible to vary the RF frequency as the beam energy increases so as to match the time-of-flight variation, this requires a great deal of RF peak power, and is therefore generally impractical. If one does not vary the RF frequency, there is a minimum amount of RF voltage required to accelerate over a given energy range, irrespective of how many turns

over which the beam is accelerated [7]. For a given type of lattice design, this minimum voltage is proportional to the total range in the time-of-flight over the energy range of the accelerator. Thus, achieving cost reductions by reducing RF voltage requires that the time-of-flight variation over the energy range of the accelerator be kept as low as possible.

3.3.1.1 *RF Cavities*

In general, if the lattice cell is kept shorter, the time-of-flight variation will be kept lower. One of the dominant factors determining the length of the cell is the length of the straight section required for RF cavities. Some of the scenarios described here use 200 MHz cavities, where a single cell would require a length of around 1 m for the cell plus associated hardware. One could shorten this length by using higher frequency RF, but there are two likely problems with doing so. First of all, the minimum required voltage described above is proportional to the RF frequency; thus, it is likely to be more costly to use higher frequency RF, despite the reduction in cell length. Second, because the beam passes through the cavities several times, and it would be prohibitive to put power into the cavities as fast as the beam is extracting it, beam loading may become problematic at higher frequencies, since there is less energy stored in the cavity at higher frequency.

Comparing superconducting RF to normal conducting, superconducting RF appears to be must more cost effective due to its substantially reduced peak power requirement. However, there is a disadvantage to superconducting RF: there must be a substantial separation between the magnets and the RF cavities to shield the cavities from the magnetic field. Previous work has suggested a separation of around 1 m is required [3], leading to a drift length of 3 m. This will substantially increase the time-of-flight range from what it would have been if the drift were only 1 m. A preliminary study by Shlomo Caspi [8] indicated that this magnet-cavity distance could be shortened to 0.5 m. It is clear that further study of how to shield magnets from RF cavities, and in particular obtaining scaling laws for the relationship between shielding distance and magnet type, field, and aperture, is required.

One very interesting solution to this problem is to shield the cavities from the magnets only to around 0.1 T, instead of the approximately 10 mG that the above distances correspond to. One would cool the cavities down to cryogenic temperatures with the magnets off, and then power the magnets. The fields from the magnets would be excluded by the superconducting cavity surface [9]. The main disadvantage to this mode of operation is that if a cavity does quench, the cavity temperatures must be raised, all the surrounding magnets must be powered down, the cavities cooled, and then the magnets powered again; this can take a very long time, potentially having an enormous negative impact on machine availability.

3.3.2 Specific Machine Types

I will classify the machine types based on the lattice cell on which they are constructed. It turns out that the different lattice cells described here all deal with the issue of avoiding linear resonances with a different one of the methods listed above. In addition, they have various advantages and disadvantages which will be described as each lattice is described.

3.3.2.1 *Low Emittance Lattice[6]*

This lattice is based on a lattice cell that would give a low emittance for an electron ring. Both the dispersion function and the beta functions are small at the bending magnet. The primary appeal of this lattice is that both the closed orbit variation and the variation in the time-of-flight with energy are extremely small, much smaller than in other lattices presented here. The ring is also very short compared to other lattices. This should lead to an extremely inexpensive ring, due to low magnet counts, low magnet apertures, and low RF voltage requirements due to the ability to accelerate for a large number of turns.

Unfortunately, these exemplary characteristics come at a severe cost: the dynamic aperture of this lattice is unacceptably small. The lattice gets its ability to operate over a large energy range (as well as its small range in time-of-flight) through the use of strong sextupoles to control chromaticity. Those sextupoles unfortunately reduce the dynamic aperture significantly. Work is progressing on improving the dynamic aperture without significantly compromising the performance of the lattice. Some significant progress has been made, but the dynamic aperture is still far from what is needed to transport a muon beam.

3.3.2.2 *FODO Lattice [5]*

A very simple approach to designing an FFAG lattice is to simply make a FODO lattice using gradient dipoles for the two quadrupoles, with drift spaces in between them for RF cavities and other hardware. Such a lattice turns out to be very linear, and therefore has an extremely large dynamic aperture. This lattice avoids the linear resonances by keeping the cell tune well below 0.5 over the entire energy range.

Designing such an FFAG lattice cell is fairly straightforward: fix the cell length and the total bend angle per cell, allow the bend fields and gradients in the magnets to vary, and fit the tunes at the lowest energy in the range to around 0.3 and the frequency slip factor at the central energy to zero. The latter condition arises because the variation of time-of-flight with energy is well approximated by a parabola, and placing the extremum of the parabola at the central energy minimizes the total height of the parabola over the full energy range.

This procedure allows one to design lattices for given cell lengths and bend angles per cell. Several general conclusions can be made from this procedure. First, the range in the time-of-flight is proportional to the cell length, which should be obvious from scaling considerations. Thus, the RF voltage required is proportional to the cell length as well: there is a clear advantage in reducing the drift length required for the RF cavities. Second, the total range in time-of-flight (per turn) is inversely proportional to the number of cells in the ring. Thus, a tradeoff between arc costs and linac costs occurs which is similar to that which one has for a multiple-arc recirculating accelerator: arc costs increase roughly in proportion to the number of cells, RF costs are inversely proportional.

An additional conclusion that one can draw is that for a given cell length and bend angle, the RF cost is proportional to the cube of the energy gain that one desires. One power is obviously because the voltage needed for a given number of turns is proportional to the energy gain desired. The other two powers are because of the parabolic time-of-flight variation with energy. As a result, it is not clear that fewer accelerating stages is better.

In all likelihood, the above considerations apply to most any FFAG lattice (except that the RF cost goes like the square of the energy gain for the scaling FFAG lattice to be described next). The only difficulty is in finding a method for designing lattices automatically with arbitrary parameters for the purposes of optimization.

If the arc cells did not need to contain RF cavities, they could be made very short, and thus the time-of-flight variation per cell would be small. If the bend angle per cell is very small, the time-of-flight variation is also small. One could try to combine these and get the best of both worlds: make straight (or nearly straight) sections that contain drifts for the RF, and arcs which contain no drifts, forming a racetrack (or oval) shape [10]. This turns out to be a very cost-effective solution. The one challenge is matching the dispersion and beta functions from one type of cell to the other over the large energy range of the accelerator. Recent attempts at doing this by Eberhard Keil [11] seem to be meeting with a great deal of success.

3.3.2.3 *Scaling FFAG Lattice [12—13]*

The so-called "scaling FFAG" is the original type of FFAG [4]. It is the only type of FFAG that has actually been built [14—16]. The tunes and the momentum compaction of the lattice are independent of energy. The closed orbits at different energies are simply geometrically scaled from one another. To achieve this, the magnets have fields that are proportional to r^k, where r is the distance to the center of the ring. As k increases, the gradient relative to the bending field increases, reducing the required magnet apertures and the momentum compaction. Unfortunately, as k increases, the nonlinearities in the field also increase, resulting in a decrease in the dynamic aperture. Thus, one generally wants the largest k (often several hundred) that will still give an acceptable dynamic aperture. The NufactJ Working Group in Japan has done an extensive design study [13] for a neutrino factory using a sequence of FFAGs for acceleration, and much study has occurred subsequently.

Compared to the previous designs, these accelerators require relatively low frequency RF (24 MHz, as opposed to 200 MHz in the non-scaling designs). The reason is related to the path length variation with energy: first of all, since the momentum compaction is constant, the path length is a monotonic (nearly linear) function of energy, as opposed to being parabolic as in the previous ("non-scaling") designs. This tends to lead to a larger total variation in time-of-flight (for a given maximum slope the parabola has a much smaller difference between maximum and minimum). In addition, the parabolic time-of-flight variation with energy allows the bunch to cross the crest three times [7] whereas it can only cross twice with the monotonic time-of-flight variation; thus, for a given time-of-flight range, the range of motion in time of a bunch is less with the parabolic variation. To accelerate, a stationary RF bucket is created which has a very large energy width, encompassing both the minimum and maximum energy. The bunch is accelerated by undergoing half of a synchrotron oscillation in this bucket [17]. It may be possible to reduce the RF requirements by having two RF systems which create two buckets, one to accelerate from the low energy to an intermediate energy, then a second to accelerate to the final energy. There has been some preliminary success with this scheme, but more work remains to be done.

Preliminary designs for superconducting magnets for the highest energy accelerator (10—20 GeV) have been made[18]. They use a cos θ style of design (with an elliptical vacuum chamber), but the coils are distributed highly asymmetrically to give the r^k field

dependence. In addition, a trim coil has been introduced to allow the adjustment of *k* over a limited range.

3.3.3 Cost Estimation [10]

Robert Palmer has created a model for magnet and RF costs [10] and used it to estimate the cost of several FODO-based accelerators and the scaling FFAG accelerator. The results are summarized in the following table:

	Magnets (M$)	RF (M$)	Other (M$)	Total (M$)
FODO, 3 m Drift, 6-20 GeV	105	89	36	230
FODO, 1 m Drift, 6-20 GeV	45	117	19	181
FODO, Racetrack, 6-20 GeV	46	34	14	94
FODO, 3 m Drift, 10-20 GeV	19	37	17	73
Scaling, 10-20 GeV	89	89	25	203

The numbers should not be taken as absolute numbers, but should be taken relative to each other. The "Other" costs are for vacuum, diagnostics, and civil construction. These designs are not cost optimized but are optimized to have roughly the same decay (corresponding to an average accelerating gradient of around 1 MV/m).

The high cost of the FODO lattice with 3 m drifts comes from the larger magnet apertures (due to the longer cell length) and the large amount of RF needed (because the range of time-of-flights is relatively long). Shortening the drifts to 1 m decreases the costs substantially for the reasons just mentioned. The RF cost is increased since one is forced to use normal conducting RF, but the shorter cell length reduces the RF voltage requirement, so the additional cost of superconducting over normal conducting RF is partially compensated. The racetrack, as expected, gives the best of both worlds: the time-of-flight range is kept under control, allowing a small amount of RF voltage to be installed, the magnet apertures are kept reasonably small, and it is still possible to use superconducting RF. This lattice has not been analyzed completely self-consistently, so one should be careful in this comparison, but these results indicated that the racetrack design is likely to be optimal if the matching can be done properly.

Reducing the energy range from 6-20 GeV to 10-20 GeV indeed results in a substantial cost reduction for the accelerator. Note that in this example, cost reduction techniques applied to the 6-20 GeV FODO design have not even been applied, and so the optimal design will probably cost far less than this. Of course, one must add in the costs associated with making more stages, including in particular transfer lines between the accelerators, so it is not clear to what extent going to more stages will be beneficial.

Using these costs estimates, the scaling FFAG is coming out substantially more expensive. The magnets are more expensive because a substantially larger aperture is required in the defocusing quadrupoles (the non-scaling designs have a smaller orbit swing in the defocusing quadrupoles, whereas the scaling designs do not) and the ring is substantially longer (due at least partly to the smaller time-of-flight range in the non-scaling design). The RF costs are higher because of the low frequency and large voltage required, and the fact that the RF must be normal conducting.

The comparison of the scaling FFAG design to the FODO-based FFAG designs is not completely fair. The FODO-based designs have not been analyzed nearly as extensively as the scaling FFAG design. In fact, an examination of the dynamic aperture has not even been done on most of them (although based on tracking done for one of them, it is expected that their dynamic aperture will be high). The nature of the

magnets in the two designs is likely to be very different. However, this comparison does indicate where improvements in the scaling FFAG design should be made in order to lower its cost.

3.3.4 Conclusions

FFAGs appear to be an effective way of reducing the cost of accelerating muons. A great deal of research is being done to verify and improve their performance and cost. Individuals are constantly coming up with new and better ideas for how to design these systems (in particular, Carol Johnstone has proposed using triplets instead of FODO cells, and initial results indicate that this improves the time-of-flight range [19]). This work has the potential to be used for many other types of acceleration applications as well, such as high-intensity proton sources.

References

[1] Don Summers, "Accelerating muons to 2400 GeV/c with dogbones followed by interleaved fast ramping iron and fixed superconducting magnets," in *Proc. of the APS/DPF/DPB Summer Study on the Future of Particle Physics (Snowmass 2001)*, ed. N. Graf, arXiv:hep-ex/208010.
[2] N. Holtkamp and D. Finley, eds., "A Feasibility Study of a Neutrino Source Based on a Muon Storage Ring," Fermilab-Pub-00/180-E (2000).
[3] S. Ozaki, R. Palmer, M. Zisman, and J. Gallardo, eds., "Feasibility Study-II of a Muon-Based Neutrino Source, BNL-52623 (2001).
[4] K. R. Symon *et al.*, "Fixed-Field Alternating-Gradient Particle Accelerators," Phys. Rev. **103**, 1837 (1956).
[5] C. Johnstone and S. Koscielniak, "Recent progress on FFAGs for rapid acceleration," in *Proc. of the APS/DPF/DPB Summer Study on the Future of Particle Physics (Snowmass 2001)*, ed. N. Graf, SNOWMASS-2001-T508.
[6] D. Trbojevic, M. Blaskiewicz, E. D. Courant, and A. Garren, "Fixed field alternating gradient lattice design without opposite bend," in *Proceedings of EPAC 2002, Paris, France* (EPS-IGA/CERN, Geneva, 2002), p. 1199.
[7] J. S. Berg, "Dynamics in Imperfectly-Isochronous FFAG Accelerators," in *Proceedings of EPAC 2002, Paris, France* (EPS-IGA/CERN, Geneva, 2002), p. 1124.
[8] Shlomo Caspi, presentation given at the Neutrino Factory and Muon Collider Collaboration workshop on FFAG Acceleration, Berkeley, CA, Oct. 28—Nov. 8, 2002.
[9] M. Ono *et al.*, "Magnetic field effects on superconducting cavity," in *9th Workshop on RF Superconductivity 1999* (Los Alamos, NM, 2000), Los Alamos National Laboratory report LA-13782-C.
[10] Robert Palmer, presentation given at the Neutrino Factory and Muon Collider Collaboration workshop on FFAG Acceleration, Berkeley, CA, Oct. 28—Nov. 8, 2002.
[11] Eberhard Keil, unpublished note, http://keil.home.cern.ch/keil/MuMu/Doc/FFAG02/adiabatic.pdf (2002).
[12] Y. Mori, "Neutrino Factory in Japan: Based on FFAG Accelerators," in *Proceedings of EPAC 2002, Paris, France* (EPS-IGA/CERN, Geneva, 2002), p. 278.
[13] NufactJ Working Group, "A Feasibility Study of a Neutrino Factory in Japan," http://www-prism.kek.jp/nufactj/ (2001).
[14] F. T. Cole *et al.*, Rev. Sci. Instrum. **28**, 403 (1957).
[15] D. W. Kerst *et al.*, Rev. Sci. Instrum. **31**, 1076 (1960).

[16] M. Aiba *et al.*, "Development of a FFAG Proton Synchrotron," in *Proceedings of EPAC 2000, Vienna, Austria*, p. 581.
[17] T. Uesugi and C. Ohmori, presentations given at the Neutrino Factory and Muon Collider Collaboration workshop on FFAG Acceleration, Berkeley, CA, Oct. 28—Nov. 8, 2002.
[18] T. Ogitsu, presentation given at the Neutrino Factory and Muon Collider Collaboration workshop on FFAG Acceleration, Berkeley, CA, Oct. 28—Nov. 8, 2002.
[19] Shinji Machida and Carol Johnstone, work presented at the Neutrino Factory and Muon Collider Collaboration workshop on FFAG Acceleration, Berkeley, CA, Oct. 28—Nov. 8, 2002.

3.4 Ionization Cooling of Muons

Klaus Hanke, CERN

Klaus.Hanke@cern.ch

3.4.1 Introduction

Recent years have seen renewed interest in the generation of high- intensity, high-brilliance muon beams. Their application is twofold:

Muon colliders open the possibility to collide particles with a well-defined initial state (energy, polarization) and obtain a simple event topology as known of electron-positron annihilation. However, contrary to electron-positron storage rings, there is essentially no energy limitation imposed by synchrotron radiation, which makes it possible to achieve a high center-of-mass energy with a relatively compact machine.

Secondly, neutrino factories based on muon storage rings are widely considered as the ultimate tool to study neutrino oscillations and leptonic CP violation. Such a machine could be thought of as a first step towards a - in terms of muon intensity and brilliance more demanding - muon collider.

Muons for such applications can be obtained from the decay of pions, which in turn are generated by bombarding a target with a high-power (few MW) proton beam. Such a secondary beam has an enormous energy spread and transverse emittance, and most particles will be far outside the acceptance of the subsequent accelerator chain. This does not meet the specifications of a neutrino factory, which requires about 10^{21} muons per year to decay into neutrinos in a dedicated decay ring. Moreover, it is not only the number of decaying muons which determines the neutrino flux at the detector location, but also their divergence. Neutrino physicists agree on a maximum divergence of the decaying muons of $0.1/\gamma$, where γ is the relativistic factor. In order to obtain the required neutrino flux at the detector location, the muon population inside the phase space acceptance of the accelerator chain has to be increased by roughly an order of magnitude.

For the accelerator design this means that between target and muon accelerators a dedicated beam line is required to prepare the muons for acceleration. This section of the machine, frequently referred to as the "front-end", has to fulfill three main tasks:

1.) Collect the pions from the target and let them decay into muons.

2.) Reduce the energy spread of the secondary beam.

3.) Reduce the transverse phase space; future developments may open the possibility to reduce in addition the longitudinal phase space.

Various technical designs have been proposed to accomplish these tasks. For pion collection both a tapered solenoid as well as a magnetic horn have been studied. The pion decay usually takes place in a solenoid channel. The reduction of the energy spread, frequenly called "phase rotation", can be accomplished either by an induction linac or by a series of rf cavities. This article will focus on the third item, the reduction of the phase space or cooling.

3.4.2 Cooling Theory

Different techniques have been used in the past to reduce the transverse phase space of particle beams. They apply all to beams stored in circular accelerators, such as electron cooling of ions or protons, synchrotron radiation damping of electrons and positrons, stochastic cooling of protons and antiprotons and laser cooling of ions [1]. The short lifetime of muons does not allow long storage in a ring to manipulate the phase space. Instead, a technique is required to reduce the phase space in a single pass through a linear channel, respectively in a very few turns in a circular device. As a possible solution, ionization cooling has been proposed by Skrinksky and Parkhomchuk in the early eighties [2]. This technique works as follows: particles are passed through a material, in which they loose momentum in all three planes according to the Bethe-Bloch formalism. Only the longitudinal momentum is then restored by subsequent rf cavities. The net effect of this procedure is a reduction of the transverse momenta, or transverse cooling. However, multiple scattering in the material counteracts the emittance reduction and hence leads to a finite minimum emittance which can be achieved by ionization cooling, the equilibrium emittance.

Ionization cooling is hence a balance between multiple scattering and energy loss in the absorber material. The two counteracting terms can be nicely identified in the equation for the reduction of the normalized emittance inside the absorber material,

$$\frac{d\varepsilon_{\perp,N}}{dz} = -\frac{\varepsilon_{\perp,N}}{\beta^2 E}\frac{dE}{dz} + \frac{\beta_\perp (13.6MeV/c)^2}{2\beta^3 E\, m_\mu L_{rad}}, \qquad (1)$$

where $\varepsilon_{\perp,N}$ is the normalized transverse emittance, β is the relativistic factor, $\beta_\perp$ is the transverse beta function at the absorber, E is the kinetic energy of the muons, m_μ the muon mass and L_{rad} the radiation length. The first term represents the cooling according to Bethe-Bloch. The second term stems from the Moliere equation for multiple scattering. Equation (1) is derived in detail in [3].

The energy dependence of the Bethe-Bloch term has important consequences for the choice of the muon energy in a cooling channel. As can be seen from Figure 3.4.1, for muons of a kinetic energy larger than 200 MeV ($\beta\gamma = 2.7$), the dE/dx function is relatively flat and hence the energy loss is comparable for all particles in a bunch with large energy spread. This is one of the reasons why an energy band around 200 to 300 MeV (kinetic) is typically considered in cooling channel designs. For lower energy, the strong energy dependence and the negative slope of the dE/dx term would result an increased energy spread.

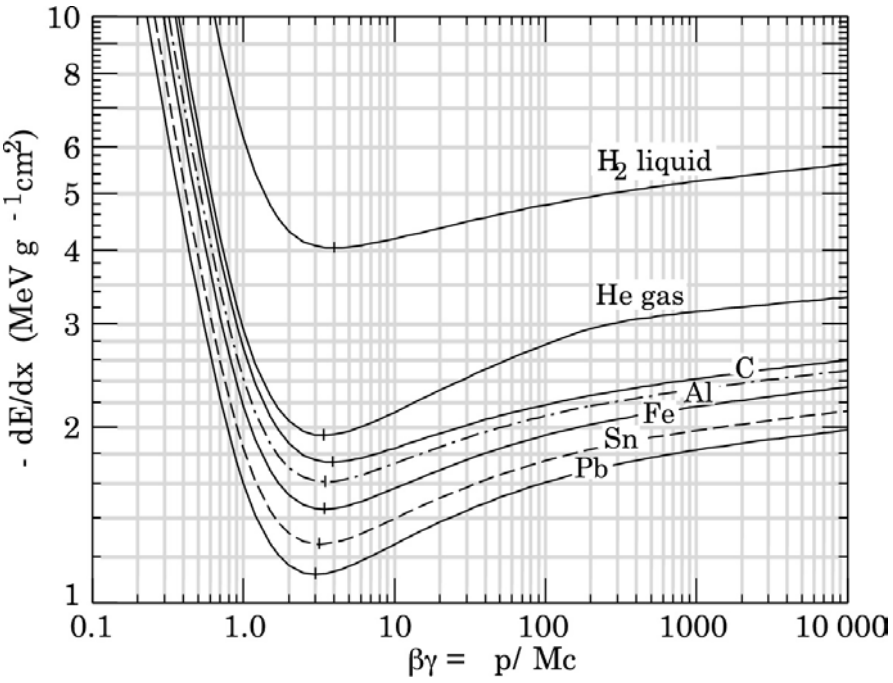

Figure 3.4.1 : Energy loss versus particle energy for various absorber materials.

Another argument to choose exactly this energy interval is given by the muon population versus kinetic energy at the exit of the pion decay channel, shown in Figure 3.4.2 for the example of a study carried out at CERN. In the energy band around 200-300 MeV, the muon population is reasonably high, while at the same time the relativistic b is not too small and hence debunching due to velocity differences within a bunch is not an issue.

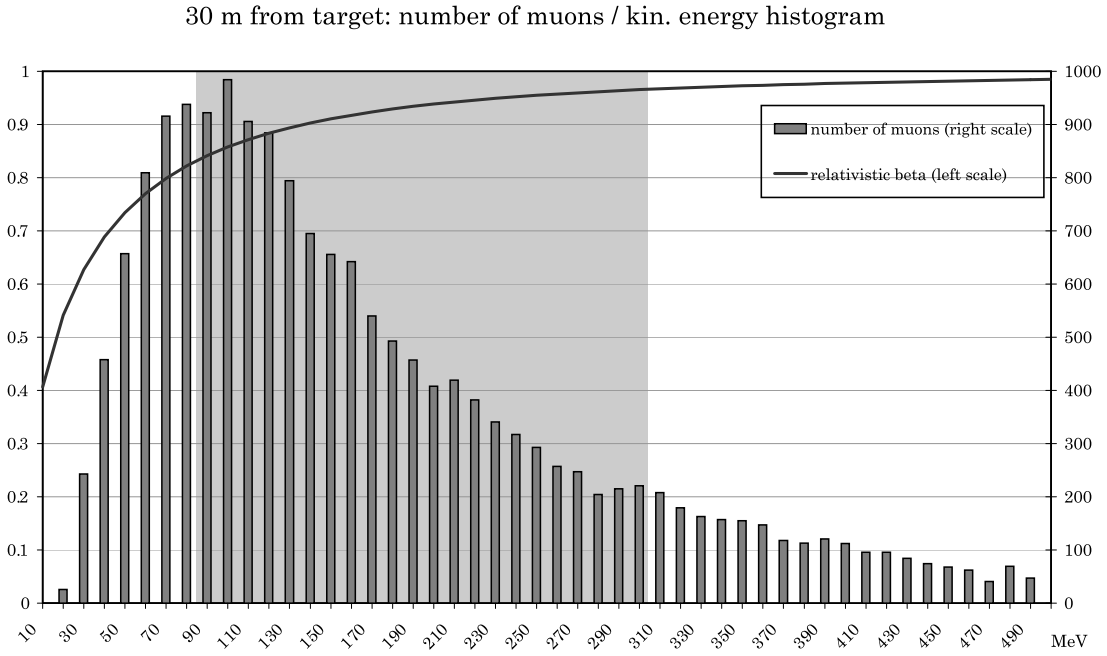

Figure 3.4.2 : Muon energy histogram at the end of decay channel and corresponding relativistic beta for the example of the CERN study. The energy acceptance of the cooling channel has been lined out grey. The energy range between 100 and 300 MeV has been chosen as a compromise between high muon densities and little debunching due to differences in the relativistic beta.

3.4.3 Linear Cooling Channels

The straightforward technical application of the ionization cooling principle leads to a linear cooling channel, where tanks filled with absorber material alternate with re-accelerating rf cavities. Focusing of the muon beam is in general accomplished by solenoids as they focus equally in both planes and have a larger acceptance than quadrupoles. As can be seen from equation (1), the heating term is proportional to $\beta_\perp$ and inversely proportional to L_{rad}. Consequently, the absorbers should be placed in low-β regions and he absorber material should have a high radiation length in order to optimize cooling.

Starting from an early proposal by Palmer, Johnson and Keil [4], three major design studies have been completed by the international community, which has organized itself in the Muon Collider and Neutrino Factory Collaboration. They differ mainly in rf frequency and magnetic lattice. The – historically speaking – first complete design, which covers all aspects of a neutrino factory complex, was led by Holtkamp and Finley at Fermilab [5]. It features a linear cooling channel based on 200 MHz rf. The cavities are pillbox cavities closed by Berillium windows to increase the accelerating gradient. Liquid hydrogen (LH2) absorbers are placed between every pair of two cavity cells. The baseline lattice is a so-called FOFO lattice, characterized by a periodic sinusoidal magnetic field with a maximum amplitude of 3.4 T. The solenoids are placed around the cavities, one coil per cavity cell. As a further evolution of the

simple FOFO lattice, a Single-Flip lattice has been proposed. Here, the absorber is housed inside a long solenoid, which provides continuous focusing and hence there is no change of the beam size. At the middle of the lattice, the solenoid field is reversed. A dedicated matching section links the two sections. The concept of this field-flip is illustrated in Figure 3.4.3.

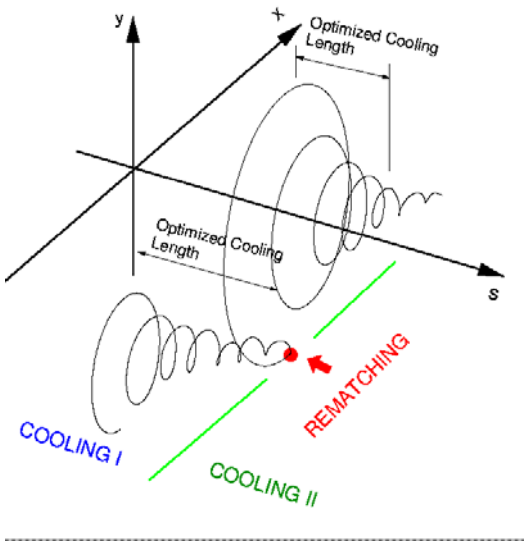

Figure 3.4.3 : The concept of field flip.

A particle traveling through the first absorber looses constantly transverse momentum and hence the amplitude of the helix decreases. However, the Larmor center of the helix remains unchanged, and hence the beam size does not decrease. In the matching section, the Larmor center is displaced such that in absorber two it coincides with the solenoid axis. The helical movement, now in opposite sense and again with large amplitude, is again damped while now both momentum and beam size decrease.

The concepts developed in this first cooling channel design were the basis for the next iteration of a neutrino factory feasibility study [6]. It features also a linear cooling channel based on 200 MHz rf and liquid hydrogen absorbers. The main difference is found in the lattice, now called super–FOFO or SFOFO. Rather than modulating the magnetic field sinusoidally, a second harmonic is added resulting in a field on axis as shown in Figure 3.4.4: the axial field vanishes at the location of the absorbers, where the beta function has its minimum. However, unlike in the simple FOFO optics, the field does not go sinusoidally but is flattened by coupling coils, which are placed around the center of the cavities. Figure 3.4.5 shows the corresponding engineering drawing of a section of the SFOFO cooling channel. The arrangement of the focusing coils around the absorbers and the coupling coils around the cavities can clearly be seen.

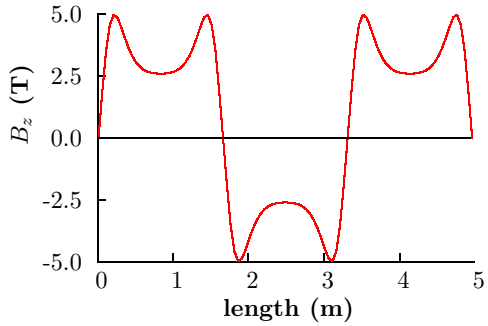

Figure 3.4.4 : Bz along z for three lattice cells of the SFOFO lattice.

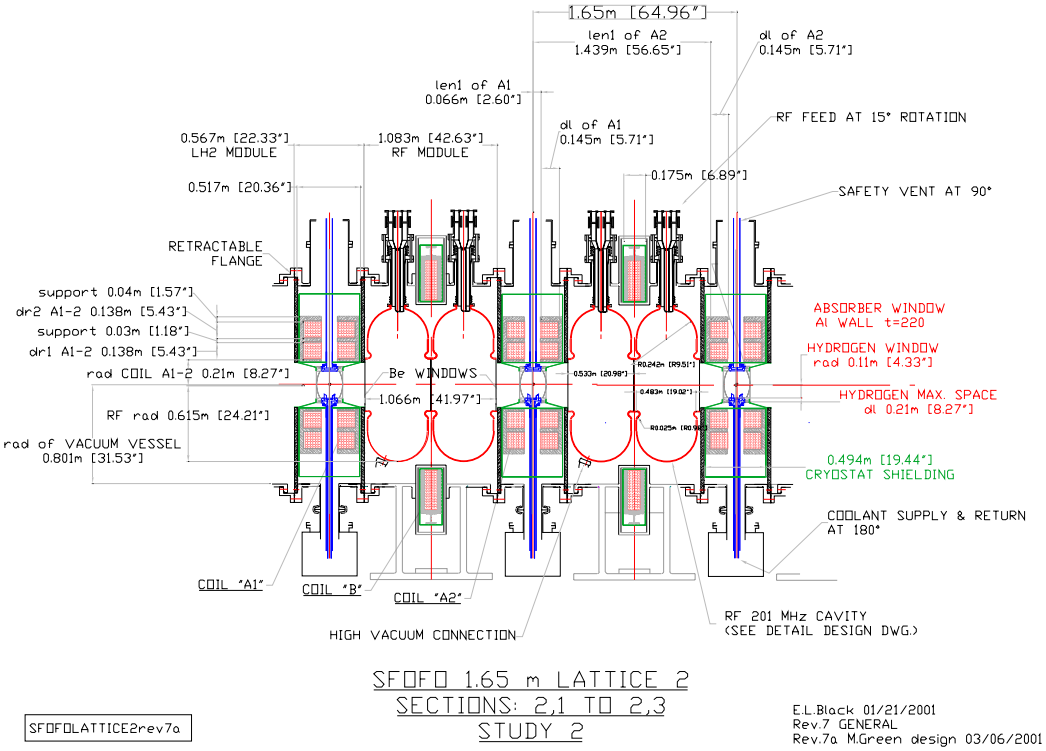

Figure 3.4.5 : Engineering drawing for a SFOFO lattice cell.

The main advantages of the SFOFO lattice over the simpler, sinusoidal FOFO lattice are stable transverse motion within the momentum range of interest, a longer period length allowing for longer absorbers – and hence fewer absorber windows – per lattice cell and focusing coils of relatively small diameter, as they are placed around the absorbers and not around the whole cavity. The latter fact results in significant cost savings. It is worth noting that the SFOFO cooling channel described in [6] comprises lattice cells as shown in Figure 3.4.5 with a length of 1.65 m as well as another type of lattice cell, used in the first part of the channel, which comprises two 4-cell cavities

with analogous coil arrangement and has a length of 2.75 m. The complete channel consists of a first section with 2.75 m lattice cells and a second one with 1.65 m lattice cells, as well as a matching section between them.

The cooling performance can be measured in two different ways. The transverse emittance decreases from 12 π mm rad (normalized) to 2 π mm rad along the channel, but particle loss makes the interpretation of this result difficult. It is more obvious to count the number of muons inside the acceptance of the subsequent accelerator. For the SFOFO channel reported in [6], the number of muons inside the acceptance considered is increased by a factor of three.

A technically very different design for a muon cooling channel has been studied CERN [7]. The cooling channel in this scenario is based on cavities with a much lower frequency of originally 44 and 88 MHz [8], in a later evolution only 88 MHz [9]. This has important consequences for the lattice, as in the case of these big cavities the focusing solenoids can be placed around the bore of the cavity (Figure 3.4.6).

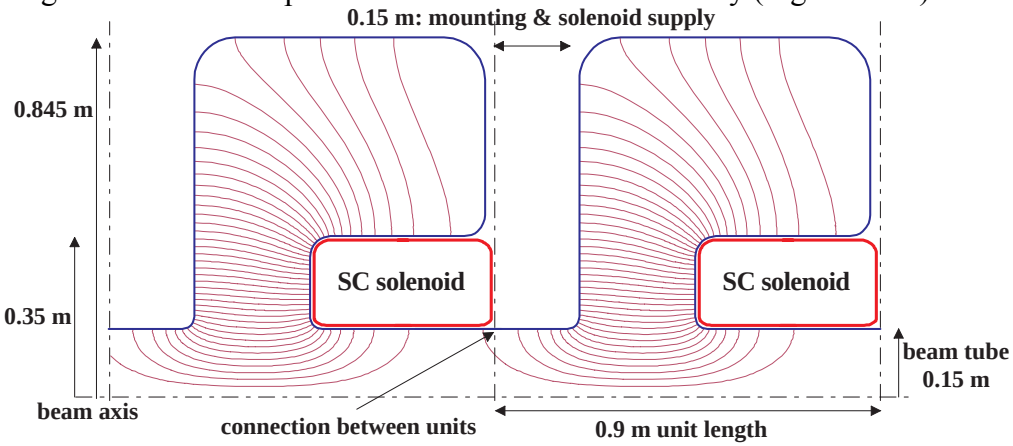

Figure 3.4.6 : 88 MHz cavities with integrated focusing solenoids as used in the CERN cooling channel.

The resulting lattice is completely periodic and the coupling between the transverse and longitudinal planes minimized. The low frequency results in a large longitudinal acceptance. However, the accelerating gradient, which determines the cooling efficiency per unit length of the channel, drops down with frequency. For an 88 MHz cavity without windows, 4 MV/m are assumed but remain experimentally to be verified. Other than the FOFO and SFOFO lattices, the CERN cooling channel has no beam waists at the absorber location but features an almost constant beta function along the channel.

The cooling efficiency of the CERN cooling channel is best characterized by counting the number of muons inside the acceptance of the subsequent accelerator (in the CERN scenario 1.5 cm rad normalized transverse, 0.1 eVs longitudinal). Directly after the target, about 5×10^{19} muons per year are found within this acceptance cut. This number is increased in the cooling channel by a factor of 20 in order to achieve the required number of 10^{21} muons per year in the decay ring. Figure 3.4.7 shows the horizontal phase space population at the entry and exit plane of the cooling channel.

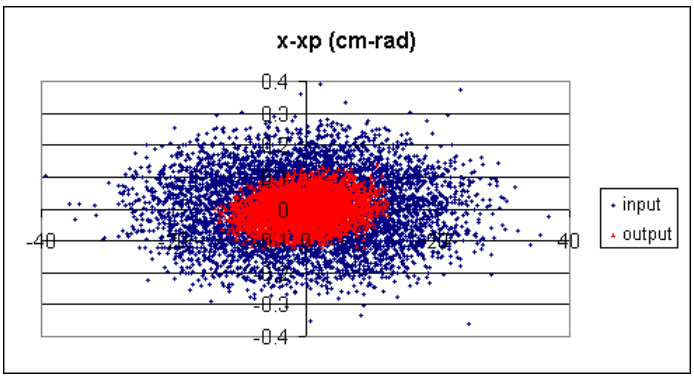

Figure 3.4.7 : Horizontal phase space population at the entry and exit of the CERN cooling channel. The number of muons inside the acceptance of the subsequent accelerator is increased by a factor 20.

3.4.4 Longitudinal Cooling

We will finally address the question how the cooling efficiency can be increased beyond the performance of the presently designed linear cooling channels and eventually come in the range of interest for a muon collider. In the schemes for transverse, or 4D, cooling discussed in the previous sections, the longitudinal emittance remains at best unchanged, but will in general slightly increase. The obvious way to increase the cooling efficiency is to perform in addition to the transverse cooling longitudinal, i.e. 6D cooling. The way to accomplish this is known as emittance exchange. The beam is, after having been transversely cooled by the previously described principle, passed through a bending where dispersion is generated. Due to its energy spread, the beam will transversely become larger. In other words, longitudinal emittance has been transformed into transverse emittance. The transverse emittance is then again reduced by ionization cooling. The absorbers are in this case not symmetric, but have a wedge shape (wedge absorbers) which ensures that high-energy particles loose more energy than low-energy particles. Figure 3.4.8 illustrates the principle of emittance exchange.

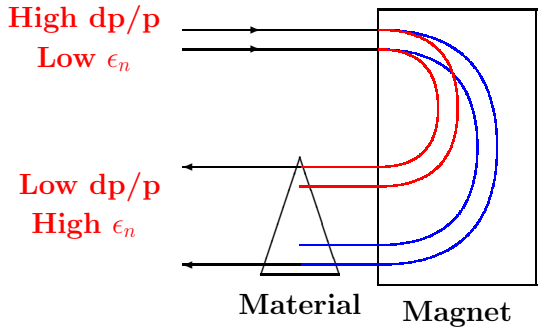

Figure 3.4.8 : Principle of emittance exchange (from [10]).

Practically speaking, the concept of emittance exchange can be accomplished in a variety of ways. Early proposals have included either dipoles or bent solenoids in the linear cooling channels. They were based either on wedge absorbers in bent solenoids or in helical channels [11]. However, the cooling efficiency of these systems was relatively

poor. The logical continuation of this thought leads to a circular machine (ring cooler), which comprises bending magnets, wedge absorbers, focusing and accelerating rf. A design by Balbekov [12], based on alternating cooling and emittance exchange, showed for the first time in a simulation cooling in all six dimensions. However, there were practical problems left with this design: there was no space forseen for injection and ejection kickers, and including them would disturb the lattice so much that the cooling efficiency dropped down. The cooling efficiency was increased with respect to a linear channel, but still out of range of what is required for a muon collider. Finally, rings with combined cooling and emittance exchange were considered. Garren et al [13] designed a ring with quadrupole focusing, and more recently Palmer et al presented a ring design with very good cooling performance [14]. The design uses solenoid focusing, and cools longitudinal and transverse emittance in the same cell. Figure 3.4.9 shows the lay-out of the ring. Injection and extraction into this ring is accomplished by dedicated kicker magnets, which are technically challenging. Further technical issues are the rf windows, which have to be very thin, as well as the design of the wedge absorbers. This ring shows for the first time a cooling efficiency interesting for the muon collider. At present, three of these rings would provide the cooling efficiency required by a muon collider, but this would require a complete re-design of the front end. Work is under way to better understand and improve ring coolers, which may eventually open the road towards a muon collider.

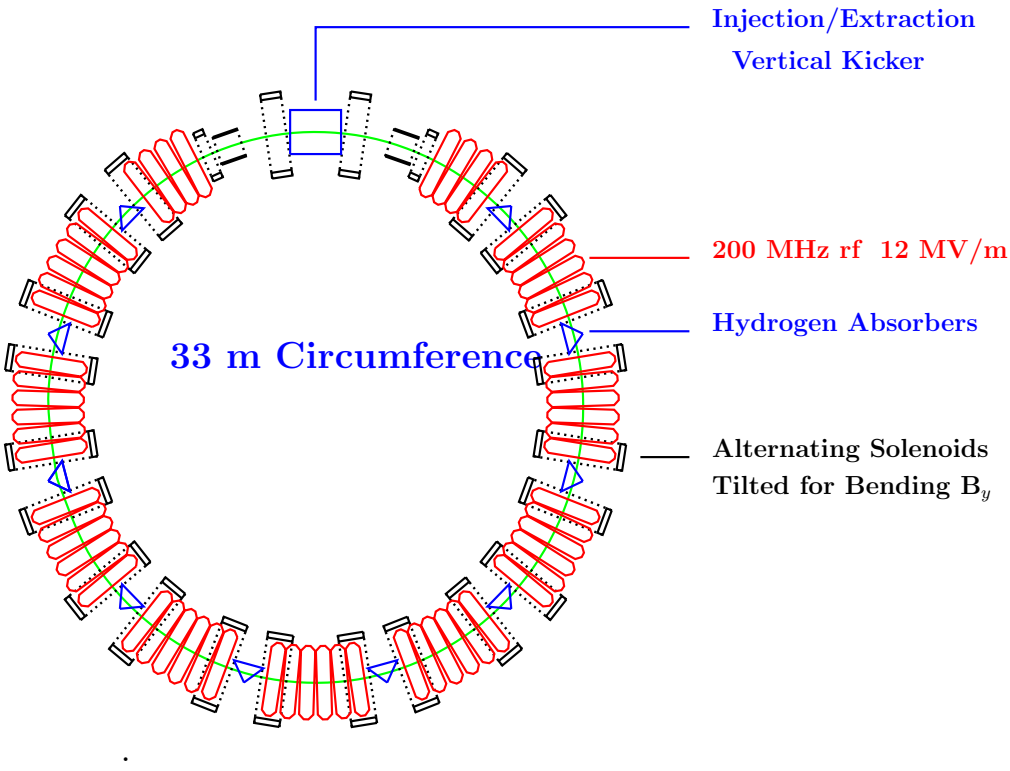

Figure 3.4.9 : RFOFO ring cooler design (from [10]).

References

[1] D.Möhl, Beam Cooling: Past, Present and Future, conf. proc. Workshop on Beam Cooling and Related Topics, Bad Honnef, May 13-18, 2001 and CERN PS 2001-021(AE).

[2] A.N.Skrinsky, V.V.Parkhomchuk, Sov. J. of Nuclear Physics, 12,3 (1981).
[3] K.T.McDonald, Comments on Ionization Cooling, Princeton/mm/98-17 (1998).
[4] R.B.Palmer, C.Johnson, E.Keil, A Cost-Effective Design for a Neutrino Factory, BNL-66971, CERN SL/99-070 AP and CERN Neutrino Factory Note 09 (1999).
[5] N.Holtkamp, D.Finley (ed.), A Feasibility Study of a Neutrino Source Based on a Muon Storage Ring, Nucl. Instr. Meth. A472, p. 388-394, (2000).
[6] S.Ozaki, R.B.Palmer, M.S.Zisman, J.Gallardo (ed.), Feasibility Study-II of a Muon-Based Neutrino Source, BNL-52623 (2001).
[7] P.Gruber (ed.), The Study of a European Neutrino Factory Complex, CERN-PS 2002-080 (PP) (2002).
[8] A.Lombardi, A 40-80 MHz Scheme for Phase Rotation and Cooling, CERN Neutrino Factory Note 37 (2000).
[9] G.Franchetti et al, Muon Phase Rotation and Cooling: Simulation Work at CERN, conf. proc. Nufact02, London, and CERN Neutrino Factory Note 119 / CERN PS Note 2002-076 (PP) (2002).
[10] R.Palmer, Ring Coolers, conf.proc. Nufact02, London, 2002.
[11] MUCOOL Notes MUC-147, MUC-148, MUC-187, MUC-189.
[12] MUCOOL Notes MUC-232, MUC-246.
[13] A.Garren et al, Snowmass 2001.
[14] R.Palmer et al, Mucool Note MUC-239.

3.5 The MICE Experiment

Rob Edgecock, RAL

R.Edgecock@rl.ac.uk

3.5.1 Introduction

The ability to cool the muons is one of the most important requirements for a Neutrino Factory, otherwise the efficiency of capture in the first muon accelerator is very poor. All existing accelerator cooling techniques either do not work for muons or simply take too long. As a result, a new technique has been derived, ionization cooling [1]. In this the muons are passed through an absorber in which they lose both longitudinal and transverse momentum via ionization energy loss. The lost longitudinal momentum is then restored using radio-frequency cavities following the absorber, giving a net reduction in transverse momentum and transverse cooling. In practice, as shown in Figure 3.5.1, the cooling is applied in a series of cooling cells, each consisting of a thickness of absorber and enough RF-voltage to restore the energy lost in the absorber.

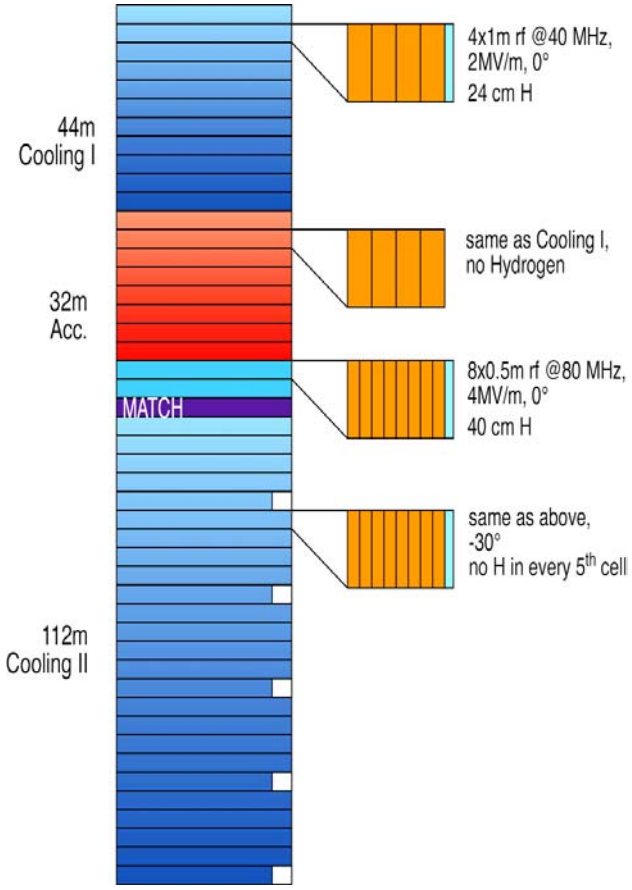

Figure 3.5.1 : Layout of the CERN 44/88MHz cooling channel showing a number of the cooling cells in detail.

However, as well as cooling coming from the energy loss, there is also heating coming from multiple scattering of the muons. The net cooling is a delicate balance between these contributions, the change in normalized transverse emittance $\varepsilon_{\perp,N}$ as a function of position z being given by

$$\frac{d\varepsilon_{\perp,N}}{dz} = -\frac{\varepsilon_N}{\beta^2 E}\frac{dE}{dz} + \frac{\beta_\perp (13.6MeV/c)^2}{2\beta^3 E m_\mu L_R}$$

where β and E are the muon's velocity and energy, respectively, $\beta_\perp$ is the beam betatron function and L_R is the radiation length of the absorber. To keep the second, heating term as small as possible requires a small $\beta_\perp$ and a large L_R. The former requires a highly divergent beam, created using super-conducting magnets, while for the latter the best compromise between energy loss and radiation length is liquid hydrogen. The resulting cooling cell is a complex structure, as shown in Figure 3.5.2.

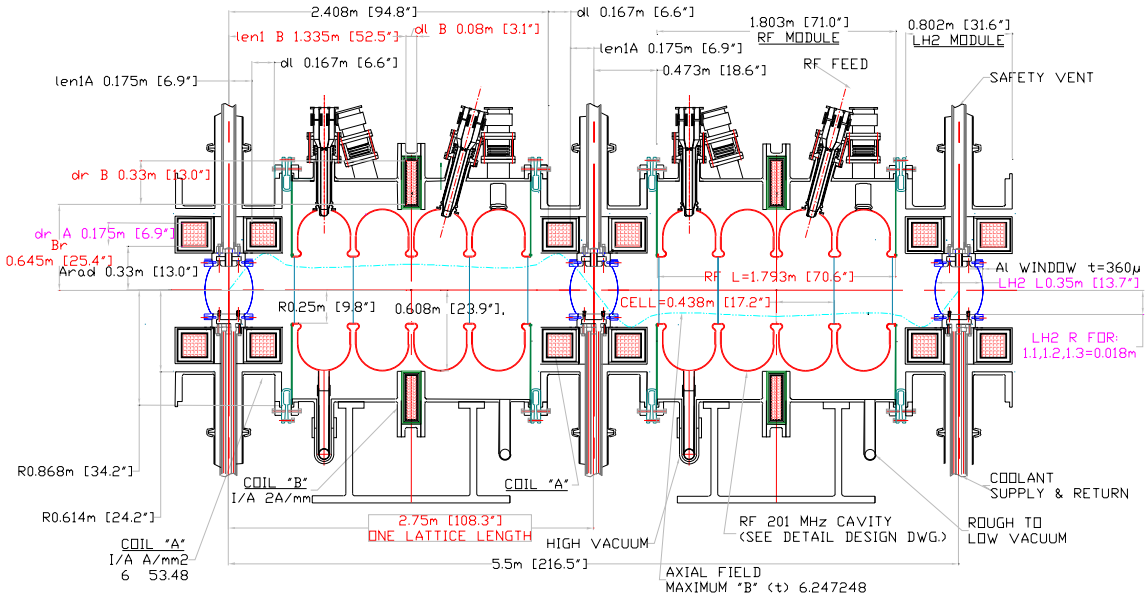

Figure 3.5.2 : Two SFOFO cooling cells from US Study2 [2].

Due to the complexity of the cooling cell and the fact that ionization cooling is not been demonstrated experimentally, a series of R&D projects are required to show that a cell can be built and will cool. The MuScat experiment [3] is measuring the multiple scattering distribution of muons in the correct momentum range and the MuCool project [1] is showing that a cooling cell can be built and the components will work together. The MICE experiment will show that it will cool and will investigate the cooling process in detail.

3.5.2 The MICE Experiment

The experiment is shown conceptually in Figure 3.5.3. The components are described in more detail below, but basically it consists of the two SFOFO cooling cells shown in Figure 3.5.2 surrounded by instrumentation to measure the parameters of muons entering and leaving the cells. The current plan is use muons with a range of momenta around 200MeV/c and produce a 6D emittance reduction of around 10%. This corresponds to an energy loss of about 12 MeV and would require a thickness of about 45cm of liquid hydrogen and enough RF voltage to restore the lost energy in the cooling cell. In addition, the instrumentation sections of the experiment must be able to make a significant measurement of this emittance reduction and hence have a total resolution, statistical plus systematic, of 1% or less.

The MICE collaboration consists of more than 100 physicists and engineers from 44 institutes in Europe, the US and Japan. It is currently preparing a proposal to be submitted to the Rutherford Appleton Laboratory for the experiment to take place there.

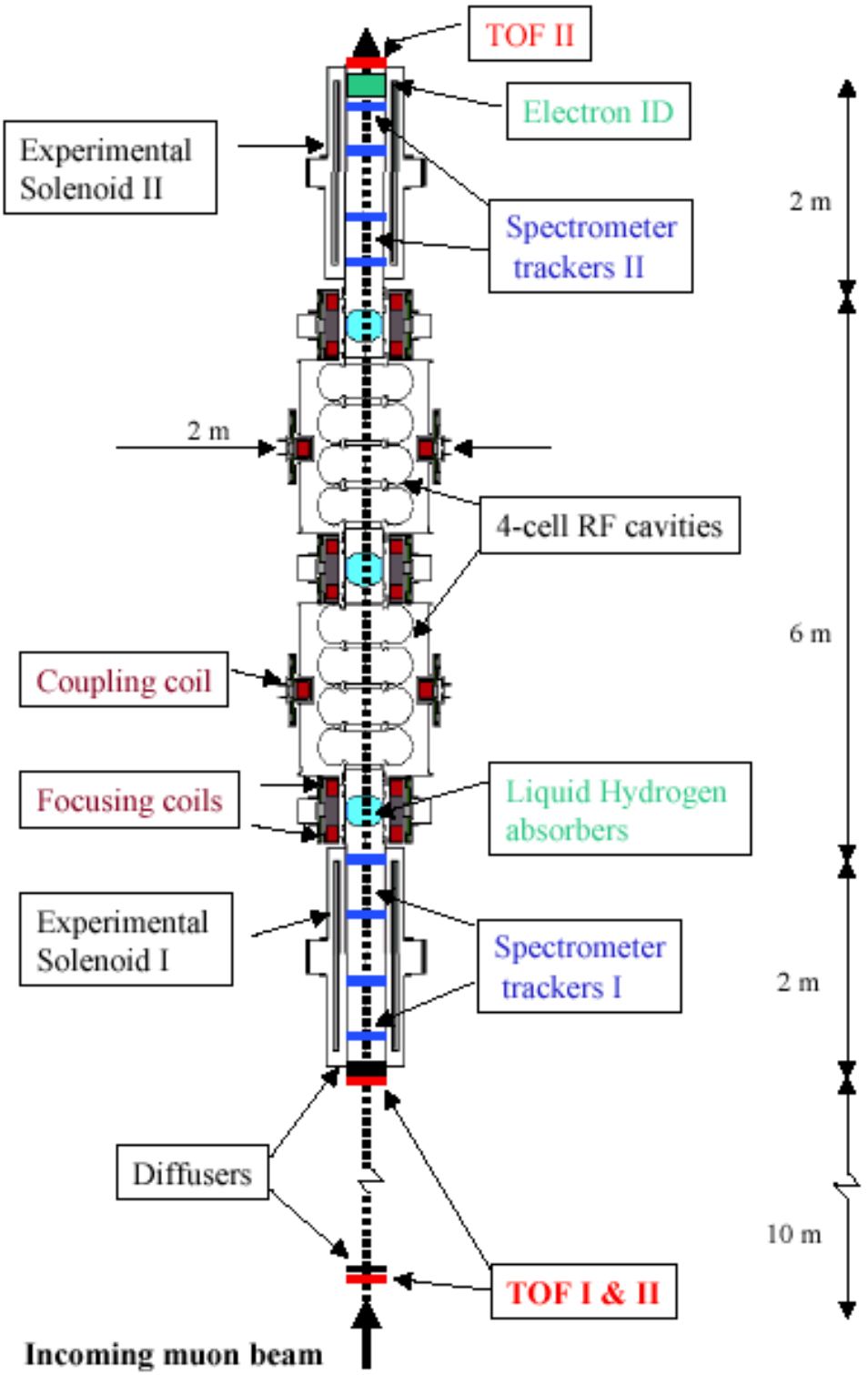

Figure 3.5.3 : The schematic layout of the MICE Experment.

3.5.2.1 *Muon beam*

It is not possible to measure the emittance of the muons for MICE with the required precision using collective emittance measurement techniques as the best such measurement precision is about 10%. As a result, MICE will use a single particle beam, with no more than one muon passing through the detector every 10ns or so. This will allow all the required parameters of each muon to be determined.

To supply the muon beam for MICE, an existing beam line at RAL, the HEP test beam, is being modified to provide a clean beam with the required intensity. Two main changes are planned: (1) a new target and pion capture mechanism to increase the flux of muons and (2) a super-conducting decay solenoid to allow the rejection of most of the proton, pion and positron backgrounds to the muons. In addition, much new infrastructure is being added to the experimental hall to satisfy the requirements of MICE. The new beam line and the layout of MICE in the hall are shown in Figure 3.5.4.

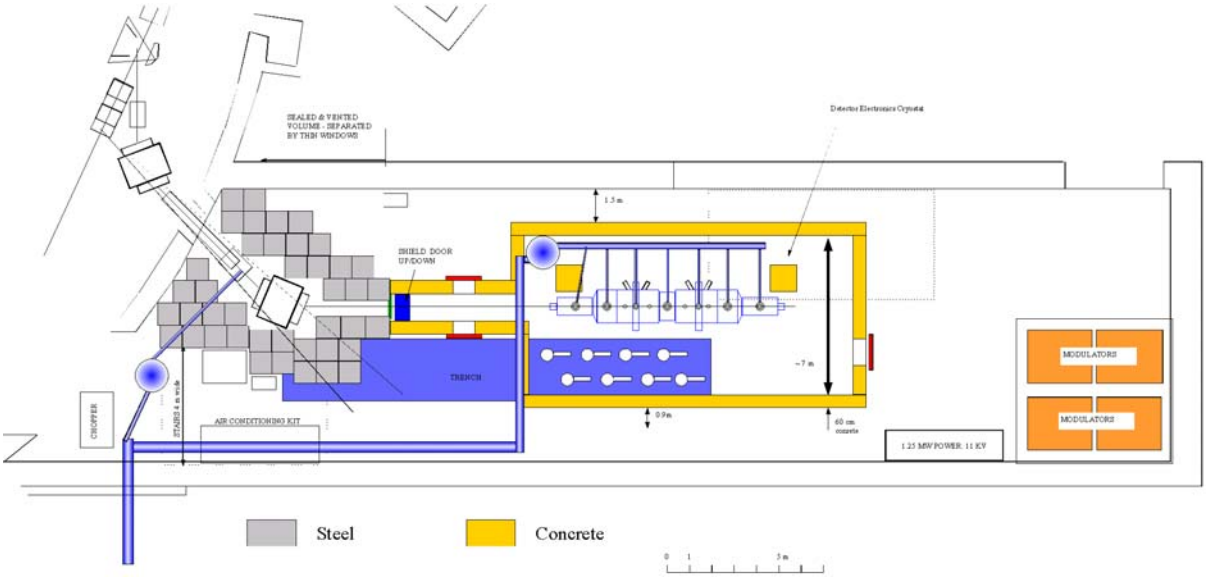

Figure 3.5.4 : Layout of the new muon beam and MICE in the HEP test beam at RAL.

3.5.2.2 *Instrumentation*

MICE needs to measure the 6D parameters of each of all the particles passing through it and eliminate any backgrounds to the level of 0.1% or less. It thus has two types of instrumentation: one for measuring the particle parameters and the second for identifying the type of particle.

Five of the particle parameters are measured using tracking detectors placed inside super-conducting solenoids placed on either side the cooling cells. There are two candidates for these detectors: scintillating fibre chambers or Time Projection chambers using GEMs (TPGs), with the former being the current baseline. The final design of

both these detectors will be strongly affected by an important source of background: dark current and X-rays from the RF-cavities. As the level of these will not be known until a real cavity is built, the current designs assume a pessimistic background rate.

The scintillating fibre tracker (FT) will consist of four or five detectors in each spectrometer section, each detector incorporating three double planes of offset fibres at 120 degrees to each other, as shown in Figure 3.5.5. This will give one space point per detector, with a very high and uniform efficiency. It is planned to read the fibres out using Visible Light Photon Counters [4]. These are avalanche photo-diodes with a very small band gap, so they have an excellent quantum efficiency. However, due to this small band gap they have to be run at cryogenic temperatures, ~9K, to reduce the noise.

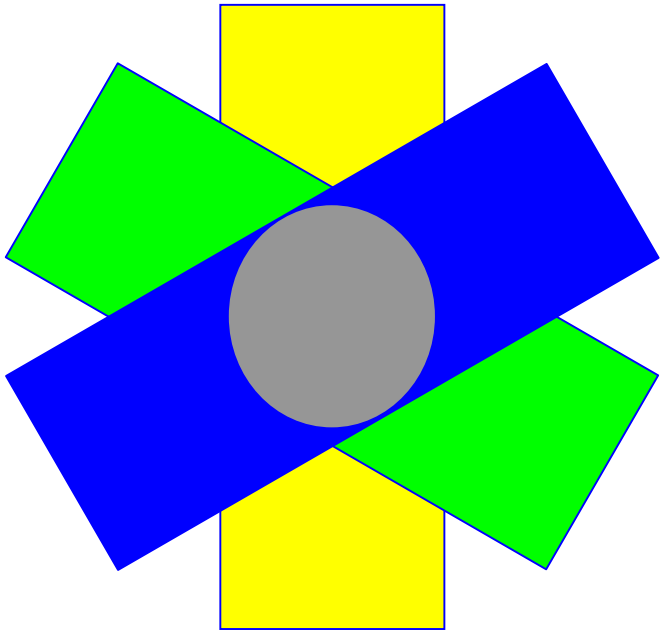

Figure 3.5.5 : The arrangement of the three double fibre planes in a scintillating fibre detector.

The alternative tracker, the TPG, will consist of a single chamber in each spectrometer section. These chambers will be standard TPCs, except for four components:

1) To keep the number of tracks drifting through the chamber at any one time down and hence maintain the pattern recognition performance, it is necessary to have a fast drift velocity. To achieve this, a drift voltage of 50k volts will be required, which could be a major safety hazard close to the liquid hydrogen absorbers.

2) It is planned to use a light gas, consisting mainly of helium, to reduce multiple scattering.

3) The electron avalanche will be created using Gas Electron Multipliers (GEMS) [5].

4) The TPGs will have 800k pads for readout, but to keep the cost down, rather than reading out each pad, they will be readout in u, v and x strips, as for the FT.

The main advantage of the TPG is it will give many points per muon track, about 120, compared to the 5 from the FT. This will make pattern recognition easier. However, backgrounds from the RF may be a problem due to the long TPG gate, 15ms.

The sixth muon parameter, time, will be measured using a very fast scintillator system, with a time resolution of about 50ps. This system will also be used for identification of the in-coming particle using time-of-flight and to provide a trigger. Identification of out-going electrons from muon decay in MICE will be made with an electron identifier placed in the rear of the experiment. There are two possibilities for this: a threshold Cherenkov detector or a sampling calorimeter and it is possible that both will be used.

3.5.2.3 *Cooling cells*

As already mentioned, two cooling cells will be used based on the US Study 2 design [2], as shown in Figure 3.5.2. Each will contain a four cell 201MHz RF cavity surrounded by large super-conducting coupling coils. There will be three absorbers, two at each end of the cooling cells, to provide shielding of the instrumentation sections from the dark current from the RF, and one in the center. The absorbers will be closely integrated with pairs of super-conducting focus coils.

3.5.2.4 *Absorbers*

The most important absorber for use by MICE is liquid hydrogen and the experiment is being designed around this. One of the main issues with using this absorber is safety and the absorber windows and hydrogen system are being designed in close collaboration with the relevant safety committees. In order to minimize the amount of material in the way of the beam, various window designs are beings studied which have more material at the edges than in the middle. A number of torispherical windows have been built and tested at Fermilab (see Figure 3.5.6).

Figure 3.5.6 : Liquid hydrogen absorber window built for safety tests in the US.

In addition to liquid hydrogen, it is also planned to use other absorbers in MICE. In particular, a solid absorber (beryllium, aluminium or plastic) will be used during the setting up period and possibly liquid helium or lithium hydride for cooling studies.

3.5.2.5 *RF cavities*

As already mentioned, MICE will use two four cell cavities running at 201.25MHz. These will need to provide an accelerating voltage of more than 20MV on peak. In addition, to reduce the backgrounds they will produce, careful conditioning and possible treatment of the cavity surface will be necessary. To obtain the required accelerating field, it is planned to close the cavities and two types of window will be tested on a single cell prototype, a thin beryllium foil or a grid (see Figure 3.5.7). To provide the RF power, it is hoped to recuperate existing power components to create two amplifier chains, each of 4MW, from CERN, RAL or Fermilab. This will provide the required 23MV on crest. It is hoped to start construction of the single cell prototype in the near future.

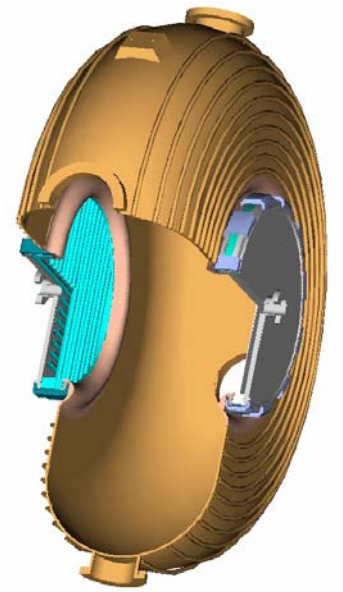

Figure 3.5.7 : Design for a single cell prototype cavity for MICE, allowing both a thin foil window and a grid to be tested.

3.5.2.6 *Super-conducting magnets*

As shown in Figure 3.5.8, MICE will have three basic types of magnet, all super-conducting:

Spectrometer solenoids: These surround each of the instrumentation sections and are used for the momentum measurement of the muons. They actually each contain five coils: the main solenoid, correction coils at each end of this and two additional coils on the end of the spectrometer towards the cooling cells. These are used to match the solenoid field to the field in the cooling cells.

Focus coils: these are pairs of coils surrounding each of the absorbers and closely integrated with them. The fields in the pairs of coils are reversed, creating significant stresses on the support structure. The integrated focus coils and absorber unit is probably the most complex in MICE (see Figure 2.5.9).

Coupling coils: these are the large coils, >1.2m diameter, surrounding the RF-cavities. They are necessary to maintain a focusing field through the cavity sections.

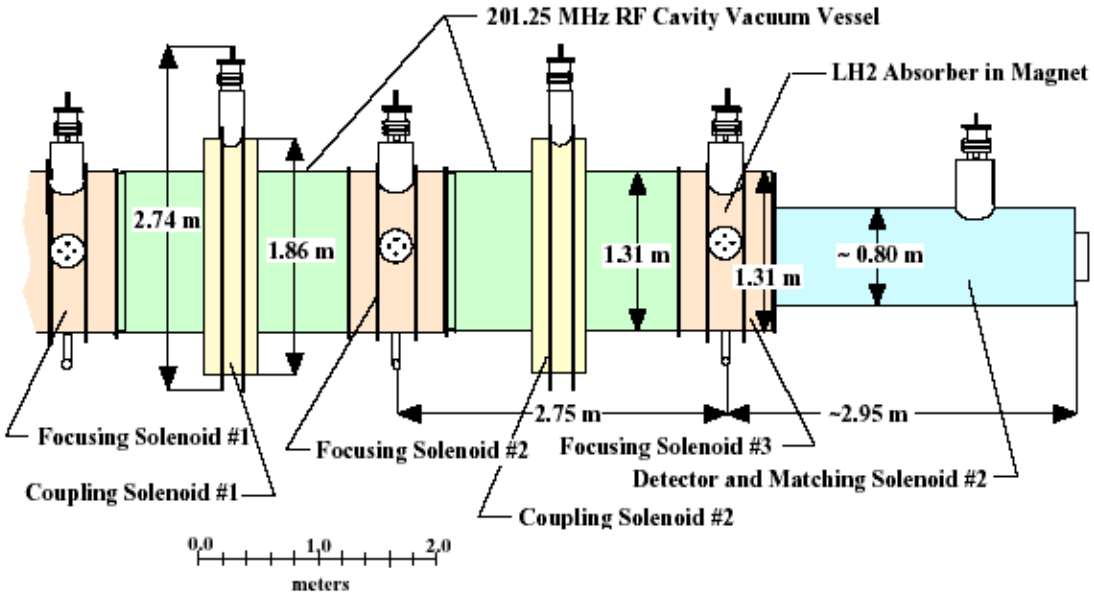

Figure 3.5.8 : The MICE magnet system

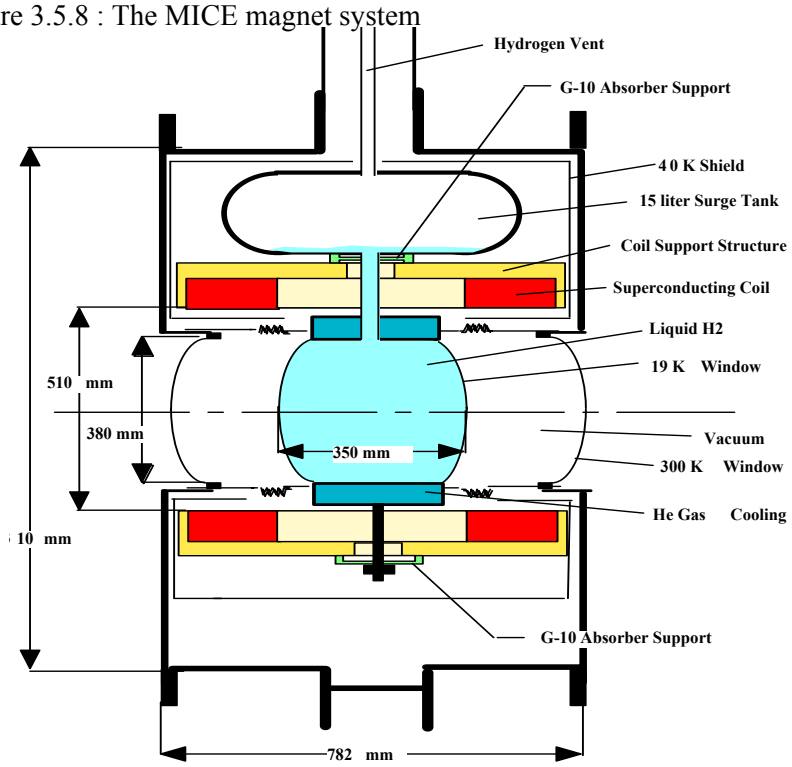

Figure 3.5.9 : The integrated focus coils and liquid hydrogen absorber unit.

3.5.2.7 *Performance*

A Geant 4 [6] simulation of MICE is currently being written and will be used to study the performance of the whole experiment. For the moment, the MICE performance has been assessed from two separate simulations, one looking at the instrumentation and the other at the cooling cells. The first of these is a home-built Monte Carlo which uses four planes of scintillating fibre detectors, with 0.5mm thick fibres, in a uniform 5T magnetic field. The statistical error on the emittance reduction obtained by this with only 1000 muons is shown in Figure 3.5.10 as a function of the length of the solenoidal field or alternatively on the inverse of the momentum. This is for the case of no cooling and perfect electron and pion identification, so there are no backgrounds. Note that the resolution achieved is smaller than one would naively expect from this number of muons due to the strong correlation between the emittance in and the emittance out.

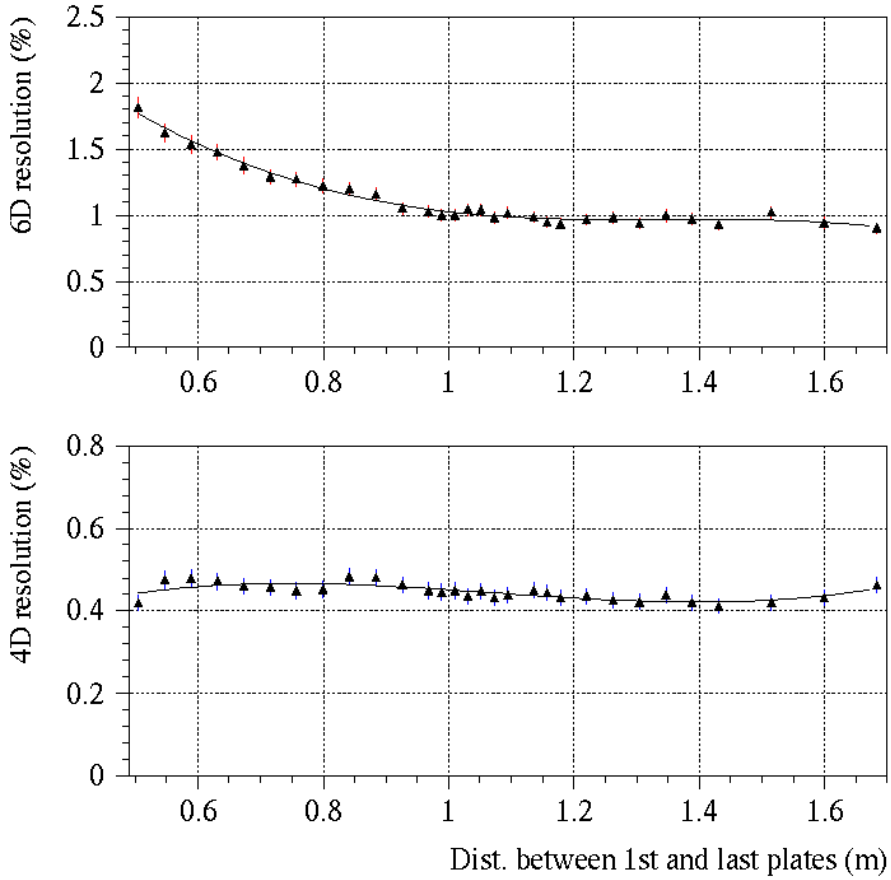

Figure 3.5.10 : Resolution on the 6D and 4D emittance reduction achievable by MICE with 1000 muons, without cooling and with no backgrounds, as a function of the solenoid length.

Due to the different kinematics, the effect of introducing backgrounds is to produce a dramatic reduction in the resolution of the emittance reduction. The simulations suggest that to have a minimal effect the pion and electron contamination must be kept below 0.1%. This leads to the requirement for excellent particle identification in MICE.

The cooling performance of MICE has been studied using ICOOL [7] and the results are summarised in Figure 3.5.11. This shows the rms transverse, longitudinal and 6D emittance along the length of MICE and the net change in the emittance. There is a 11% emittance reduction in each transverse plane and a 11% increase in the longitudinal emittance, giving a net reduction of 11% in the 6D emittance. Note that the longitudinal emittance growth was expected to be 6% rather than 11%, the difference arising because the magnetic fields were not properly matched when these studies were done. This was fixed in later studies. The last plot shows the percentage muon loss.

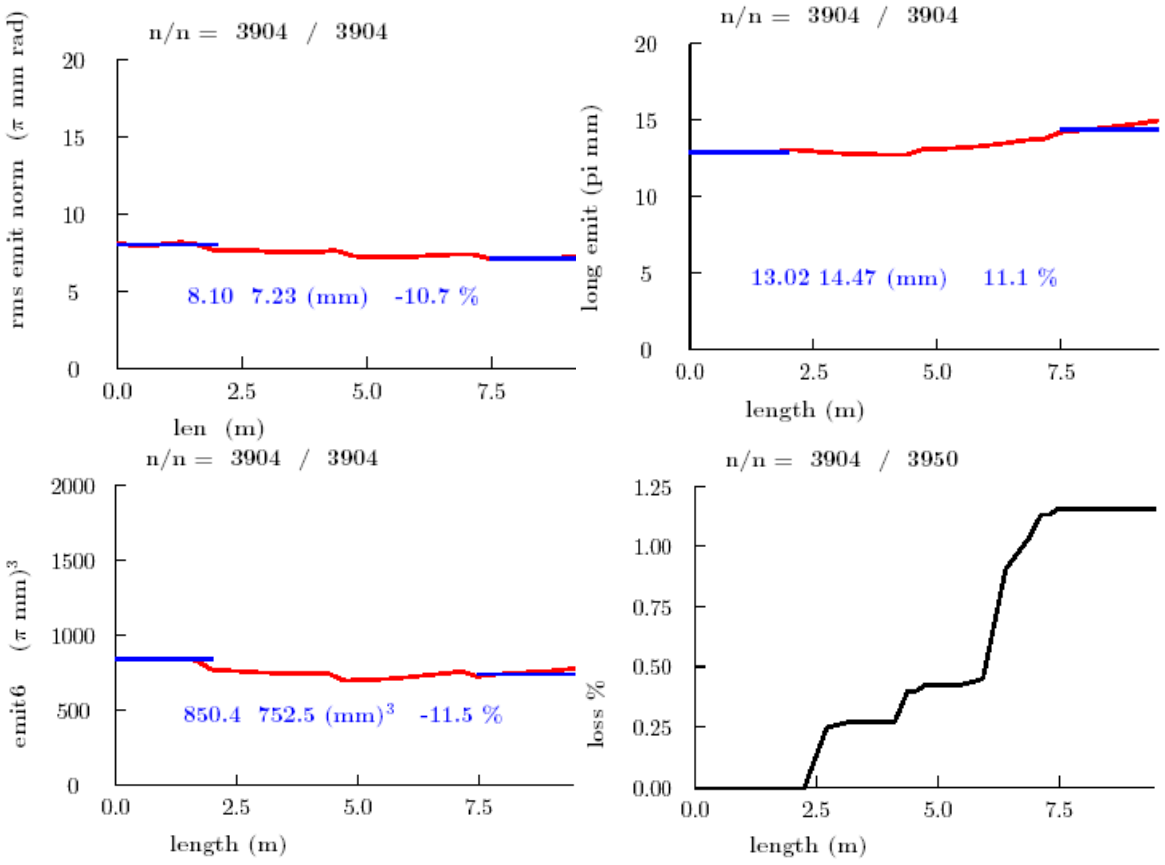

Figure 3.5.11 : Performance of the MICE cooling cells.

3.5.3 MICE schedule and cost

As a Technical Design Report for the Neutrino Factory cannot be completed until the results of MICE are known, the aim is to do this as quickly as possible. In particular, it is important that cooling has been demonstrated by about the time that the LHC starts. This defines the end point for MICE. The starting point is affected by two main things: approval by the Rutherford Appleton Laboratory and obtaining funding. It is hoped to obtain the former in spring 2003 and that the latter will quickly follow. The time schedule this leads to is shown in table 3.5.1.

The cost of MICE is currently being assessed, but the latest situation is shown in table 3.5.2. There are a number of major uncertainties in this, in particular the cost of the liquid hydrogen safety systems, which tracking detector will be used and whether refurbished or new RF power amplifiers will be used. These uncertainties will be resolved during 2003.

3.5.4 Conclusions

The MICE experiment is an essential component of the R&D taking place for a Neutrino Factory. It will demonstrate that the process of ionization cooling can be used to cool the muons. The MICE Collaboration is currently preparing a proposal that will be submitted to the Rutherford Appleton Laboratory in the UK on 15th December. Much of the MICE design is being finalized in preparation for this. It is hoped to receive approval in spring 2003 and to start construction of MICE late in 2003 or at the start of 2004. Although there is still some R&D to be done, it looks feasible to build the current MICE design and simulations suggest that it will work as required.

MICE will be constructed and tested in the muon beam in approximately seven stages, starting with only the tracking detectors in 2005 and finishing with the complete MICE in 2007. It is hoped that all data taking and analysis will be finished before the end of 2008.

For further information on MICE, please email Rob.Edgecock@rl.ac.uk.
Further collaborators are always welcome!

References

[1] MuCool Collaboration, Fermilab Proposal P904 (1998)
[2] US Muon Collaboration, BNL-52623 (2001)
[3] The MuScat Collaboration, RAL-TR-2002-022 (2002) 33
[4] A.Bross et al, FERMILAB-Pub-97/015 (1997)
[5] S. Bachmann et al, CERN-EP/2000-151 (2000)
[6] See http://cern.ch/geant4
[7] See http://pubweb.bnl.gov/people/fernow/icool/readme.htm

ID	Task Name
1	**MICE project**
20	**RAL beam line**
1	**ISIS Schedule (Provisional)**
13	**Prepare Sync.**
17	**Prepare MICE hall**
23	**Beam Line**
35	**Target**
40	**Final Installation**
45	**Solenoid**
51	**Cryogenics**
56	**Water Services**
61	**Electrical Services**
21	**RF system**
25	**Magnets**
26	**Focusing solenoid**
42	**Coupling coil**
54	**Spectrometer/matching solenoids**
55	**LH2 absorbers**
78	**Detectors**
1	**MICE Detectors**
2	TOF
3	Ecal
4	CKoV
5	**DAQ**
8	**Trackers**
9	SciFi
10	TPG R&D
11	TPG Construction
12	Tracker decision point
13	**Software project**

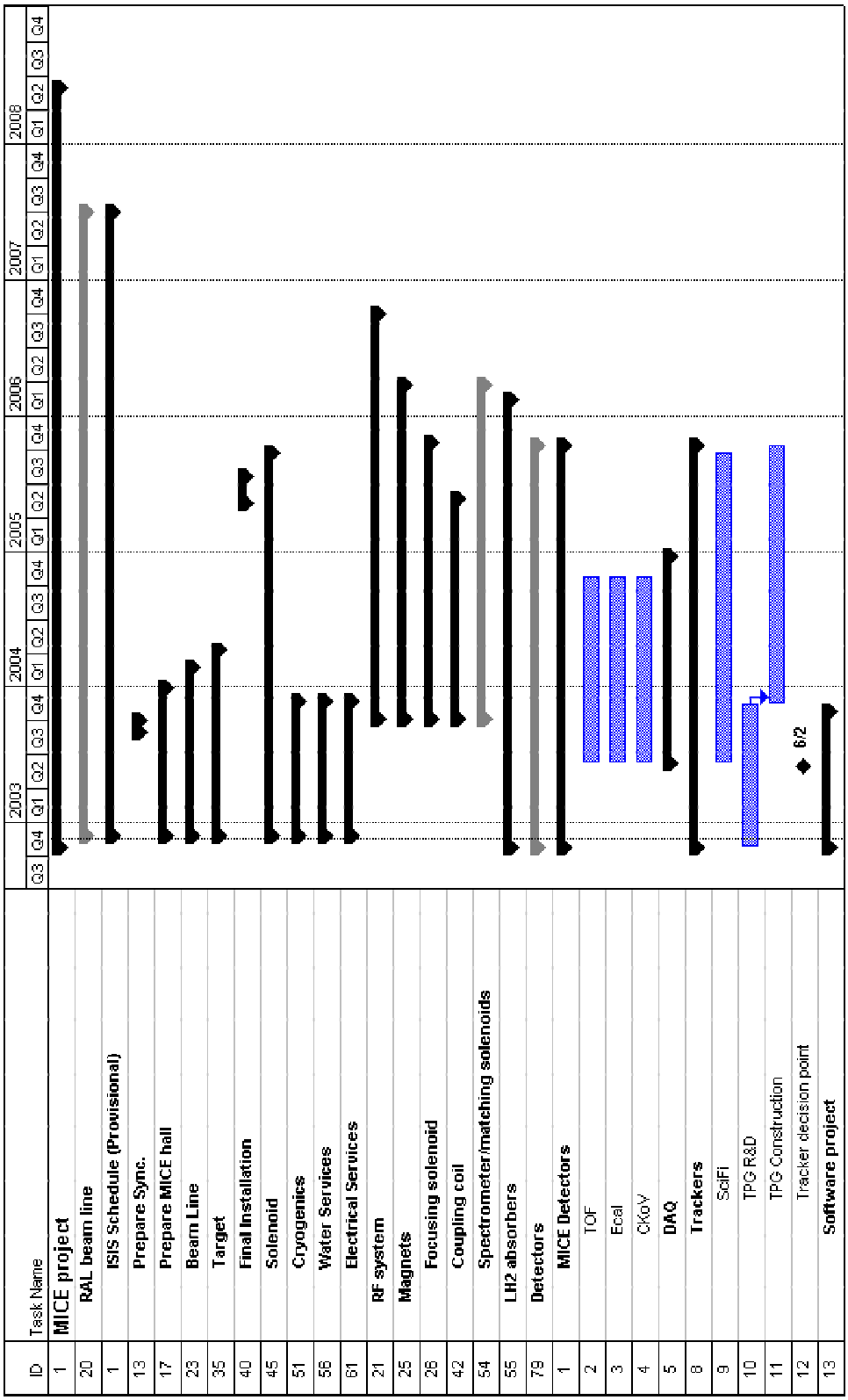

Table 3.5.1: The MICE construction schedule.

Item	No. reqd.	Cost (kEuros)	Responsible	Funding Source			
				U.S. (kEuros)	Europe (kEuros)	Japan (kEuros)	UK (kEuros)
Cooling Section		**11283**					
Magnets							
Focus coil pairs	3	2491	Oxford-RAL				2491
Coupling coils	2	2560	LBNL	2560			
Power supplies	6	135	LBNL	135			
Magnetic measurements	1	100	UK				100
RF Cavities							
Cavities	8	1686	LBNL	1686			
Windows	16	855	U-Miss.	855			
Tuners	8	259	U-Miss.	259			
Cryostat	2	96	IIT	96			
System integration	2	235	IIT	235			
Power distribution	1	950	EU		950		
Power source + LLRF	2	940	EU		940		
Absorbers							
Body (manifold)	3	349	Japan			349	
Windows	6	199	U-Miss.	199			
System integration	1	57	Oxford-RAL				57
Hydrogen safety	1	200	RAL	100	100		
Diagnostics							
RF cavities	2	44	ANL/ICL	22			22
Vacuum	2	10	EU		10		
Cryogenics	3	117	NIU	117			
Spectrometer Section		**9128**					
Magnets							
Spectrometers	2	2745	INFN-Genoa		2745		
Power supplies	8	280	LBNL	280			
Magnetic measurements	1	50	UK				50
Detectors							
Tracker (SciFi)	1	5596	U.S.+UK+Japan	2548	2548	500	
Tracker (TPG)	1	500	INFN+Geneva		500		
Cherenkov	2	227	U-Miss+Louvain	25	202		
TOF	1	180	Padova+Milan		180		
Calorimeter	1	50	Rome III		50		
Ancillary Items		**2718.8**					

Cryogenics						
Cooling channel	1	1300	UK			1300
Detector electronics	1	200	UK			200
Vacuum						
Pumps & valves		62	EU	62		
Beam spoiler		20	RAL			20
Supports/stands						
Cooling section		25	UK			25
Spectrometer section		15	UK			15
Data Acquisition	1	220	Bari	220		
Alignment	1	50	UK			50
Consumables						
Travel		827		827		
Experiment Support (5 years)						
Engineer/Technician (FTEs)				64.3		
Scientific (FTEs)				71.7		
TOTAL		**23130**		**9943**	**8007**	**849**	**4330**
				43.0%	34.6%	3.7%	18.7%

Table 3.5.2: Current estimated cost of constructing MICE.

3.6 Single Particle Description of Ionisation Cooling

Giuliano Franchetti, GSI

giuliano@lxi005.gsi.de

In future accelerator development neutrino factories are an investigated issue [1]. Experimental requirements for neutrino physics and muons lifetime impose a set of constrains which are challenging for the design of the front-end linac after the target [2]. In order to meet design constrains, the large 6D beam emittance obtained after the target needs an effective fast cooling. Ionization cooling has been proposed as a method to cool transverse 4D emittance while longitudinal cooling might be reached through a transverse-longitudinal emittance exchange [3] where the longitudinal emittance is transferred to the transverse plane and there cooled out. The main issue for an ionization cooling scheme becomes its effectiveness and optimization. In the international

collaboration [4] efforts both theoretical [5,6] and computational [7] have been dedicated to investigate beam dynamics in ionization cooling channels. We report here a theoretical description of ioniziation cooling channels based on a single particle dynamics. We present in some approximations the effects of absorber on the final value of the cooled emittance.

3.6.1 Modeling of an Ionization Cooling Channel

Typically a cooling cell is built with focusing structures, absorbers, and cavities [8]. We restrict ourself to the study of linear cooling cell (no bends) and start considering the dynamics in the horizontal plane. The single particle dynamics is described in an orthogonal reference frame *x,z*. The transverse coordinates of one particle are $x,x' = dx/ds = p_x/p_z$. . The cooling principle is the following [2]: the absorber reduces the particle's energy, but the cavity increases only the longitudinal momentum p_z. The global effect is a decreasing of x'. A focusing structure can be described in first approximation as harmonic oscillator with equation such as

$$x'' + kx = 0, \qquad (1)$$

where *k* is the focusing strength.

The motion of the particle in an absorber is affected by the muon-atom interaction which produces an absorption of energy ε and an angular deviation ψ from the incoming direction. These two effects are characterized by two distributions f_ε, f_ψ with standard deviations σ_ε and σ_ψ. . The muon-atom interaction is repeated many times, say *n*, along the muon path through the absorber. The total energy absorption δE and angular deviation ϑ at the exit of the absorber have standard deviations $\sigma_{\delta E} = \mathrm{sqrt}\{n\}\sigma_\varepsilon$ and $\sigma_\vartheta = \mathrm{sqrt}\{n\}\sigma_\psi$ and averages E_a , and ϑ_a . In a statistical sense, if each particle experiences the same number of interactions *n*, we expect that the distributions of δE, and ϑ are gaussian; for big deviations of *n* the distribution present deviations from a gaussian tail [9]. Since for $|\vartheta| << 1$ we can write $\delta x' = \vartheta$, the absorber can be modelled with the map

$$\begin{pmatrix} x \\ x' \\ E \end{pmatrix}_{out} = \begin{pmatrix} x + x' L_a + \delta x \\ x' + \delta x' \\ E - E_a + \delta E \end{pmatrix}. \qquad (2)$$

Here we consider δx, δx', δE as gaussian random noises with standard deviations $\sigma_{\delta x}$,$\sigma_{\delta x'}$,$\sigma_{\delta E}$. L_a is the length of the absorber, and E_a is the average energy taken by the absorber when the average exit angle ϑ_a is x'. Note that the 3 random variables are de-correlated and that δx' is not (δ x)'. The cavities are used to restore the longitudinal momentum reduced by the absorbers.

In first approximation a cavity affects only the longitudinal momentum, the transport through the cavity is then approximated by

$$\begin{pmatrix} x \\ x' \\ E \end{pmatrix}_{out} = \begin{pmatrix} x \\ x'/(1 + \Delta p_z/p_z) \\ E + E_c \end{pmatrix}, \qquad (3)$$

E_c is the energy supplied by the cavity, according to the phase, and Δp_z is the variation of the longitudinal momentum according with E_c .

3.6.2 Single Particle Equation of Motion

If transverse focusing, absorbers, and cavities have a 'weak' effect on the particle dynamics, then we can use a smooth approximation for the cooling channel. We suppose then to spread uniformly along the cooling cell cavities and absorbers. We lose then the concept of cooling cell, introducing that one of *uniform* cooling channel. An infinitesimal part of such a uniform channel of length ds can be approximated as a composition absorber + cavity + focusing kick + drift. Composing the drift map with the kick we obtain the map of the microcell

$$\begin{pmatrix} x \\ x' \\ E \end{pmatrix}_{out} = \begin{pmatrix} x + x' ds + \delta x + o(1) \\ x' - x' \Delta p_z / p_z - k\, ds\, x + \delta x' \\ E + E_c - E_a + \delta E \end{pmatrix}. \qquad (4)$$

When we track a particle by using Eq. 4, at each application of the map we should create δx, δx', and δE. We postpone the discussion on δE and consider δx' be a gaussian noise whose variance depends on the distance ds according to

$$\sigma^2(\delta x') = \alpha ds, \qquad (5)$$

where α is a constant typical of the absorber and the beam energy. Note that Eq. 5 keeps the consistency with the composition of noise errors along the absorber. For muons we have [9]

$$\alpha = \frac{f}{X_0}\left(\frac{13.6 MeV}{\beta c p}\right)^2 \quad [m^{-1}], \qquad (6)$$

where f is the absorber filling factor of the real periodic cooling cell, X_0 is the radiation length of the absorber, β= v/c, and p the particle momentum. From [9] we find also

$$\sigma^2(\delta x) = \frac{\alpha}{3} ds^3. \qquad (7)$$

Note that for small ds the noise δx becomes much smaller than the noise in δx'. This suggests that on the continuum δx will have a negligible effect on the dynamics.

From the first two rows of Eq. 4 we find

$$\begin{aligned} \Delta x &= x'\, ds + \delta x + o(1) \\ \Delta x' &= -x' \Delta p_z / p_z - k\, ds\, x + \delta x', \end{aligned} \qquad (8)$$

dividing by ds the previous equations become

$$\begin{pmatrix} \Delta x/ds \\ \Delta x'/ds \end{pmatrix} = \begin{pmatrix} 0 & 1 \\ -k & -(\Delta p_z/p_z)/ds \end{pmatrix} \begin{pmatrix} x \\ x' \end{pmatrix} + \begin{pmatrix} \delta x/ds \\ \delta x'/ds \end{pmatrix}. \qquad (9)$$

In order to extend to the continuum this difference equation we guess a sequence of N errors $\delta x'_j$=1,...,N corresponding to the N application of the map Eq. 4. Each of these errors is generated by the same source which is gaussian with variance Eq.5 . The second term in the rhs second row of Eq.9 can be extended to the continuum with the interpolation $\xi_{x'}(s) = \delta x'_j / ds = \xi'_j / \mathrm{sqrt}\{ds\}$ if j ds < s < (j+1) ds, where now ξ'_j is a random variable such that $\langle \xi'_j\, \xi'_j \rangle = \alpha$. When ds →0, $\xi_{x'}(s)$ becomes the derivative of the Wiener stochastic process [10,11] which has the formal property

$$\langle \xi_{x'}(s) \xi_{x'}(s') \rangle = \alpha \delta(s - s'). \qquad (10)$$

The same argument can be repeated for δx/ds, the second term on the first row in the rhs of Eq. 9 .The extension to the continuum is $\xi_x(s) = \delta x_j / ds = \xi_j\, \mathrm{sqrt}(ds)$ if j ds < s < (j+1) ds, where now ξ_j is a random variable such that $\langle \xi_j\, \xi_j \rangle = \alpha/3$. When ds →0, $\xi_x(s) \to 0$: the stochastic noise on the spatial coordinates can be neglected. On the limit of ds going to zero, $\xi_x(s)$ converges formally to a function which has the property

$$< \xi_x(s)\xi_x(s') >= \frac{\alpha}{3} ds^2 \delta(s - s'). \qquad (11)$$

With these definitions we finally write the transverse stochastic equation of motion for a particle in a uniform cooling channel

$$\begin{pmatrix} x \\ x' \end{pmatrix}' = \begin{pmatrix} 0 & 1 \\ -k & -d \end{pmatrix} \begin{pmatrix} x \\ x' \end{pmatrix} + \begin{pmatrix} \xi_x \\ \xi_{x'} \end{pmatrix}. \qquad (12)$$

Next we compute the term $d=(\Delta p_z/ p_z)/ds$. By using the cooling principle the energy taken by the absorber E_a should balance the energy supplied by the cavity E_c .

With the assumption of $|x'| << 1$ the longitudinal momentum lost and regained, Δp_z, is a constant quantity throughout the uniform cooling channel. On the other hand energy conservation between the entrance and exit of the cavity leads to

$$\sqrt{p_{z,in}^2 (1 + x_{in}'^2) c^2 + \left(mc^2\right)^2} + qV = \sqrt{p_{z,out}^2 (1 + x_{out}'^2) c^2 + \left(mc^2\right)^2}$$

here $x_{out}' = x_{in}'(1 - \Delta p_z/ p_{z,out})$. Since qV is small with respect to the energy of the particle, an expansion at the first order gives

$$d = (\Delta p_z / p_z)/ds = \frac{V}{ds} \frac{q}{E_0 \beta_z^2}. \qquad (13)$$

The average electric field (longitudinal RF density) V/ds depends from the energy taken by the absorber $E_a+\delta E$, in fact along each ds the RF voltage has to restore the lost momentum Δp_z and this happens when

$$\frac{E_a + \delta E}{1 + x_{in}'^2} = qV, \qquad (14)$$

that with smooth approximation becomes $E_a + \delta E = q\ V$. In order to simplify the problem we assume here that ds is such that $\sigma_{\delta E} /E_a << 1$ so that we can neglect the energy fluctuation δE and assume $E_a = q\ V$.

For a cooling cell of length L the coefficient d can be approximated as $d = (\Delta E/E_0)/(L\beta_z^2)$where ΔE is the energy lost and gained per cell. A generalization of Eq. 12 at the 2D case is given by the set of equations

$$\mathbf{X}' + M\mathbf{X} = \mathbf{N}, \qquad (15)$$

with

$$\mathbf{X} = \begin{pmatrix} x \\ x' \\ y \\ y' \end{pmatrix}, \quad \mathbf{N} = \begin{pmatrix} \xi_x \\ \xi_{x'} \\ \xi_y \\ \xi_{y'} \end{pmatrix}, \quad M = \begin{pmatrix} 0 & -1 & 0 & 0 \\ k_q & d & \hat{k}_q & -k_s \\ 0 & 0 & 0 & -1 \\ \hat{k}_q & k_s & k_q & d \end{pmatrix}. \qquad (16)$$

These equations include the constant focusing uniform channel modelled by Eq. 12: the strength is now represented by the coefficient k_q; it includes the uniform solenoidal cooling channel, in the form

$\mathbf{x''} = \mathbf{x'} \wedge \mathbf{s}\ k_s + d\ \mathbf{x'}$ with **s** longitudinal versor and $k_s = qB_0/p_z$; or more general combinations of uniform focusing, uniform solenoid, and uniform skew quadrupole (the coefficient $\hat{k}_q$) in the cooling channel. Next we show the method to solve Eq. 15.

3.6.3 Single Particle Dynamics

The simplest cooling channel is obtained by using quadrupoles as focusing structures: the transverse planes are decoupled. However it has been proposed a more efficient scheme [12] which uses alternating solenoids. For an axially symmetric beam

in a solenoidal channel, envelope equations have been derived by R. K. Cooper [13], and recent works had included the effect of the absorbers [5,6]. In the next discussion we calculate the effect of the noise on the single particle dynamics in a uniform channel where the cooling channel properties are constant along the longitudinal direction. We first solve Eq. 15 considering **N** as a well-defined function. The solution of Eq. 15 is

$$x_k(s) = \sum_{ij} P_{ki} C_{ij} e^{\lambda_j s} + \sum_{ij} P_{ki} e^{\lambda_i s} \int_0^s e^{-\lambda_i s'} (P^{-1})_{ij} \mathrm{N}_j(s') ds', \qquad (17)$$

where C_{ij} is a matrix determined by the initial conditions, P_{ki} is the matrix which diagonalizes M, i.e. $\Lambda = P^{-1} M P = \mathrm{diag}(\lambda_1,\lambda_2,\lambda_3,\lambda_4)$. The first term on the rhs represents the homogeneous solution of Eq. 15 that we call $\hat{x}_k(s)$ while the second term represents the contribution of **N** called next Δx_k. The evolution of Δx_k (s) depends on the noise **N** (s) which is a function that has a certain probability to be found in the set of all the possible choices for **N**. We indicate this dependence by writing Δx_k [**N**]. We can't characterize the dynamics of a single particle with a unique solution, but rather we can give a probability that the noise has the functional form and then compute the motion. It follows that the frame for a predictive analytical investigation must be statistical. At the longitudinal position s each coordinate of the particle has the value x_k (s) $= \hat{x}_k(s) + \Delta x_k$ [**N**] (s) with probability P[**N**] d[**N**]. We can average with respect to the noise and find

$$\langle x_k \rangle_{\mathrm{N}}(s) = \hat{x}_k(s) + \langle \Delta x_k[\mathrm{N}] \rangle_{\mathrm{N}}(s), \qquad (18)$$

where with $\langle \bullet \rangle_{\mathrm{N}}$ we mean average over the noise. Since the noise has average zero the second term of Eq. 18 disappears. We can also characterize the spread of x_k (s) computing the variance

$$\langle (x_k(s) - \hat{x}_k(s))^2 \rangle_{\mathrm{N}} = \langle \Delta x_k^2[\mathrm{N}] \rangle_{\mathrm{N}}(s). \qquad (19)$$

However for an rms approach to the beam description, moments as <x x'> are needed requiring the evaluation of all the noise correlations. We call to simplify the notations $\Delta_{kp}(s) = \langle \Delta x_k [\mathbf{N}] \Delta x_p [\mathrm{N}] \rangle_{\mathbf{N}}$ (s).

By using the second term on the rhs of Eq. 17 we find

$$\Delta_{kp}(s) =$$

$$= \sum_{ijqt} P_{ki} (P^{-1})_{ij} P_{pq} (P^{-1})_{qt} \int_0^s \int_0^s e^{-\lambda_i (s'-s) - \lambda_q (s''-s)} \langle \mathbf{N}_j(s') \mathbf{N}_t(s'') \rangle_{\mathrm{N}} ds' ds''. \qquad (20)$$

However

$$\langle \mathbf{N}_j(s') \mathbf{N}_t(s'') \rangle_{\mathbf{N}} = \int_{\mathcal{F}} \mathbf{N}_j(s') \mathbf{N}_t(s'') \mathcal{P}[\mathrm{N}] d[\mathrm{N}] = Q_{jt} \delta(s' - s''), \qquad (21)$$

where F is the space of the noises and δ (s'-s") is Dirac's function. The matrix Q_{jt} has the form

$$Q = diag(\alpha \frac{ds^2}{3}, \alpha, \alpha \frac{ds^2}{3}, \alpha), \qquad (22)$$

where ds is the integration length used in Eq. 4. The diagonal form of Q stems from the de-correlation of the noises in the four coordinates. Since we are considering very small integration step we can drop the second order terms in Eq. 22 neglecting then the noises ξ_x, ξ_y. With this approximation and defining the matrix L = diag(0,1,0,1) Eq. 20 gets the form

$$\Delta_{kp}(s) = \alpha \sum_{ijqt} P_{ki} (P^{-1})_{ij} P_{pq} (P^{-1})_{qt} L_{jt} \frac{1 - e^{(\lambda_i + \lambda_q) s}}{-(\lambda_i + \lambda_q)}. \qquad (23)$$

Defining the symmetric matrix $B = P^{-1} L P^{-1} T$ and

$$F_{iq}(s) = \frac{1 - e^{(\lambda_i + \lambda_q)s}}{-(\lambda_i + \lambda_q)}, \qquad (24)$$

we can express the noise correlations in the compact form

$$\Delta_{kp}(s) = \alpha \sum_{iq} P_{ki} P_{pq} B_{iq} F_{iq}(s). \qquad (25)$$

From this expression we see that a crucial role is played by the sum $\lambda_i + \lambda_q$: if this sum has real part negative the function F_{iq} approaches an asymptotic value for big s, if $Re(\lambda_i + \lambda_q) > 0$ the effect of the noise increases exponentially; if $Re(\lambda_i + \lambda_q) = 0$ then $F_{iq} = s$.

3.6.4 Uniform Quadrupolar Cooling Channel

In a quadrupolar uniform cooling channel the horizontal and vertical planes are decoupled. We consider then only the horizontal plane. The general solution of the equation

$$x'' + dx' + kx = \xi_{x'}, \qquad (26)$$

is

$$x = Ae^{\lambda_1 s} + Be^{\lambda_2 s} - \frac{e^{\lambda_1 s}}{\lambda_2 - \lambda_1} \int_0^s \xi_{x'} e^{-\lambda_1 s'} ds' + \frac{e^{\lambda_2 s}}{\lambda_2 - \lambda_1} \int_0^s \xi_{x'} e^{-\lambda_2 s'} ds', \quad (27)$$

where λ_1 = -d/2 + (sqrt{d^2-4 k})/2 and λ_2 = -d/2 - (sqrt{ d^2-4 k})/2 are the eigenvalues. A and B are coefficients determined by the initial conditions. Eq. 27 is just the x component of Eq. 17. It is valid if $d^2 \neq 4$ k. First we study the solution when the absorber noise is absent.

Unperturbed Solution $\xi_{x'} = 0$

In this case the solution becomes

$$x = e^{-d/2s}[Ae^{(\sqrt{d^2-4k}s)/2} + Be^{-(\sqrt{d^2-4k}s)/2}], \qquad (28)$$

the factor $e^{-d/2}$ s is the exponential damping of the particle motion.

We distinguish two regimes, one where the focusing strength dominates the damping i.e. when sqrt{d^2-4 k} is pure imaginary and the terms in the square brackets express an oscillation.

The other regime is dominated by the damping over the focusing strength, in this case sqrt{ d^2-4 k} is real.

Focusing Dominated Regime

In the focusing dominated regime $d^2 < 4$ k and calling sqrt{4 k - d^2} = K the solution in terms of the initial condition becomes

$$x = e^{-d/2s}\left[x_0\left(\frac{d\sin(K/2s)}{K} + \cos(K/2s)\right) + \frac{2x_0'}{K}\sin(K/2s)\right]. \qquad (29)$$

We observe that if d→0 then K/2 →sqrt{k}and the previous solution approaches the

$$x = x_0\cos(\sqrt{k}s) + \frac{x_0'}{\sqrt{k}}\sin(\sqrt{k}s), \qquad (30)$$

which expresses the betatronic motion in a uniform focusing channel. When d > 0 the oscillations are damped according to $e^{-d/2\ s}$. If we are in a regime where k >> d^2 the

term d sin(K/2 s)/K is smaller than cos(K/2 s) and the exact solution can be approximated by

$$x = e^{-d/2s}[x_0 \cos(\sqrt{k}s) + \frac{x_0'}{\sqrt{k}} \sin(\sqrt{k}s)]. \qquad (31)$$

Envelope and Emittance Evolution

Since the focusing strength is uniform the Twiss parameters of the cooling channel are $\beta_x = 1/\text{sqrt}\{k\}$, $\gamma_x = 1/\beta_x$ and the initial coordinates x_0, x'_0 can be expressed as

$$x_0 = \sqrt{\beta_x \epsilon_{x,0}} \sin\hat{\delta}, \qquad x_0' = \sqrt{\gamma_x \epsilon_{x,0}} \cos\hat{\delta}, \qquad (32)$$

with δ an initial phase and $\varepsilon_{x,0}$ the initial single particle emittance. By using these expressions in Eq. 31 we find

$$x = e^{-d/2s}\sqrt{\beta_x \epsilon_{x,0}} \sin(\sqrt{k}s + \hat{\delta}), \qquad (33)$$

consequently the single particle emittance evolves according to

$$\epsilon_x(s) = \epsilon_{x,0} e^{-ds}. \qquad (34)$$

The same relation holds for the matched beam and the envelope evolves according to $\hat{x}_{env} = \hat{x}_{env,0} e^{-d/2s}$

When we approach the transition condition ($4k = d^2$) Eq. 33 does not hold, however Eq. 29 holds giving a solution as

$$x = e^{-d/2s}[oscillating \quad terms], \qquad x' = e^{-d/2s}[oscillating \quad terms], \quad (35)$$

Again by using $\varepsilon_x = \beta_x x'^2 + \gamma_x x^2$ one finds

$$\epsilon_x(s) = e^{-ds}[oscillating \quad terms], \qquad (36)$$

which shows the exponential damping of the single particle emittance. The damping rate of the emittance can be explained in another way. The dissipative term in Eq. 29 causes a damping of energy. However in the quadrupolar channel the particle energy changes continuously form between potential energy and kinetic energy. If the change energy is not to fast compared with the period of one betatron oscillation an equipartition argument leads to the relation $E = \langle x'^2 \rangle$ (over one betatron oscillation). We find then the equation $E' = -d\,E$ which shows a dump of the energy with the factor exp(-ds).

Damping Dominated Regime

This regime happens when $4k < d^2$. Defining $\text{sqrt}\{d^2 - 4k\} = K$ the solution of the motion becomes

$$x = \frac{1}{2K}[(x_0(K+d) + 2x_0')e^{(-d+K)s/2} + (x_0(K-d) - 2x_0')e^{-(d+K)s/2}]. \quad (37)$$

Since $-d \pm K < 0$ the motion is dumped and no betatron motion can be found. The transverse kinetic energy is not converted in potential but rather taken by the absorber.

3.6.5 Noise Effect

We apply now the theory described in Section 3.6.4 to the uniform quadrupole channel for $d^2 \neq 4k$.

First we note that $\lambda_1 + \lambda_2 = -d$ which determines the evolution of the second order moments: they approaches an asymptotic values. Applying Eq. 25 we find

$$\begin{aligned}
\Delta_{11} = \Delta_{33} &= \frac{\alpha}{d^2-4k}\left\{\frac{1}{2k}\left[d - e^{-ds}\left(d\cosh(\xi s) + \xi \sinh(\xi s)\right)\right] - \frac{2}{d}\left(1 - e^{-ds}\right)\right\} \\
\Delta_{22} = \Delta_{44} &= \frac{\alpha}{d^2-4k}\left\{\frac{1}{2}\left[d + e^{-ds}\left(-d\cosh(\xi s) + \xi \sinh(\xi s)\right)\right] - \frac{2k}{d}\left(1 - e^{-ds}\right)\right\} \\
\Delta_{12} = \Delta_{34} &= \frac{\alpha}{d^2-4k}\left\{e^{-ds}\left(\cosh(\xi s) - 1\right)\right\}
\end{aligned} \tag{38}$$

where ξ= sqrt{d^2 - 4 k} = K in the damping dominated regime and ξ= -i K in the focusing dominated regime. All the missing moments are zero.

We can visualize how the noise disturbs the particle dynamics integrating the equations of motion Eq. 4.

We have considered as example a uniform quadrupolar cooling channel with parameters k=1 m^{-2}, d=0.1 m^{-1}, α=5.9 10^{-4} rad^2/m. Given a particle with initial coordinates x=0.3 m, x'=0.3 rad, in order to show the stochastic nature of the motion, we repeated the integration 50 times. Figure 3.6.1 shows this result. The picture shows that when the spread of the particle equals the betatron amplitude the cooling stops to be effective. Figure 3.6.2 shows the computed standard deviation of the particle's position compared to the theoretical prediction: the agreement is very good.

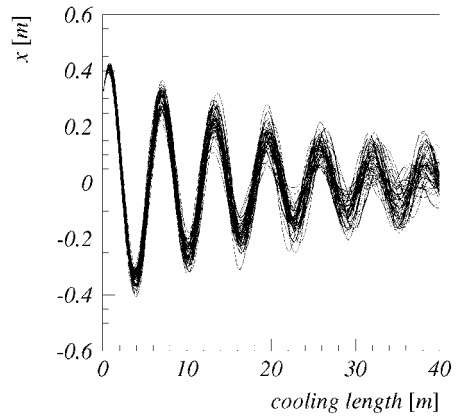

Figure 3.6.1 : Example with 50 repetitions of a particle's trajectory: each time the absorber noise builds up an error in a different way.

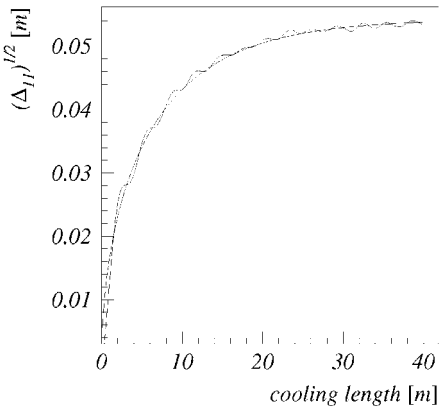

Figure 3.6.2 : Comparison between the theoretical standard deviation and that one obtained from simulations by repeating the integration of the equation of motion with noise 10000 times.

Next we include the noise effect on the particle dynamics in a focusing dominated regime.

Envelope with Noise in a Focusing Dominated Regime

For practical considerations the maximum deviation can be taken as Δx_{max} = 3 sqrt{Δ_{11}}. The envelope can be computed as the unperturbed envelope plus Δx_{max}, i.e.

$$x_{env}(s) = \hat{x}_{env}(s) + 3\sqrt{\Delta_{11}}, \qquad (39)$$

and neglecting small oscillating terms we find

$$x_{env}(s) = \sqrt{\beta_x \epsilon_0} e^{-d/2s} + 3\sqrt{\frac{\alpha}{2kd}(1 - e^{-ds})}. \qquad (40)$$

This equation can be rewritten in normalized units dividing by $\hat{x}_{env}(0)$ and defining R = $\hat{x}_{env}(s) / \hat{x}_{env}(0)$

$$R = e^{-d/2s} + \frac{1}{\chi}\sqrt{1 - e^{-ds}}, \qquad (41)$$

where χ= (sqrt{$\beta_x \varepsilon_0$}/3) sqrt{2 k d/α} is a dimensionless characteristic parameter which combines beam parameters and cooling channel parameters.

A numerical check of Eq. 41 was performed. Figure 3.6.3 shows the dumped oscillating motion of one particle, the dashed curve the theoretical dump of the envelope when the absorber noise is absent. The dash-dot curve is the maximum contribution of the noise (3 times the standard deviation of the absorber noise), while the upper continuous curve represents the sum of the two curves (Eq. 40). The figure shows how the noise perturbs the dumped betatronic motion and that the theoretical prediction bounds this motion. In Figure 3.6.4 is shown that the theoretical envelope really bound most of the possible trajectory that the absorber noise may build.

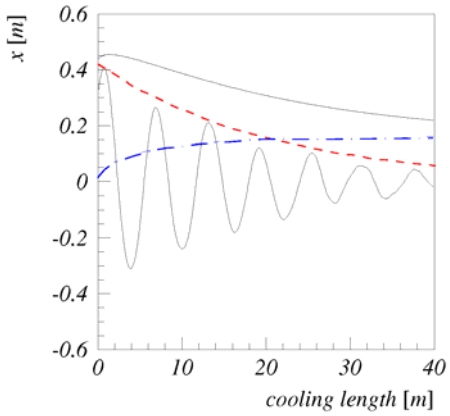

Figure 3.6.3 : The dumped oscillating motion of one particle and the theoretical dump of the envelope (dashed curve) when the absorber noise is absent

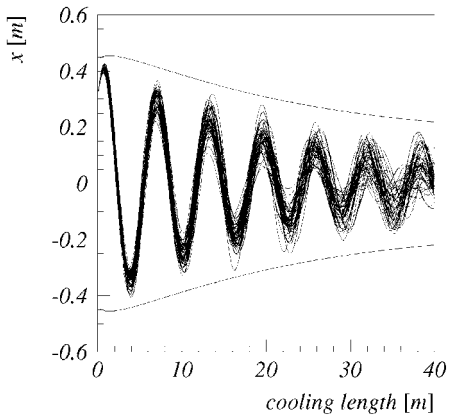

Figure 3.6.4 : Comparison of the theoretical envelope with a set of 50 curves. The picture shows that the theoretical prediction bound practically all the trajectory evolution.

References

[1] H. Haseroth, in CERN Ideas and Plan for a Neutrino Factory, edited by S. Chattopadhyay (Elsevier Science, NORTH-HOLLAND, 2000), p. 17, proceedings of the Nufact conference, Monterey CA, held March 29th - April 2nd.
[2] D. Neuffer, Part. Accel. {14}, 75 (1983).
[3] D. Neuffer, FERMILAB-Pub-96 140, Fermilab (unpublished).
[4] C.~M. Ankenbrandt et~al., Phys. Rev. ST Accel. Beams {2}, 081001 (1999).
[5] K.-J. Kim and C. xi~Wang, Phys. Rev. Lett. {85}, 760 (2000).
[6] G. Penn and J.~S. Wurtele, Phys. Rev. Lett. {85}, 764 (2000).

[7] R.~C. Fernow, in ICOOL: a simulation code for ionization cooling of muon beams, edited by A. Luccio and W. MacKay (IEEE, 445 Hoes Lane Piscataway, NJ 08854-4150, USA, 1999), Vol.~3, p. 3020, proceedings of the 1999 Particle Accelerator Conference, New York NY, held March 29th - April 2nd.
[8] A. Lombardi, CERN-NUFACT Note 34, CERN, (unpublished), http://molat.home.cern.ch/molat/neutrino/nfnotes.html .
[9] D.~E. Gordon and S.~R. Klein, The European Physical Journal C {15}, 163 (2000).
[10] G. Turchetti, in Dinamica Classica dei Sistemi Fisici, edited by Zanichelli (Zanichelli, Bologna, 1998), p. 584.
[11] C.~W. Gardiner, in Handbook of Stochastic Methods for Physics, Chemistry and Natural Sciences}, edited by Springer (Springer, Berlin, 1983), Vol.~13, p. 442.
[12] R.~B. Palmer and R. Fernow, in Beam Physics for Muon Colliders (lectures given at the Accelerator School, Vanderbilt University, 1999).
[13] R.~K. Cooper, Part. Accel. {7}, 41 (1975).

3.7 The HARP Experiment

Maria-Gabriella Catanesi , INFN Bari

Maria.Gabriella.Catanesi@cern.ch

3.7.1 Pion Production in a Neutrino Factory

A neutrino factory requires a sophisticated front-end: the proton target, pion capture, muon phase rotation and muon cooling.

For the proton source several options from a 2 GeV proton Linac to 24 GeV rapid-cycling synchrotron are under discussion. Deuterons, which provide more symmetric yields of positive and negative pions than protons, are discussed as an alternative to protons [1],[2].

In this context, accurate pion production yields are very important to achieve the desired neutrino fluxes and to design a cost effective machine. The design goal for a Neutrino Factory is to maximize the number of accelerated positive/negative muons in the decay ring [3].

Current simulations of the pion yield with FLUKA and MARS show a 30%-100% discrepancy in pion production [4], [5]. It is reasonable to assume a similar uncertainty for the momentum distribution. The reason for this uncertainty is the small amount of experimental data for the simulation programs. It is not surprising that at relatively low-energy (in the 1 GeV-to- 50 GeV range) this lack of data exist despite the fact that several hadron production experiments are being operated, built or proposed [6], [7], [8]. Such experiments all share a basic design, consisting of an open-geometry spectrometers, as close as possible to full angular coverage, and the aim of a full particle identification. However, they are limited in acceptance or, most frequently, in statistics (small event sample, only one beam momentum, limited number of target materials).

The variables affecting the pion production are the proton energy, the target material and the target geometry (diameter and length). The total proton-beam power is only a scaling parameter. A pion production experiment should give the set of data necessary to choose the optimum proton energy and target material.

The transverse capture and the first phase rotation are strongly dependent on the pion production data. Both the transverse the longitudinal momentum distribution of the pions must be known to a high precision as it affects the efficiency of transverse capture and the design the phase rotation. Moreover to enhance the polarization (by correlating time with forward/backwards decay of pions) a precise knowledge of the longitudinal phase plane is essential.

A high-precision pion production experiment with full angular coverage and full particle identification capability would thus be a requirement for the simulation of a neutrino factory.

The necessary data to optimise the neutrino factory design are summarized in Table 3.7.1

Table 3.7.1

Parameter	***Range***	***Precision***
p longitudinal momentum	100-700 MeV/c	< 25 MeV/c
p transverse momentum	0 -250 MeV/c	< 25 MeV/c
Number of secondary p/proton		5%
p+/p- ratio		5%

3.7.2 Setup and expected performances

The HARP experiment at the CERN PS [9] has carried out in the last 2 years (2001-2002), a vast program of measurements of secondary hadron production, over the full solid angle, produced on thin and thick nuclear targets by beams of protons and pions with momenta in the range 2 to 15 GeV/c.

The first aim of the experiment is to acquire an adequate knowledge of pion yields for an optimal design of the proposed neutrino factory. The second aim is to reduce substantially the existing 30% uncertainty in the calculation of the absolute atmospheric neutrino fluxes and the 7% uncertainty in the ratio of neutrino flavours.

The main goal of the experiment is the measurement of secondary hadrons with a 4π angular acceptance using various beams energies and targets. An overall precision of 2% for the inclusive cross-section of secondary particles is the primary aim. This is motivated by the wish to obtain 5% precision on the production of accepted muons in the neutrino factory's front stage. A 2% overall accuracy requires some 10^6 events for each measured point to minimize the statistical error. The challenge lies in understanding efficiencies with an error of the order of few %. This calls for as much redundancy as can be afforded, with a view to cross-calibrating efficiencies and to keep under control the systematic. Furthermore, at different energies the purity of the pion sample is affected by different backgrounds that require good particle identification detectors.

In addition to the standard set of target geometries and materials, HARP is also measuring production cross section on special targets provided by the K2K[10] and MiniBooNE [11] collaborations.

The HARP experiment is located on the T9 beam line in the East Hall of the CERN PS complex. HARP has been designed with the aim of collecting up to 1000 events in each PS spills (400ms) , which represents a relatively high rate, especially for the Time Projection Chamber (TPC). Since the beam is a mixture of several particle (deuterons, protons, kaons, pions, muons, electrons) all of the same momentum, the beam line is instrumented with threshold Cerenkov and Time-Of-Flight detectors to tag the incoming particle (Figure 3.7.1). To predict the impact position on the HARP target, trajectories of beam particles are recorded by 3 sets of X-Y multi-wire proportional chambers.

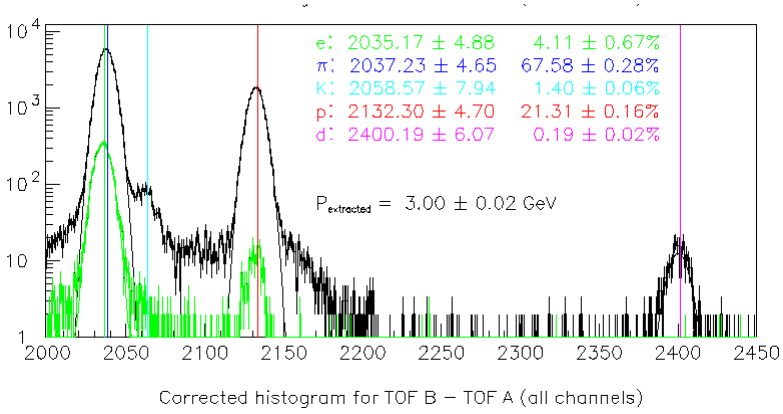

Figure 3.7.1 : Beam composition at CERN PS as seen by the HARP experiment

3.7.2.1 *Large-angle detectors*

Particles with high transverse momentum are detected in a large-angle spectrometer, consisting of the Time Projection Chamber (TPC) for particle identification by tracking in magnetic field and measurement of dE/dx, and by a high-precision Resistive Plate Chambers (RPCs) time-of- flight arranged in a cylinder around the TPC. In order to detect backward-going particles, the target is placed inside the TPC volume. The TPC consists of a cylindrical volume (1.5m long and 0.8m in diameter) filled with a gas mixture composed of 91% Ar and 9% CH4. The trajectories of charged particles are bent by a 0.7T solenoid magnetic field. A 12 kV electric field drives the ionization charges at a velocity of 5.1 cm/s to the read-out plane, where 3972 pads arranged in 20 concentric rows collect the induction signals. The pad signals are digitized in 100 ns time bins, corresponding to about 5 mm bins in the longitudinal direction. The RPC system consists of 4 layers of RPC chambers with a 0.3mm gap. They allow for Time-Of-Flight measurement, e / p separation in the 100-250 MeV/c region and rejection of tracks from piled-up events by measuring the time of crossing tracks with a precision of about 150 ps.

Figure 3.7.2 shows a 3 GeV proton interaction in a Tantalum target as seen by the large angle spectrometer.

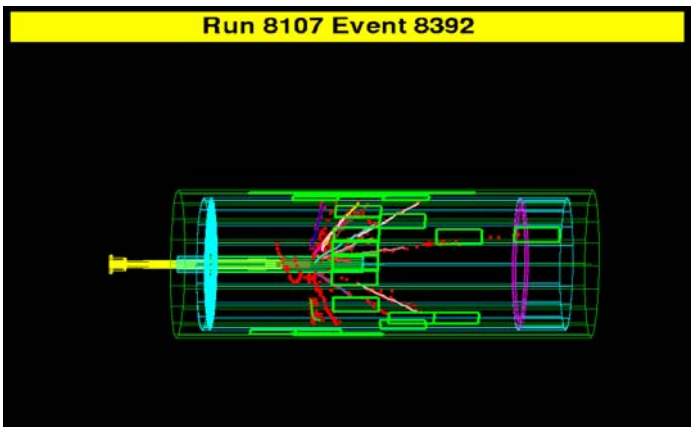

Figure 3.7.2 : Proton interaction in a Tantalum target as seen by the large angle spectrometer (simulated).

3.7.2.2 *Forward detectors*

Immediately after the TPC, a forward trigger scintillator plane selects events with small-angle particles. It is complemented by a further set of RPC chambers for e / p separation. Particles leaving the target in the forward direction are poorly seen in the TPC, and are therefore measured and tagged by the forward spectrometer. The spectrometer is built around a 4-station Drift Chamber system, where a 0.68T dipole magnet is inserted between the first and the second station. The chambers are filled with a gas mixture consisting of 90% Ar, 9% CO2 and 1% CH4. The drift chamber modules have been designed for the NOMAD experiment. They are made by 4 sets of 3 planes inclined at angles of -5,0,+5 degrees and are expected to deliver 200ps resolution in the horizontal plane; A 30m^3 Cerenkov detector sits after the second drift chamber station. It is filled with C4F10 at atmospheric pressure. A set of cylindrical mirrors guides the light to 38 photo-multipliers. Its main purpose is the particle identification in the high-energy region. The thresholds are 2.6GeV/c for pions, 9.3GeV/c for kaons and 17.6GeV/c for protons. After the third drift chamber station, a large Time-Of-Flight wall made of 39 scintillation counters identifies particles in the intermediate-energy range. A preliminary analysis of data taken in the 2001 indicates a resolution of about 200ps.

As an example of the expected performance, a simulation has been run with 15 GeV/c protons impinging on a beryllium target of a thickness equal to 2% of the interaction length In Figure 3.7.3 we can see the distribution of events in the transverse-longitudinal momentum plane *(d2N/dpT* dPL) for the secondary pions produced in the interactions. Overlaid on this plot one can see the approximate regions of parameter space covered by the u/p identification capabilities of the TPC and the TOF. In Figure 3.7.4 we can see the three-dimensional plot of the PL-PT-plane in which the third coordinate is the acceptance of the TPC for pions produced by 15 GeV/c incident protons (dark grey) or the corresponding acceptance of the magnetic spectrometer (light grey). This plot shows that the acceptance of pions over the full phase space is almost 100% and confirms the 4π capabilities of the HARP detector.

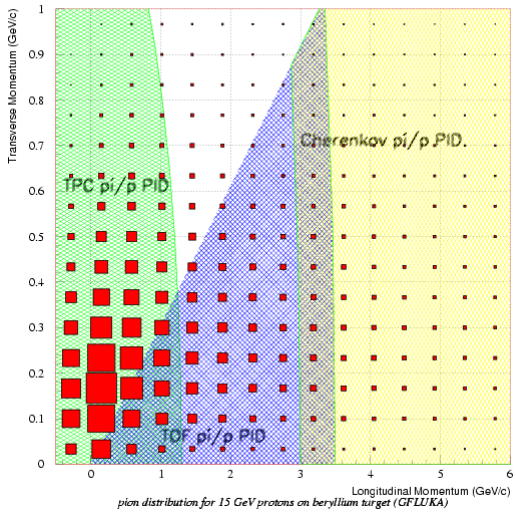

Figure 3.7.3 : Transverse-longitudinal momentum plane *(d2N/dpT* dPL) distribution for the secondary pions produced by a 15 GeV/c protons impinging on a thin beryllium target

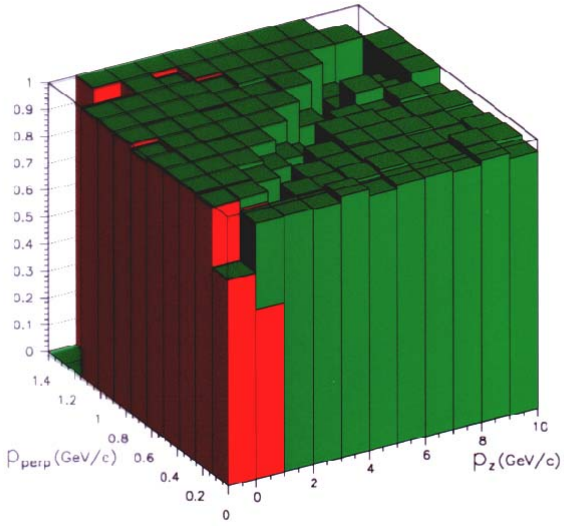

Figure 3.7.4 : Longitudinal and transverse momentum vs. TPC acceptance for pions produced by 15 GeV/c protons.

3.7.3 Collected data and preliminary results

Tables 3.7.2 and 3.7.3 summarize the data collected by the HARP experiments in the years 2001 and 2002. Each entry in the table is the number of recorded events per setting in units of Million of events. A setting is a combination of a given beam energy, target (material and depth) A pilot analysis was done in the spring 2002 using a 3GeV

protons beam impinging on a Tantalum Target and selecting large-angle' tracks in the TPC . The main aim of this analysis was to test the reconstruction software and the data analysis chain. No sophisticated detector calibration and inter-calibration was performed so the results can be largely improved. The analysis of large-angle tracks is clearly focused on the reconstruction of tracks in the TPC. The extrapolation of reconstructed tracks to small radii into the ITC, and to large radii into the barrel RPC chambers, permitted the determination of the efficiency of these devices. The efficiency of the ITC trigger was confirmed to be higher than 99%, the efficiency of the RPCs is at least 95%.

The reconstruction of tracks in the TPC shows a high pattern recognition and momentum fitting efficiency. The efficiency for finding tracks was estimated to be 98%, for tracks with at least 10 points. To select events occurring in the target and to remove overlay events, tracks are extrapolated to the nominal beam axis and are required to originate from the target position. In addition, the tracks are required to point to an RPC hit inside the trigger time window. The combination of these criteria reduces the background to below the 1% level.The two criteria select largely overlapping samples, allowing the determination of their efficiency.

In Figure 3.7.5 the two-dimensional distribution of the transverse and longitudinal momentum are shown for a thin (2% of the interaction length) Ta target with the corresponding distribution for tracks with negative charge.

The geometrical acceptance of the track selection removes tracks with small angles with the beam axis in the backward and forward direction. A cut of 2 GeV/c was applied on the momentum to remove measurements outside the present sensitivity range (only about 10^{-3} of the tracks were removed).

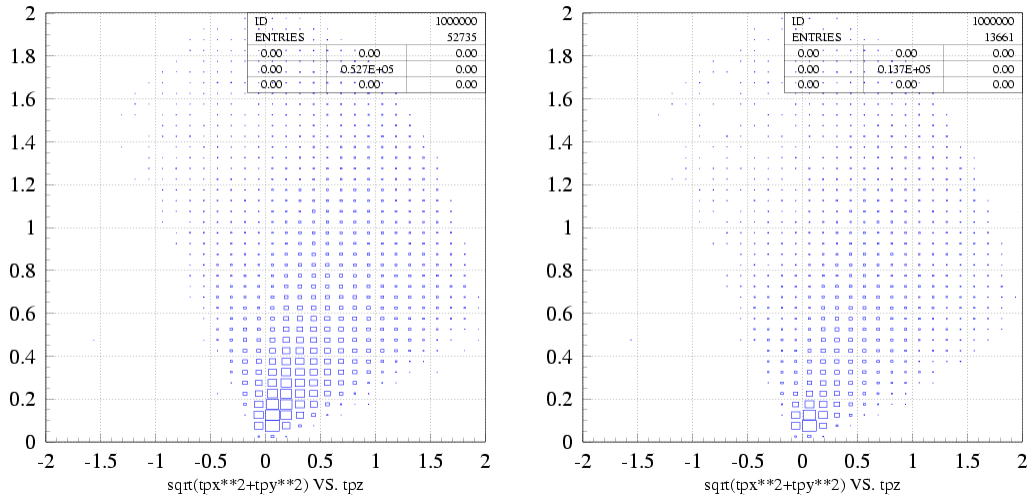

Figure 3.7.5 : Measured two-dimensional distribution of the transverse and longitudinal momentum for a thin (2% of the interaction length) Ta target with the corresponding distribution for tracks with negative charge.

Table 3.7.2

Target	+3 GeV/c	+5 GeV/c	+8 GeV/c	+12 GeV/c	+15 GeV/c
Be 2%	2.2	2.3	—	5.9	1.8
C 2%	2.4	—	—	—	2.7
C thick	—	—	—	—	—
Al 2%	2.4	2.1	—	3.8	2.3
Cu 2%	3.6	1.5	—	2.0	3.0
Cu thick	—	—	—	—	—
Sn 2%	1.3	—	—	—	2.2
Ta 2%	4.9	1.5	—	1.6	2.6
Ta thick	1.1	—	—	—	—
Pb 2%	4.4	1.5	—	2.5	2.3
Pb thick	1.0	—	—	—	—
empty	1.0	1.2	—	1.4	0.1
Target	-3 GeV/c	-5 GeV/c	-8 GeV/c	-12 GeV/c	-15 GeV/c
Be 2%	0.2	0.76	—	1.2	1.3
C 2%	—	—	—	0.86	1.1
Al 2%	0.27	0.79	—	0.88	0.90
Cu 2%	—	—	—	1.11	0.7
Sn 2%	—	—	—	—	1.2
Ta 2%	0.82	0.80	—	0.6	2.1
Pb 2%	0.94	0.34	—	0.7	1.4
empty	—	0.86	—	—	0.06
Special Targets					
K2K at 12.9GeV /c		thin: 1.5M,		medium: 2.2M,	thick: 1.4M
MiniBoone Be at 8. GeV /c		3.2M			
Cu "button" at 12.9 GeV /c		1.45M			

Table 3.7.3

Target	+3 GeV/c	+5 GeV/c	+8 GeV/c	+12 GeV/c	+15 GeV/c
Be 5%	1.54	1.95	2.23	0.63	0.91
empty	0.13	0.10	0.14	0.18	0.15
Be thick	1.16	1.09	1.09	1.81	0.74
C 5%	1.63	3.37	2.27	2.15	0.81
empty	0.37	-	0.32	0.23	0.14
C thick	1.11	1.12	1.01	0.66	0.96
Al 5%	1.93	2.07	2.22	0.73	0.71
empty	0.12	0.20	0.16	0.14	0.14
Al thick	1.34	1.29	1.27	1.15	0.70
Cu 5%	1.16	2.49	2.95	0.85	0.65
empty	0.16	0.14	0.14	0.14	0.15
Cu thick	1.12	1.58	1.40	1.93	0.83
Sn 5%	1.87	3.25	3.15	2.05	0.63
empty	0.21	0.14	0.17	0.14	0.15
Ta 5%	2.62	2.38	2.33	1.04	0.62
empty	0.15	0.10	0.20	0.15	0.08
Ta thick	1.01	1.33	1.49	1.56	0.61
Pb 5%	2.49	3.41	3.32	0.72	0.64
empty	0.10	0.10	0.16	0.08	0.09
Pb thick	0.76	1.26	0.98	1.12	1.10
Target	-3 GeV/c	-5 GeV/c	-8 GeV/c	-12 GeV/c	-15 GeV/c
Be 5%	2.33	1.39	1.76	1.21	0.85
empty	0.17	-	0.05	0.06	0.04
C 5%	2.26	1.81	1.63	0.74	0.62
empty	0.24	0.10	0.07	-	0.05
Al 5%	2.17	1.11	1.38	0.75	0.62
empty	-	-	0.7	0.09	0.05
Cu 5%	3.20	1.23	2.28	0.85	1.06
empty	0.08	0.24	-		0.03
Sn 5%	2.08	1.82	1.58	1.35	0.27
empty	-	-	0.07	0.08	-
Ta 5%	1.66	1.60	1.38	1.03	0.40
empty	0.25	-	0.07	0..08	-
Pb 5%	1.54	2.33	1.65	1.92	1.08
empty	0.11	-	0.10	0.06	0.04
Special Targets					
K2K at 12.9GeV /c	thin: 3.4 , medium: 3.1, replica: 3.67				
MiniBoone Be at 8.9 GeV /c	thin:7.3 , medium: 5.17, thick: 2.84 replica: 4.05				
Cu "skew" at 12 GeV /c	1.71M				
Cu "button" at 15 GeV /c	0.24M				

References

[1] R. Palmer et al., Draft parameters of a neutrino factory, Muon Collider Note 46.
[2] R. Palmer, C. Johnson and E. Keil, A cost effective design for a neutrino factory. talk at Nufact 99 in Lyon, published in Nucl. Instrum. Meth.
[3] B. Autin et al., Prospective study of muon storage rings at CERN, CERN 99-02 (1999).
[4] R. Engel, T. K. Gaisser and T. Stanev, Pion production in proton collisions with light nuclei: Implications for atmospheric neutrinos," Phys. Lett. B 472, 113 (2000)
[5] J. Collot et al., Particle production comparisons between MARS, FLUKA and E910, talk at Nufact 99 in Lyon, be published in Nucl. Instrum. Meth.
[6] J.V.Allaby et al. CERN report 70-12 (1970).
[7] T.Eichten et al.,Nucl. Phys B44, (1972) 333.
[8] T.Abbot et al. Phys. Rev. D45 (1992) 3906.
[9]M. G. Catanesi et al., Proposal to study hadron production for the neutrino factory and for the atmospheric neutrino flux," CERN-SPSC-99-35.
[10]Y. Oyama [K2K collaboration], K2K (KEK to Kamioka) neutrino oscillation experiment at KEK-PS.

[11]E. Church et al. [BooNe Collaboration], A proposal for an experiment to measure muon- neutrino ! electron-neutrino oscillations and muon-neutrino disappearance at the Fermi- lab Booster: BooNE," FERMILAB-P-0898.

4 Activity Reports

4.1 TWAC : the High-Power Accelerator-Accumulator Facility at ITEP

Boris Sharkov, Nicolai Alexeev, Dmitry Koshkarev, ITEP

Boris.Sharkov@itep.ru , naleex@vitep5.itep.ru , dmitry.koshkarev@itep.ru

The TWAC (TeraWatt Accumulator) project at Moscow's Institute for Theoretical and Experimental Physics (ITEP) has successfully passed its proof-of-principle test. This marks completion and commissioning of the new facility's main non-Liouvillian acceleration/accumulation scheme and proper operation of key systems - ion source, ion pre-injector, new RF and power supply systems for the booster ring, beam transport lines and pulsed magnetic elements. For the accelerator/accumulator facility a bunch of carbon-4+ ions from by the laser ion source was pre-accelerated in the new U-3 pre-injector, injected and accelerated in the UK booster ring to 300 MeV/amu, stripped down to 6+ and stacked into the U-10 storage ring. By repeating this cycle several tens of times the batch of about 10^{10} Carbon ions have been accumulated.

4.1.1 Introduction

A former proton synchrotron dedicated to research in nuclear physics and recently mainly applied to radiation therapy, is converted to a medium energy heavy ion complex Figure 4.1.1.

The project takes advantage of an accelerator facility based on both synchrotron and storage rings (34 and 13 TM), and using a non-Liouvillian stripping technique for stacking pulses accelerated in the UK booster synchrotron into the U-10 storage ring. Its aim is to produce a particle beam power of one TeraWatt with ~10^{13} Cobalt ions in bursts of 100 ns, to be accelerated to nearly 0.7 MeV/amu.

Due to the very high particle density aimed at in phase space, an energy deposition of more than 100 kJ/g can be expected in focal spots of ~1 mm in diameter.

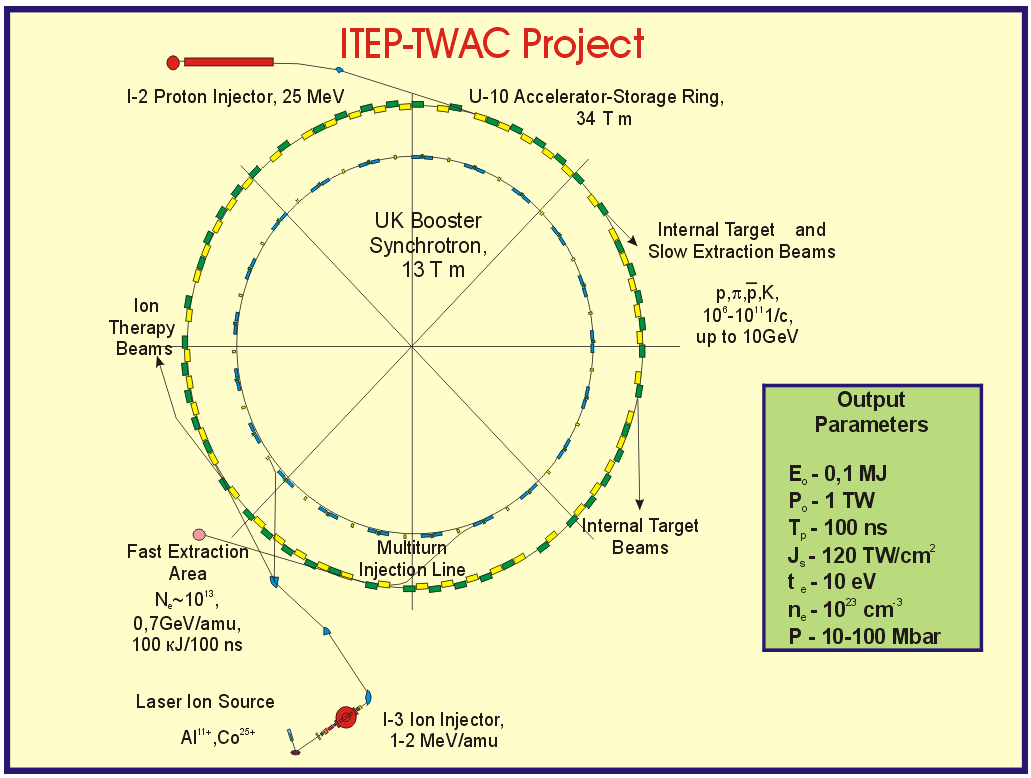

Figure 4.1.1 : Schematic layout of ITEP-TWAC Accelerator Facility.

To achieve the necessary efficiency (= high particle densities at relativistic energies) at TWAC, many challenges on topics in accelerator physics itself can be identified:

(i) only a laser ion source is capable of producing 10^{10} - 10^{11} highly charged heavy ions in pulses of some microseconds length at repetition rates of 1 Hz,

(ii) Non - Liouvillian stacking technique is needed to accumulate sufficient ions before extraction to, and bombardment of any experimental target,

(iii) pulse compression of almost a factor of ten in time has to be mastered just before extraction and

(iv) an ultra high vacuum must reduce the recombination of the fully stripped atoms circulating in the accumulator ring.

For this first phase, the ion source [2], based on 5J/0.5 Hz TEA CO_2-laser, has been operated and installed in the U-3 pre-injector area. The 20 mA/10 μs carbon ion beam was matched to the 2 MV/2.5 MHz pre-injector.

The accelerated 16 MeV carbon-4+ ion beam was guided by the new beam transport line to the UK booster ring and injected . The intensity measured at the injection point is around 1.5 x 10^{10}/10μs. The power supply of the UK booster ring magnets, of the vacuum system, and of the RF accelerating cavities has been upgraded, and the carbon beam accelerated up to 300 MeV/amu.

Pulsed magnetic components of the beam-transfer line connecting the UK booster and U-10 rings required for the multiple injection scheme have been manufactured, installed and tested.

Stripping target (5 mg/cm^2 of mylar) providing non-Liouvillian operation has been designed and installed. The whole acceleration/accumulation scheme has been tested by repetition of several tens of pulses sequence for C^{6+} ions.

A 86 m long new beamline for fast extraction to the beam-target interaction area has been constructed. Focusing elements and the interaction vacuum chamber are manufactured and installed in the experimental area. First beam-target interaction experiments by using γ-diagnostic were performed.

For the second phase of the project, two new beam transport lines and a slow extraction systems will be designed for beam delivery to the medical and relativistic nuclear physics experimental areas.

The application of electron cooling for increasing of the phase space density of accumulated beam will be investigated, and design of the new linac-injector completed.

A powerful CO_2-laser with 100 J/30 ns output at 1 Hz will be set in operation. Together with the upgrading of the main accelerator-accumulator systems and with implementation of the pulse compression system, the intensity of the heavy ion beam will then reach the maximal (target) values:

- In ion **acceleration mode** supplying up to 4.3 GeV/amu and up to 10^{10} particles/s;
- In ion **accumulation mode**, 300-700 GeV/amu and $10^{12} – 10^{13}$ particles per ca.100 ns pulse;
- In **medical application** mode, some 250 MeV/amu, 10^{9} - 10^{10} particles/s.

The TeraWatt Accumulator (TWAC) project ITEP Moscow, is a multi-disciplinary scientific undertaking. Its essence is to upgrade and modify the ITEP accelerator complex to new unique capabilities for investigating the following fields:

extreme states of matter with high density and temperature and their relation to the physics stellar interiors;

basic research into the properties of the nuclear matter (relativistic nuclear physics); and

medicine and radiobiology for tumour therapy using carbon ions.

Former research in relativistic nuclear physics will get a new boost: TWAC will - for modest ion beam intensities - also allow accelerating ions to 4.3 GeV/amu. None of the new research areas will stop the accelerator complex to continue to service for cancer treatment. The C^{6+} will become a second, very effective, projectile.

4.1.2 General scheme

The layout of the ITEP Accelerator Facility upgraded to the TWAC project is shown in Figure 4.1.1. Project parameters of the TWAC are listed in Table 4.1.1. The laser ion source is being used for generation of highly charged ions (Z/A ~ 0.25÷0.45) with atomic mass of up to ~60 and at extraction potential of about 50 kV. Preliminary acceleration of ions is carried out in the linear injector I3 up to the energy of 1÷2 MeV/amu. The booster synchrotron UK accelerates an ion beam to a nearly relativistic energy for stacking the energetic beam into the accumulator ring U10 by using a non-Liouvillian charge exchange injection technique. The multiple injection system adjustment has been completed by demonstrating the C^{4+}=>C^{6+} beam stacking at the

energy of 200 MeV/amu. The current growth of the stacked beam by factor of 10 at the accumulation test has been limited by the beam vacuum loss in accumulator ring (10^{-8} Torr), low repetition rate (<0.3 Hz), and diminished dynamic aperture of the U10 in the shortage of magnetic field correction. The nearest term goal for the TWAC advance is the accumulation of $2 \cdot 10^{12}$ bare C nuclei reaching the predicted space charge limit for the available facility configuration.

4.1.3 Laser ion source

The laser ion source is the best one for the TWAC as there is no other type of ion source with comparable value of output current and pulse length for a high charge state heavy ion beam (A~60, Z/A ~ 0.25÷0.4) [2]. Those features of the laser ion source make it possible to fill the synchrotron ring in single turn injection mode. The $5J/CO_2$ laser ion source with carbon target installed in the linear injector I3 line is good enough for adjusting of a stacking technology implemented in the TWAC project, but it's not suitable for generation of heavier ions to be used in the teraWatt level facility. That means the present ion source has to be replaced by the laser ion source based on 100J/30 ns CO_2-laser. Recent modifications in the laser ion source have been implemented for improvement of beam stability and increasing of output beam current. The peak current of carbon ions is observed at the output of extraction gap is in the range of 500 mA. This value of current is too high for the I3 acceptance and cannot be transferred without loss through the I3 matching channel designed for the beam current of no more than 50 mA. The optimum current of the C^{4+} beam for the I3 input is of the order of 30 mA. A Wien filter is used in the I3 matching channel for the beam separation. The charge state distribution changes along the beam : . C^{4+} and C^{5+} ions are more abundant in the front part of the beam whereas C^{3+} ions near the tail.

4.1.4 Features of the I-3 injector

The Ion Injector I3 was modified in accordance with the requirements of the TWAC project. It's a single drift tube linac whose parameters are listed in Table 4.1.2. This injector is not a best choice for a high intensity ring accelerator because of low energy, low accelerating frequency (2.5 MHz) and a high bunch current requiring very long travelling distance for debunching. The current of the C^{4+} beam at the output of the I3 has been shaped into 80 mA/2.5 MHz short bunches. Therefore, high bunch current cannot be transferred without losses through the U3/UK beam line and cannot provide stable beam circulation in the UK ring because of excessive space charge forces. Transmission of the beam from the I3 output to the UK input is in order of 50%.

4.1.5 Beam acceleration in booster synchrotron UK

Present configuration of the booster synchrotron UK is suited for acceleration of partially stripped C^{4+} ions with energy raise from 1.3 MeV/amu to 300 MeV/amu at repetition rate up to 1 Hz (Table 4.1.3). The maximum energy for the C^{4+} beam in the UK ring is limited presently by the RF variation factor, which is the order of 15 for the acceleration system available. This variation factor is obtained from two ferrite loaded resonators working in sequence and modulated in the frequency ranges of 0.6÷2.2 MHz and of 2.2÷10 MHz correspondingly. The change of bucket for the bunch beam, on the

ramp of the accelerating cycle, is provided without particle loss by matching RF phases and amplitudes in both resonators. The reached intensity of the C^{4+} beam in the UK is now of the order of 3 10^9 and it is limited by three main factors: the relatively low injection energy, large travelling distance for the injected beam (~50 m) and the vacuum losses of the beam during acceleration cycle. Subsequent improvement of the vacuum in the UK ring by factor of 2 or 3 will be achieved with implementation of additional non-evaporable getter pumping. Improvement of the ring magnet correction system and implementation the adiabatic beam capture will increase the UK intensity by factor of 2-3. Thus it is reasonable to reach in the UK ring the intensity of (5÷6) 10^9 for the accelerated C^{4+} beam.

The beam accelerated in the UK is extracted fast for transfer and injection into accumulator ring U10. Extraction kicker magnet consists of six identical modules each of effective length 300 mm. The pulsed magnets are excited from individual pulse generators charged to 45 kV. The pulse rise time is 300 ns, the flat-top time is 500 ns. The total kick strength is up to 0.16 T·m. The kicker magnets are equipped by a bakeable ceramic vacuum chamber matched by the 80 mm aperture to the UK circulating beam at injection.

To obtain a practically loss and dilution-free extraction and transfer of the accelerated beam from the UK to the U10 providing reasonable gaps for kickers, a rebunching RF system with harmonic number 1 has to be adjusted in the UK ring by using one of accelerating resonators. The control for RF gymnastics is being prepared for tests.

The position of the extraction kicker magnet and a schematic layout of the transfer line between the UK and the U10 are presented in Figure 4.1.2. This transfer line is designed to have a transverse acceptance of 15 π·mm·mrad. Transverse matching in both planes is achieved by four quadrupole magnets positioned between two chains of C-core bending magnets. The magnets are laminated to be pulsed from a capacitor discharge power supply with a half sine waveform 10 ms long for the magnet SM and 19 ms for the magnet BM. The deflection in the BM is 90 mrad, maximum field is 1.5 T and the magnetic length is 0.6 m.

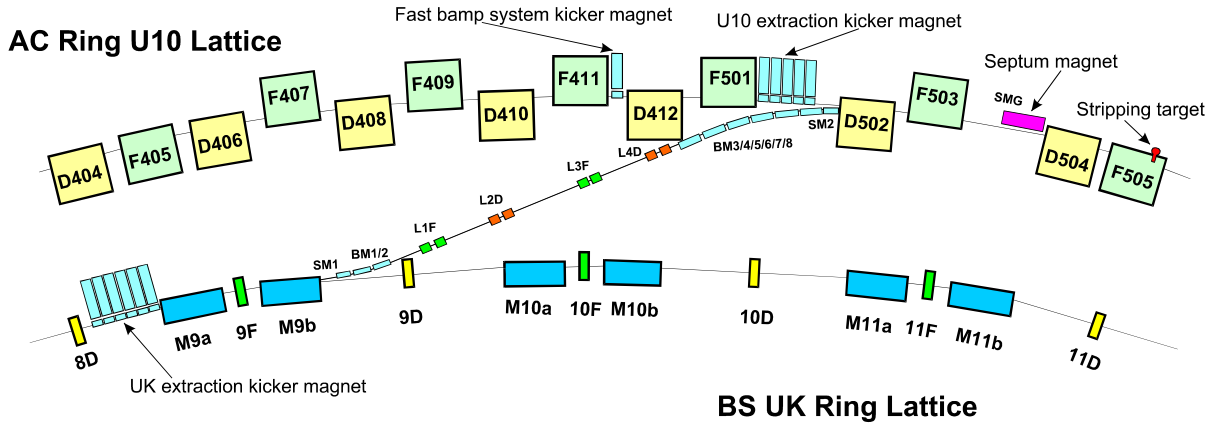

Figure 4.1.2 : Schematic layout of Beam Transfer Line UK/U10.

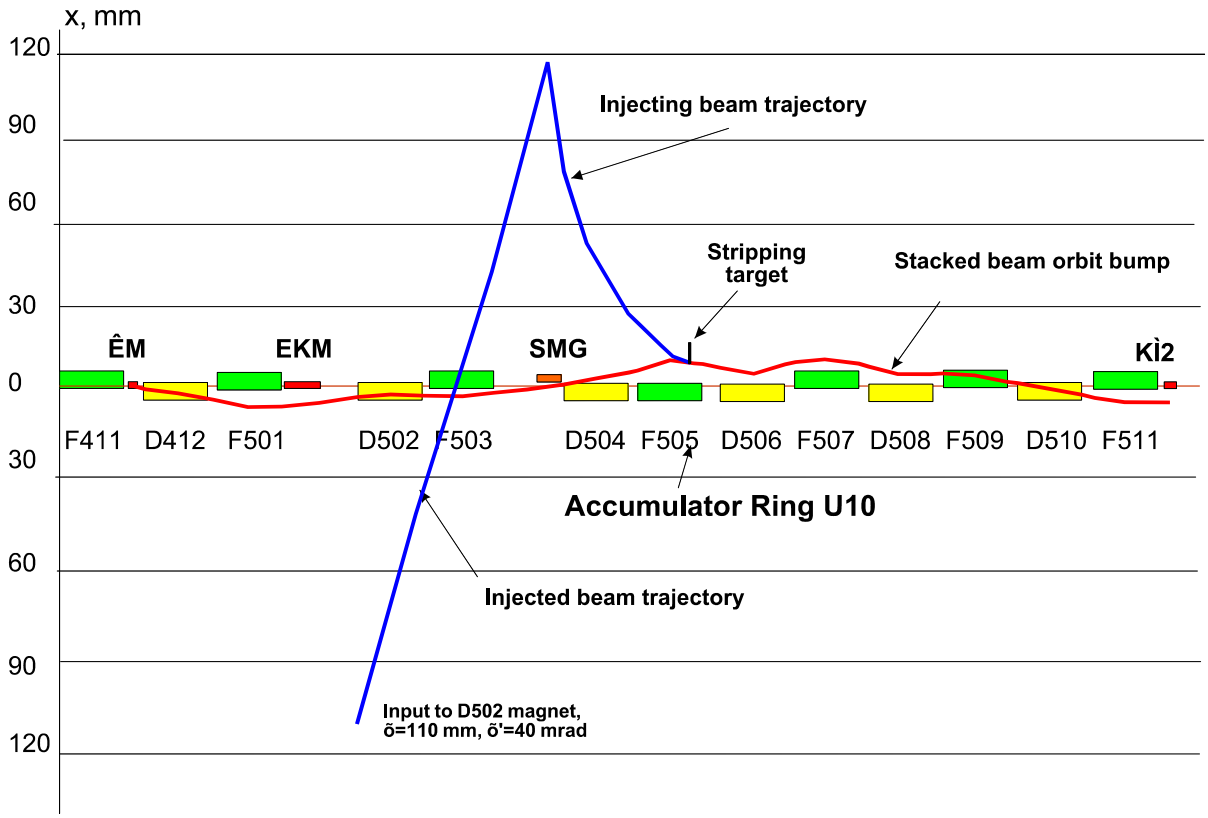

Figure 4.1.3 : Beam trajectory and multiple injection system elements in the accumulator ring U10.

4.1.6 Accumulator ring U-10.

Parameters of the U10 ring are listed in Table 4.1.4. This ring is adapted for ion accumulation from the 10 GeV proton synchrotron. The ion accumulation procedure [3,4] is based on the charge-exchange injection using a fast bump system for minimising the stacked beam perturbation by crossing the stripping foil material. Schematic layout of the beam trajectory at injection and the injection elements are shown in Figure 4.1.3. The septum magnet SMG with magnetic length of 0.8 m is placed outside of the U10 ring between magnets F503 and D504. It's pulsed from a capacitor discharge power supply with a half sine waveform lasting 20.3 ms. This magnet is used not only for the beam injection but also for extraction. The deflection of the C^{4+} beam in the septum magnet at injection is 98 mrad, the maximum field is 1.2 T. Slight gradient of the magnetic field in the septum magnet focuses the beam at extraction. The SMG steers the injected beam to the centre of the stripping foil of 5x10 mm size, which is placed in the vacuum chamber of the F505 with a displacement of 20 mm from the ring equilibrium orbit. The fast bump system matching of both injected and circulating beams includes three kicker magnets installed in the short straight sections after of the magnets F411, F511 and F711. The rise- and fall-time for the kicker magnet pulse is 300 ns, the pulse flat-top is 500 ns. The first kicker magnet gives the kick of 3 mrad deflecting the stacked beam to the stripping foil at a moment when the

injected beam is passing through the transfer line. The two beams, becoming one after passing through the stripping foil, are set to the ring closed orbit downwards by the kicker magnets in straight sections of F511 and F711. The foil material is 5 mg/cm^2 mylar, that yields >90% of bare carbon ions at projectile energy of >50 MeV/amu.

4.1.7 Experiments on carbon beam stacking.

The adjusting of the multiple injection system has been carried out in several steps. The first step was to transfer the beam through the small aperture of 30x55 mm in the five meter long, seven dipole modules, bending magnet with total deflection of 28.8^0. The transferred beam would be observed on the screen in the station after the magnet F502.

The second step was to hit the stripping foil with the beam by steering the magnets SM2 and SMG. The centre of the foil has been positioned at the point of the ring equilibrium orbit. The beam penetrating through the foil and ions stripping was identified by the negative signal from the foil indicating electrons tearing off.

When the charge-exchange process has been obtained, the next step was to get the first revolution of the stripped beam in the U10 ring. Steering the injected beam trajectory and the closed orbit in the point of the foil crossing, the first revolution of the ion beam was trapped confirming correctness of the calculated kinematics for the beam passing through the injection elements.

The circulation of the injected beam was a result of the stripping foil displacement to 20 mm from the closed orbit and the fast bump system activation for setting the stripped beam to the closed orbit trajectory.

The beam stacking test was the next logical step for adjusting of the accumulation process. As the repetition rate for the U10 multiple injection is less than 1 Hz, the required lifetime for circulating beam has to be at least several seconds. As soon as the construction of the shielding chamber has been changed and the perturbing field was eliminated, the beam circulation time increased to dozens of seconds according the vacuum conditions in the U10 ring.

The beam accumulation test was carried out in the U10 ring with the RF on with voltage of 1 kV and harmonic number two providing recapture of the injected beam that had been bunched before in the booster synchrotron UK with harmonic number ten. Periodicity of accelerating cycles was set to 3.5 s. Matching of both injected and stacked beams was reached by careful steering of the fast bump system, of the injected beam trajectory and of the orbit position to the stripping foil. As a result of accumulator adjusting, the stacking process has been launched and a beam current in the U10 ring started to increase from cycle to cycle up to the level of 1.4 10^{10} (Figure 4.1.4).

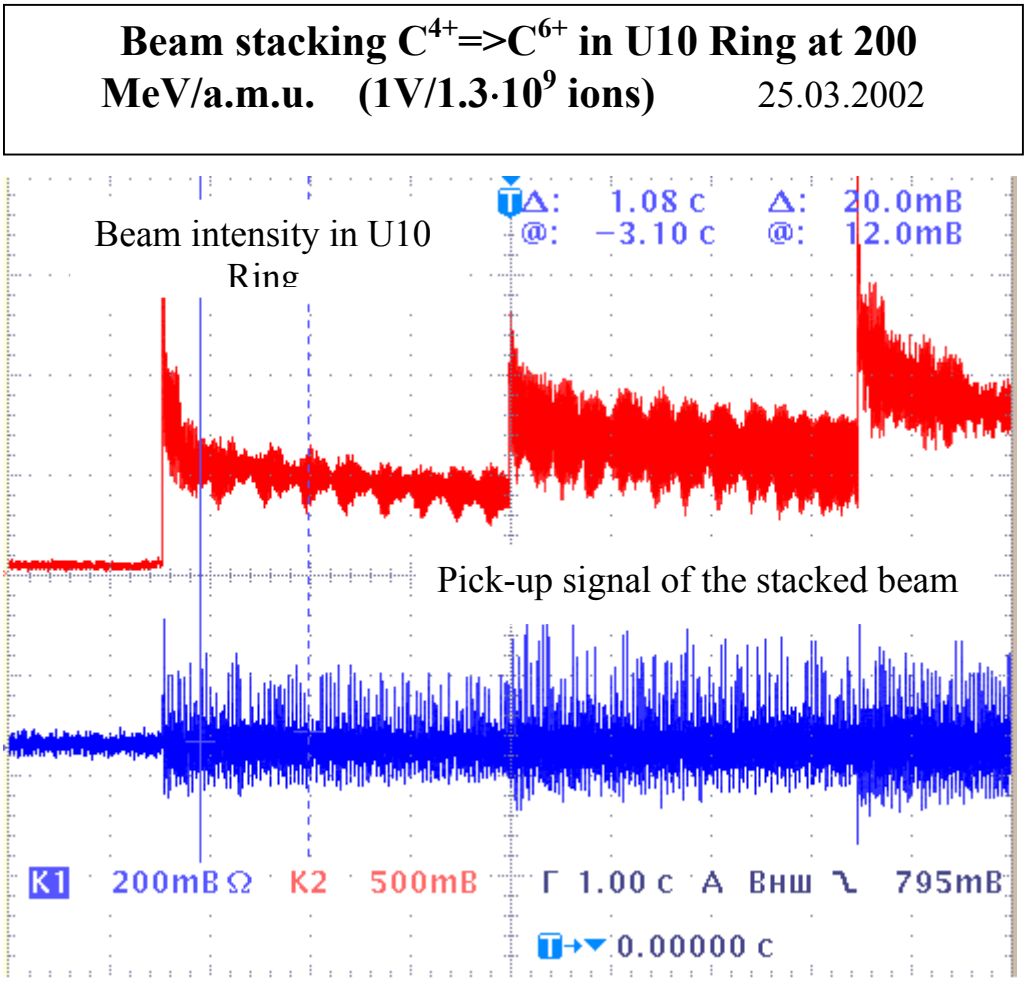

Figure 4.1.4 : The C^{6+} beam stacking in the accumulator ring U10 at the energy 200 MeV/amu.

4.1.8 Outlook for TWAC advance.

By obtaining the stacking process in the accumulator ring U10, the basic non-Liouvillian stacking technique of the TWAC project was demonstrated to be really working well. Now it can be successfully used for ion beam accumulation with increasing phase space density. Expansion of a dynamic aperture for the accumulator ring and mastering the multiple injection procedure is the nearest goal for the TWAC team activity. Parameters of the stacked beam seem to be achieved in the frame of available TWAC configuration taking into account the IBS limit for the stacked beam intensity are given in Table 4.1.5. The stacked energy increase can be achieved by substitution of the 100J laser of the ion source for the 5J one, as it was outlined in the project. Nevertheless, it becomes clear now that this solution is not optimal for the TWAC because of the IBS limit. This process can cause the limitation for the increase of the stacked beam current considerably. The only way to overcome the IBS effects is to speed up the accumulation process. Fortunately the TWAC facility has a precondition to do it as the magnets in the booster synchrotron UK are laminated for the repetition

rate of 20 Hz. The expected parameters for the 20 Hz TWAC operation mode are given in Table 4.1.6.

4.1.9 Conclusions

1. The TWAC facility is in permanent progress and the following milestones have been passed successful:

generation of high charge carbon ions in the laser ion source,

matching and pre-acceleration of the C^{4+} ion beam in 4MV injector I3,

acceleration of the C^{4+} beam in the booster synchrotron UK up to the energy of 300 MeV/amu,

stacking of 10^{10} C^{4+}=>C^{6+} ions in the accumulator ring U10.

2. The nearest term goal for the TWAC advance is the optimization of the multiple injection procedure for the stacked beam current increase up to the limit of the presently available facility configuration.

3. The proposed upgrade to the 20 Hz TWAC facility operation mode and the implementation of the e-cooling system are the subjects for detailed considerations and discussions.

References

[1] B.Yu. Sharkov, D.G.Koshkarev, M.D.Churazov, N.N. Alexeev, M.M.Basko, A.A. Golubev, P.R. Zenkevich, NIM A 415 (1998), 20-26.

[2] B.Yu. Sharkov, S.Kondrashev, I.Roudskoy, S.Savin, A.Shumshurov, H.Haseroth, H.Kugler, K.Langbein, N.Lisi, H.Magnusson, R.Scrivens, S.Homenko, K.Makarov, V.Roerich, A. Stepanov and Yu. Satov, Rev.Sci.Instrum, 69, 1035 (1998)

[3] B.Yu.Sharkov, N.N.Alexeev, A.A.Golubev, D.G.Koshkarev, P.R.Zenkevich, NIM A 464 (2001), 1-5.

[4] Alexeev N.N., Bolshakov A.E., Mustafin E.R., Zenkevich P.R. (1998) "Simulation of Accumulation Process in ITEP-TWAC", *Proc. EPAC98*, 1141-1143.

Koshkarev D.G., Alexeev N.N., Sharkov B.Ju. (1996), ITEP Accelerator Facility Upgrade, *Proc. XV Workshop on Charged Particles Accelerators, Protvino*, 2, 319-321 (1996).

Table 4.1.1 : Project parameters of the TWAC

Stacked beam energy, E_0	100 kJ
Stacked beam power, P_0	1 TW
Beam pulse length, T_0	100 ns
Beam power density, J_0	120 TW/sm^2
Electron temperature in matter, t_e	10 eV
Electron density in matter, n_e	10^{23}
Internal pressure in mater, P	10-100 Mb

Table 4.1.2 : Parameters of the injector I3

Accelerating frequency, MHz	2.504 MHz
Number of acc. gaps,	2
Voltage per gap, MV	2
Length of drift tube, mm	1920 mm
Aperture, mm	70-90 mm
Length of first acc. gap, mm	250 mm
Length of second acc. gap, mm	230 mm
Transverse acceptance	up to 2000 π mm mrad
Buncher peak voltage	10 kV
Max. output beam current, mA	5 mA

Table 4.1.3 : Parameters of the booster synchrotron UK

Orbit length, m	223
Max. magnetic rigidity, T m	9.8
No. of long straight sections	42 x 3 m
Betatron frequency	5.75
Max. of betatron amplitude function	18.2 m
Max. of momentum compaction function	2.1 m
Vacuum, Torr	5 10^{-10}
RF variation range, MHz	0.6÷10
RF amplitude, kV	10
Acceptance h/v, π mm mrad	120/90
Maximum repetition rate, Hz	20
Operation repetition rate, Hz	1

Table 4.1.4 : Parameters of the accumulator ring U10

Orbit length, m	251
Max. magnetic rigidity, T m	34
Betatron frequency, h/v	9.25/9.25
No. of long straight sections	16 x 2.3 m
Vacuum, Torr	5 10^{-9}
RF variation range, MHz	0.9÷4.9
RF amplitude, kV	50
Acceptance h/v, π mm mrad	80/50

Table 4.1.5 : Expected parameters of the TWAC in available configuration

Facility configuration	Laser energy Injector energy Repetition rate	5 J 4 MV 1 Hz
Stacked ions	$_{12}C^{4+}=>_{12}C^{6+}$	
UK intensity	$6\ 10^{9}$	
Stacked ion energy	4.9 GeV	
Stacked beam intensity/energy	$1.8\ 10^{12}$/2 kJ	

Table 4.1.6 : Target parameters for 20Hz TWAC

Facility configuration		Laser energy Injector energy Repetition rate	50 J 7 MeV/amu 20 Hz
Stacked ions	$_{12}C^{5+}=>_{12}C^{6+}$	$_{27}Al^{10+}=>_{27}Al^{13+}$	
UK intensity	$2.5\ 10^{11}$	$1.5\ 10^{11}$	
Stacked ion energy	11 GeV	21 GeV	
Stacked beam intensity/energy	$1.1\ 10^{14}$/190 kJ	$3.9\ 10^{13}$/130 kJ	

5 Recent Doctoral Thesis

5.1 3D Simulations of Space Charge Effects in Particle Beams

Andreas Adelmann ,ETH Zurich and PSI

aaadelmann@lbl.gov

Thesis number 14545
Supervisors Prof. Dr. R. Jeltsch and Prof. Dr. R. Eichler
Date: April 2002

For the first time, it is possible to calculate the complicated three-dimensional proton accelerator structures at the Paul Scherrer Institut (PSI). Under consideration are external and self-effects, arising from guiding and space-charge forces. This thesis has as its theme the design, implementation and validation of a tracking program for charged particles in accelerator structures. This work form part of the discipline of Computational Science and Engineering (CSE), more specifically in computational accelerator modeling.

The physical model is based on the collisionless Vlasov-Maxwell theory, justified by the low density (~10^{9}protons/cm^{3}) of the beam and of the residual gas.

The probability of large angle scattering between the protons and the residual gas is then sufficiently low, as can be estimated by considering the mean free path and the total distance a particle travels in the accelerator structure.

In this model a particle feels two forces: external forces from the guiding and acceleration structures, and internal space-charge forces arising from the coulomb interaction.

The external forces are obtained from a relativistic Hamiltonian using

Lie-Algebra methods and series expansion. The result of this procedure is a set of maps, which allow particle transport through arbitrary magnetic elements. The internal space-charge forces are obtained by solving the Poisson equation in an open domain.

The particle-mesh method interpolates the charge density on to a rectangular mesh. It is then Fourier transformed into the reciprocal space. The Hadamard-Product with the charge density and the Green's function (both in the reciprocal space) are then subsequently transformed back to real space allowing us to compute efficiently the time-consuming convolution. The electric field is then obtained from the scalar potential, by the use of a second-order finite difference scheme.

Again by using interpolation, we obtain the electric field in the continuum. A split-operator integration scheme is used for solving the equation of motion.

In a series of calculations of the 870 keV beam line at PSI, we could confirm the model by comparing the results with measured density profiles in vertical and horizontal directions. With the use of stochastic optimization (Simulated Annealing), the initial conditions (start distribution) are found and the space-charge neutralization factor is estimated. This set of parameters describes the initial conditions for the Injector 2 cyclotron calculations. All calculations show good to very good agreement in almost all sections of the 870 keV beam line. At a few places however we observe discrepancies which we attribute to the somewhat simplified model. (Thus there is no modeling of the residual gas, the electron distribution or the image charges). Another source of uncertainty is the initial condition, which are modeled simply by a Gaussian.

The calculations of a coasting beam in the Injector 2 cyclotron could verify 2-D simulations done by Stefan Adam. The vertical emittance appears to be almost invariant, which confirms the separation Ansatz on which the 2-D model is based. The coasting beam is very stable even up to currents as high as 30 mA.

With respect to the upgrade (increasing the intensity) of the PSI proton accelerator facility, from the beam dynamical aspects we could find no limiting factors with the present calculations.

MAD9P (methodical accelerator design version 9 - parallel) can be used over a broad range, as was demonstrated in the Neutrino-Factory design study at CERN. The calculations of the 560-meter long injection line (2 GeV and 22 to 220 mA) show small transversal and longitudinal beam blow-up, which can be easily compensated by small changes in the optics.

In a series of validation calculations using analytically traceable problems (drift in free space and FODO-structure) we obtained very good agreement. The relative errors are in the range of 0.2 … 0.8 x10-2. Two other methods of calculating the space-charge forces are compared: a serial Barnes-Hut-Tree-Code and a serial particle-particle code, as well as different integration methods like: Leap-Frog and Verlet in addition to the

Split-Operator method. The rigorous, object-oriented, parallel design and the corresponding implementation eases the extendibility and portability of MAD9P. At present the code is available on different Linux (Beowulf) Silicon Graphics and IBM SP-2 clusters.

The use of parallel Fourier transforms to solve the Poisson problem, and the full parallelisation of the split operator integration method, allows the following range of problems to be tackled: 10 to 100 million particles on meshes up to $1282 x 2048$. The parallel efficiency is 87.5% on 32 Processors; even using 128 processors we still obtain 37.5% with no code optimization.

6 Workshop and Conference reports

6.1 The 10th ICFA Mini-Workshop on high intensity and high brightness hadron beams - Slow Extraction

Kevin Brown, Ray Fliller III and Nick Tsoupas BNL

kbrown@bnl.gov , rfliller@bnl.gov , tsoupas@bnl.gov

The 10th ICFA mini-workshop on slow extraction took place at BNL on October 15-17, 2002. This was a small, highly focused workshop attended by accelerator physicists from BNL, CERN, FNAL, COSY, GSI, KEK, and TRIUMF. Presentations at this workshop covered most aspects of slow extraction, representing the current state of the art in this well-established and important area of beam dynamics. Proceedings for the workshop are located at the workshop website:

http://www.agsrhichome.bnl.gov/ICFA2002

Slow extraction can be characterized as a process of performing transverse and longitudinal state changes in order to perform a transformation of the inherent bunched structure of the circulating bunches of particles in a synchrotron into a stream of particles which match (typically) fixed target experimental specifications. Many experiments require just a simple dc beam with a duty factor defined by instantaneous rate limits and other detector characteristics. Newer experiments (e.g., the NSF RSVP experiments, http://www.bnl.gov/rsvp) require dc like beams with well-defined bunch sub-structure. Other kinds of transformations include manipulations of the number and spacing of bunches in the accelerator.

The workshop began with an introduction by BNL Collider-Accelerator Department Chair Derek Lowenstein. Derek quickly painted the big picture in terms of current directions in high energy and nuclear physics throughout the world, as well as

the increasing interest in the use of higher energy accelerators for medical applications. There are significant questions about the Standard Model that are best investigated through fixed target experiments, as is demonstrated by recent advances the understanding of the nature of neutrinos as well as next generation experiments such as RSVP.

Although slow extraction is an established technique that has been employed to produce dc beams from accelerators for well over 40 years, a definitive methodology for the accelerator physicist to use in the design of slow extraction systems does not exist. This is largely due to the difficulties of establishing an invariant Hamiltonian description of the beam dynamics. Steve Peggs, BNL, gave a very enlightening description of a methodology in which he develops an N-turn Hamiltonian that is a constant of motion. Steve reviewed the traditional formal Hamiltonian approach and then went on to describe Discrete Time Difference Hamiltonians. The One-turn Difference Hamiltonians are not constants of motion, but they connect to distortion functions and observable time series. On the other hand, the N-turn Hamiltonian, constructed from the One-turn Difference Hamiltonian, is a constant of motion and extracted particles follow the KAM surface of section contours with a speed (or step size) that is proportional to the local contour steepness. This approach provides valuable insights to the designers of slow extraction systems and for the analysis of existing slow extraction systems.

The use of accelerators for hadron-therapy is becoming an important tool for the medical community. Although such facilities are lower in energy and intensity than accelerators required by physicists, they face the same problems as the bigger machines. Marco Pullia, CERN, described existing and planned medical synchrotrons around the world, and then went through a careful analysis of what constitutes a useful beam for medical therapy. For facilities that employ slow extraction to produce uniform in time beams, the main concern is the ac structure of the dc beam. One of the common problems all slow extraction systems share is structure imposed on the extracted beam by power supply ripple. Marco has analyzed this problem, developing the method of transit time analysis. His analysis has lead to a deeper understanding of what happens as particles move from stable motion into resonance and the motion of particles along the resonant separatrices. Through transit time analysis Marco is able to simulate the amount of structure imposed on the dc beam for different slow extraction methods. He showed simulations of the amount of ac structure for three different methods of slow extraction.

The ac structure that develops on the extracted dc beam results from variations in betatron tune. There are two basic approaches to ripple structure correction. The first approach is to work at reducing the tune variations as much as possible by buying highly stable low ripple power supplies and then using harmonic correction feed-forward to a fast, typically air core, quadrupole. The second approach involves increasing the speed of the particle passage through the resonance. This approach

involves locating empty RF buckets over the resonance and accelerating the particles through the resonance between the RF buckets. This method for reducing spill structure has the side effects that RF structure will remain on the spill and extraction losses will increased. How much RF structure remains and what the characteristics are of that RF structure depends on many parameters. There is potential for creating very short bunches with very few inter-bunch particles. This is the basic method that will be used to create short bunches for the KOPIO experiment. Shane Koscielniak, TRIUMF, spoke about the RSVP experiment KOPIO which requires a long (~5 seconds) train of 25 MHz bunches with bunch widths smaller than 250 psec. Shane developed a simulator in order to study methods of making the bunch widths as short as possible. He presented the results of these calculations and the schemes that he studied in order to make narrow bunches. As a result he has learned what parameters promote narrow bunches and in the process is developing an intuition for the complicated 4 dimensional space of transverse and longitudinal coupling inherent in slow extraction systems.

Massimo Giovannozzi, CERN, described a new technique they are studying at CERN, for transferring bunches from the PS to the SPS, of multi-turn extraction using adiabatic capture in islands of transverse phase space. This technique has great potential in other applications. As accelerators achieve higher beam power it may be necessary to deliver those beams in smaller packets, to avoid target failure, pileup and other technical limitations at the detector ends, while still achieving high duty factors. Slicing the bunches up in transverse space avoids having to use rf techniques, such as harmonic changes to perform bunch splitting, which require more time with higher power, larger bandwidth and more expensive rf systems.

A good fraction the meeting consisted of talks in which people described their experiences with slow extraction, and the kinds of problems they are trying to resolve. Hikaru Sato, KEK, gave an excellent talk on their experiences with slow extraction at the KEK 12 GeV-PS main ring, where they extract on a half-integer resonance at a tune of 7.5. Masashi Shirakata, KEK, described in more detail the performance (including extraction efficiency) of the slow extraction system. Dieter Prashun, COSY, described the extraction systems for COSY, where stochastic resonant extraction is employed with control of the dispersion at the extraction septa defined by a Hardt condition (low angular spread in the extracted beam phase space). Extraction is accomplished using a third-integer resonance together with a rectangular frequency spectrum to flatten the momentum distribution resulting in a long and uniform extracted beam pulse. Rende Steerenberg, CERN, described the slow extraction systems at the CERN PS, where they use slow extracted beams for LHC detector tests and two physics experiments. They extract on a third-integer resonance and control the dispersion at the extraction septum to create a Hardt condition. They also use a phase-back phase-forward RF manipulation to produce a uniform momentum distribution. Rende also described a novel method for a dispersion sweep correction system they have employed in their DIRAC beam line. Craig Moore, FNAL, presented his experiences with slow extraction at FNAL. They

employ a half-integer resonant extraction system, which is complicated since extraction occurs from two separate locations in the main injector.

Experience in slow extraction of high intensity beams is limited. Kevin Brown discussed experiences at BNL, which has operated high intensity slow extracted beams for many years. The main difficulty in extraction of high intensity beams is correcting for collective effects. Operating with a positive vertical chromaticity above gamma-transition is required in order to avoid vertical beam blowup and high extraction losses. In addition, we see evidence that operating with a negative horizontal chromaticity begins to cause higher losses at the highest intensities. For AGS operation keeping the peak beam currents as low as possible is also an extremely important factor in avoiding instabilities. A high frequency RF cavity is used to dilute the longitudinal phase space at injection and after transition. We have observed rebunching and random period spill structure that is uncorrelated with power supply ripple and is only reduced by using this cavity as an empty bucket filter. Masahito Tomizawa, KEK, described the next generation high intensity slow extraction system designed for JHF. The goal of this extraction system is to achieve better than 1% beam loss, since residual radiation dose will be significant.

Ray Fliller, BNL and SUNY@Stony Brook, spoke about crystal channeling technologies and applications in slow extraction systems. There are many applications for using these technologies, and experience within the accelerator community is growing.

J.Woody Glenn, BNL, moderated a working group discussion on methods of increasing extraction efficiency and improving spill structure. Woody reviewed the history of improvements at the AGS for both reducing losses and improving spill structure. The basic problem in reducing losses is a matter of either reducing the thickness of the septum, or by reducing the density of the resonant beam at the septum. For example, the step size of the resonant beam can be increased, but at the expense of a larger extracted beam emittance. This is true, at least for half-integer and third-integer resonant extraction schemes. The results will be better for a half-integer system, though, since the distribution of the extracted beam is more uniform than for third-integer. Further improvements in reducing losses can be made by controlling the phase space at the second septum, which can still cause losses by clipping the corner of the extracted beam phase space. Improving spill structure is a matter of improving tune feed-forward systems, which are intrinsically difficult to get working and maintain. Using RF phase displacement (or empty bucket schemes) has proved to be an excellent method for reducing the spill structure, and is very important with high intensity beams. In principle using RF phase displacement will reduce the extraction efficiency. In practice this can be minimized by careful selection of RF parameters.

The workshop will be producing two tables. First is a table that will summarize performance parameters of slow extraction systems discussed at this meeting. The

second table provides a listing of computer codes used in the study and design of slow extraction systems. These tables are not yet complete but will appear on the workshop web site very soon. A preliminary version of the second table can be found in the appendix.

6.2 The 11th ICFA Mini-Workshop on high intensity and high brightness hadron beams - Diagnostics

John Galambos and Tom Shea , ORNL and Kay Wittenburg , DESY

galambosjd@ornl.gov , shea@ornl.gov , Kay@ntmail.desy.de

The 11th ICFA International Mini-Workshop on Diagnostics for High-Intensity Hadron Machines was held at the Spallation Neutron Source (SNS) project office in Oak Ridge TN, on Oct. 21-23, 2002. The purpose of the workshop was to summarize the state of the art in diagnostics, produce a prioritised list of diagnostic developments, and propose experiments to test new diagnostics or techniques. Twenty representatives from 13 projects/institutes attended. The workshop was divided into three sessions; 1) a summary of diagnostics at different institutes, and the accelerator physics needs, 2) general diagnostics and 3) non intercepting profile monitors. These sessions are summarized below. Presentations, an attendance list and other workshop material can be found at http://www.sns.gov/icfa

Prior to the workshop, a table of diagnostics used at high intensity hadron facilities was compiled. Input was also solicited from facilities not able to send participants to the workshop (this table is available from the above workshop web-site). For convenience, it is divided into two parts, one for linacs and another for rings (and transfer lines).

6.2.1 Session 1: Overview of Diagnostic status and Accelerator Physics Needs

There were three classes of talks in this session: 1) a summary of the SNS project and its diagnostics needs, 2) some accelerator physics diagnostic proposals, and 3) summaries of existing facility diagnostic needs and requirements. Some overall themes from this session were identified. First, more use should be made using information from existing diagnostics, and also reliable, believable output is an important characteristic for useful diagnostics. For high intensity machines, a good loss monitor display is an important, commonly used application. Finally, good glitch detection systems are recommended, which are triggered by a machine protection trip and dump circularly buffered data on local diagnostics, throughout the facility. This glitch system should be common for diagnostics, and other systems such as RF and magnets.

SNS: For the SNS, talks were given by N. Holtkamp, S. Henderson J. Galambos and A. Fedotov. A common theme is that attaining MW level beam power for a user facility requires extremely low loss levels and high reliability. Additionally there are time correlation needs of diagnostic data due to the pulsed nature of the machine. The low loss level requirements at high power levels imply not only a good loss monitor

system, but also a need to understand sources of losses, approximately 20 sources of beam "halo" producing mechanisms were identified. Additionally, a need to continuously monitor the beam profile on the neutron target is important and challenging due to the harsh radiation environment.

Accelerator Physics Proposals: S.Y. Lee presented an idea for a quadrupole-mode transfer function diagnostic, which is especially useful for high intensity space charge dominated beams, and can also be used for noninvasive emittance measurement. V. Danilov presented some analysis on beam invariants, aimed at identifying the minimum number of simultaneous phase space coordinate measurements that are needed to unambiguously use measured data in simulations.

Facility Overviews: Regarding facility overviews, the summary table described above provides lists of diagnostics used at facilities, and only highlights are presented here. E. Prebys presented an overview of the FNAL Booster diagnostics. The booster is presently loss limited, but faces a need for intensity increases of up to a factor of eight. There is a need to understand the large injection losses as well as other losses further into the acceleration. A. Feschenko presented an overview of the linac at the Institute for Nuclear Research (INR). This MW level linac is well instrumented, with careful measurement of the low energy beam, including independent bunch shape and energy measurements. J. Dooling presented an overview of the IPNS, which is a loss limited spallation neutron source. An ESEM (energy spread and monitor) system has been developed for on line measurements. Additionally bunch-by bunch measurements have been made following the beam from the linac through acceleration in the ring. P. Forck presented an overview of the GSI diagnostics, including a proposed idea for a MCP and CCD combination for a fast readout of profile measurement. Finally K. Wittenburg presented an overview of the DESY diagnostics, which included an IPM system capable of low intensity profile measurements.

Some overall desires for diagnostic development that were discussed are:

- Single linac bunch profile diagnostics – not averaged.
- Laser-based HARP (simultaneous x-y profile).
- Beam observables vs. time in linac pulse
- Diagnostics capable of handling full pulse length and rep-rate
- Halo/beam tail measurement capability to 10-4 level
- Incoherent tune (tune footprint)
- In-situ Secondary Electron Yield Monitor
- Electron Cloud Monitor (across chamber aperture)
- Beam profile on target measurement
- 6-d phase space tomography
- Higher-order instability monitor
- Laser wire for non invasive H- profile and Emittance measurements
- Good display ergonomics / easy use of measurements
- Better coupling to theory
- Non-destructive Emittance measurement over the entire linac
- Reliable diagnostics

by J. Galambos, ORNL

6.2.2 Session II General Diagnostics

This session covered a wide range of topics that do not conveniently fit in one category. The presentations covered; 1) Intercepting devices (bunch shape monitor, harp, and halo),
2) Issues for High Intensity (electron cloud, loss monitors) and 3) Techniques (superconducting resonators and tune).

Intercepting Devices

The usual issues were raised regarding the insertion of material into high intensity beams, namely lifetime, reliability, and survivability of the target (wire or foil) and that a special study mode is usually required (shorter, lower intensity), interrupting operations.

Regarding Bunch Shape Monitors, impressive bunch length resolution is observed due to continuous improvements over the years, the longitudinal halo measurement can be complicated by higher harmonic of RF in BSM, wire heating is an issue - tungsten generally used instead of carbon and measurements of longer pulses can be made by retracting the wire from core, but bunches may appear shorter.

Harps and multiwire system presentations showed that harps near target see 10 to 100 MR per year. Kapton is successfully used in the LANCE devices near the target but wire lifetime is an issue for the SNS target harp. Actuators are very bulky and complex, but without them, wires are continuously exposed to the high intensity beam.

Halo measurements at LEDA were presented and are the most extensive to date. They utilized a combined wire and foil on a single actuator device to produce excellent dynamic range. The community should encourage follow-on studies that build on this good work. Profile measurements at HERA have demonstrated high resolution measurement of tails. Calibrations with respect to the beam core are challenging and work to develop theory remains. Many proposals are being evaluated for halo measurement in SNS ring, and will be discussed at the ICFA Halo03 workshop in May 2003, Montauk, NY.

Issues for High Intensity

For high intensity rings, dedicated electron collectors are strongly recommended, but some results have been achieved with standard diagnostics. For new installations, distribution of detectors needs some consideration. Questions remain about the required number and placement of electron detectors, i.e, required azimuthal and axial distributions, and locations relative to magnets. An ionisation profile monitor with variable electric and magnetic fields may be a useful device for electron cloud studies. Electron detectors have not been generally used as a tuning device, but are rather used to verify predictions, correlate with other diagnostics/vacuum data. Sufficient bandwidth to see intra-bunch effects is important.

LHC loss monitors use nitrogen used instead of argon. The high dose behaviour may be an issue for LHC and SNS. As in most machines, loss monitors provide the primary diagnostics input to the machine protection system. Availability and reliability must be carefully addressed.

Technique

Coherent tune measurement in high intensity rings can use frequency estimation vs. spectrograph. At LANSCE, 10-3 resolution in 25 turns is attained at PSR. For SNS, multiple techniques for measurement of incoherent tune are being studied including Schottky, BTF, and Quadrupole moment variation. One issue is applicability of the Schottky method on a short/ repetitive pulsed ring like SNS.

Use of superconducting resonators as a diagnostic was discussed, driven by the lack of space for other diagnostics. Up to 20 MeV/au, the RIA driver linac requires 1 deg phase accuracy. Tuning techniques should be compared to those planned for the SNS superconducting linac.

By T. Shea, ORNL

6.2.3 Session III: Non intercepting profile monitors

Solid wire scanners are probably the most trustworthy devices for measuring beam profiles. Unfortunately the wire can be destroyed in high current (and high brilliance) machines by the beam itself. Another problem arises at SNS at scanner positions close to the superconducting cavities: A broken piece of wire might contaminate the surface of the cavity and may lead to quenches. Therefore alternatives were discussed during this session. Mainly three different types of non intercepting profile monitors were presented: 1) Beam Induced Gas Scintillation (BIGS), 2) Residual Gas Ionization Profile Monitors (IPM), 3) Laser Wire Scanners.

BIGS: Presentations by M. Plum, J. Dietrich, P. Forck

In the beginning of the workshop, the question arose of using the BIGS as a profile monitor just in front of the target. It has been shown by J. Dietrich, that this effect will create enough light to measure beam profiles even at good vacuum conditions and low beam current (2·1010 p , 10-8 mbar, 45 – 835 MeV/c). Accurate gas scintillation cross section measurements for N2 and Xe gas at high proton energies (1.4 to 40 GeV/c) were presented by M. Plum. The cross section obtained for N2 is 6.7 times smaller than that expected from dE/dx scaling of previous measurements with 200 keV protons and in addition 3.3 times smaller for Xe gas. The spectra and lifetimes for N2 and Xe were also presented. Based on these measurements one can calculate the sensitivity of this monitor for different setups in accelerators. Some profiles were presented during the workshop, but it was pointed out that there are still unsolved questions: a) This kind of profile monitor is somehow sensitive to background, probably due to adjacent beam losses. b) in the literature one can find some measurements where the BIGS-monitors gave larger beam profiles than other types of profilometers (wire scanners, etc) in the same machine (see for example Refs. 1-3). Solutions discussed were a): moving the light detector far away from the beam, while having enough light from the scintillation

and b): a black painted vacuum chamber. However, Ref. 3 claims that "the light produced does not result only from the incoming protons, but also from several secondary processes which create excited atoms". This should be a subject of further studies.

IPM: Presentations by J. Dietrich, R. Connolly, P. Forck, E. Prebys, K. Wittenburg

IPMs are used in quite a lot of proton accelerators around the world. Most of them give satisfactory results when collecting the electrons from the ionisation process in combination with a magnetic guide field of ³1 kG. For small bunch currents the use of the ions without a guiding magnetic field is also possible, but the space charge of the bunch will disturb the collection of the profile at higher bunch currents. Care should be taken in designing parallel guide fields. The turn by turn profile sampling capability of the IPM was shown by R. Connolly and other references (see for example Ref. 4), which enables the IPM to study injection mismatches (quadrupole or beam shape oscillations). However, a gas bump or gas jet inside the IPM might be necessary to increase the sensitivity of an IPM by some orders of magnitude. Nearly all IPMs use MCPs to create enough gain for signal detection. It was pointed out that the aging of the MCP (i.e. inhomogeneous decrease of the gain) is an important issue. The measured beam profile becomes larger, because the gain decrease is stronger at the centre of the profile than in the tails. The need for an online calibration tool was strongly recommended. Some possibilities were discussed like heated wires, a-source, UV-light, 900 turning of the MCP, beam steering to an unused area of the MCP, … there is still a large area for new ideas.

Sources of background and noise were discussed: RF-coupling to the anode strips might be suppressed by a clever design (?, somehow magic). Beam losses upstream as well as inside and close to the IPM should be avoided by a large aperture of the monitor and the adjacent beam pipes. It turns out, that an important issue for IPMs is the background due to electrons (secondary electrons, clouds) in the beam pipe. It was strongly recommended to extend the HV-electrodes by at least a few centimetres to get rid of the clouds before they can reach the detector.

An unexpected characteristic of the IPM at CERN was observed (B. Dehning): The measured beam width depended on the beam current by several tens of percent, while the beam width measured by a wire scanner was constant. More investigations are needed to understand this effect.

Laser wire scanner (H- photoneutralization) Presentations by R. Connolly, S. Assadi

This method has been used for transverse and longitudinal emittance measurements where transverse profiles of H- beams have been measured by laser photoneutralization. It is being used at the SNS for measurement of transverse beam profiles. Once a portion of the beam is neutralized by the thin laser beam, measurements can be made on the neutral beam, the removed electrons, or the reduced beam current with beam current transformer or BPM stripline. Experiments which measured the notch in beam current with current transformers and with BPM striplines were successfully performed at BNL and Berkeley.

R. Connolly proposed to detect directly the amount of electrons instead of the difference in the currents. This will have some advantages:

- Detection of electrons requires a far lower neutralization rate.

· A microchannel plate can amplify the electron signal by 104-106, which reduces the laser power requirement to 1W or less.

· Proposed laser is a solid-state, CW diode laser with fibre-optic output. Power ~1W and l= 975-980 nm. It is much cheaper than a high power Q-switched Nd:YAG Lasers.

· With CW laser and electron collection the beam can be scanned with optical scanner and one will get the full beam profile in one machine pulse (300ms). The laser beam can be swept with commercial optical scanners.

· Light might be transported from the laser to the beamline over optical fibres.

Drawback:

· Might suffer from beam loss background and electrons from gas ionisation.

· No longitudinal profile measurement possible

S. Assadi discussed the ideas of the complete laser wire system at SNS, including the laser light transport. It was pointed out that the jitter of both beams (laser and ion) has to be considered. Especially the jitter of different macropulses might disturb a precise profile determination when using the notch technique.

by K. Wittenburg, DESY

6.2.4 Recommended work for the future

· Extensions of LEDA halo studies
· Similar studies for ring halo
· BSM for long pulses
· Electron detector as tuning device
· Further development of incoherent tune measurement techniques
· Enhanced use of machine model for loss monitor data

References:

[1] Residual Gas Fluorescence for Profile Measurements at the GSI UNILAC
P. Forck, A. Bank, GSI, Darmstadt, Proc. Eighth European Particle Accelerator Conference La Villette – PARIS, 3 - 7 June 2002

[2] THE LUMINESCENCE PROFILE MONITOR OF THE CERN SPS
G. Burtin, J. Camas, G. Ferioli, R. Jung, J. Koopman, R. Perret, A. Variola, J.M. Vouillot CERN, Geneva, Switzerland, 7th European Particle Accelerator Conference, Vienna, Austria, 26 - 30 Jun 2000 - European Phys. Soc., Geneva, 2000.

[3] Optical Transverse Beam Profile Measurements for High Power Proton Beam
P. Ausset, S. Bousson, D. Gardes, A.C. Mueller, B. Pottin, IPN, Orsay; R. Gobin, CEA, Gif-sur-Yvette; G. Belyaev, I. Roudskoy, ITEP, Moscow, Proc. Eighth European Particle Accelerator Conference La Villette – PARIS, 3 - 7 June 2002

[4] SENSITIVITY STUDIES WITH THE SPS REST GAS PROFILE MONITOR
F. Ferioli, C. Fischer, J. Koopman, CERN Laboratory, Geneva, Switzerland
5th European Workshop on Diagnostics and Beam Instrumentation, Grenoble, 2001

6.3 International Workshop on Recent Progress in Induction Accelerators

Ken Takayama, KEK

ken.takayama@kek.jp

An international workshop on "Recent Progress in Induction Accelerators" (RPIA2002), was held at KEK, 29-31 October, 2002. The workshop was chaired by K. Takayama and jointly organized by KEK and Tokyo Institute of Technology (TIT). Information on the workshop, including all presentation materials, may be found at the workshop website:

http://www.conference.kek.jp/RPIA2002/

The purpose of the workshop was to discuss recent progress in induction accelerators and related key technologies, which are common to different communities: heavy-ion inertial fusion and high energy accelerators. This specialized workshop focused on four topics: (1) a review of the development in induction acceleration since the first demonstration by Christofilos, their applications, and up-to-date activities in energy science and high-energy physics , (2) new concepts and ideas using induction acceleration, (3) key technologies, such as magnetic materials and solid-state modulators that are indispensable to realize high-gradient accelerating fields and low-loss, high rep-rate operation, and (4) beam dynamics specific to extremely high-intensity beam linacs, circular induction accelerators, and hadron colliders employing a so-called super-bunch.

More than 55 people participated in the workshop from 15 different institutes and 3 private companies. All topics, except for a few poster presentations, were presented in plenary sessions. The attendants to the afternoon session of the last day divided into five working groups: Concept, scenario, and new ideas (G1), Accelerating cavity (G2), Modulator (G3), Beam dynamics in LINAC (G4), and Beam dynamics in Circular rings (G5) and discussed various highlights presented at this workshop and remaining unsolved issues.

In his welcome address H. Sugawara, Director-General of KEK, explained the recent ICFA activity in addition to the status of ongoing and future projects at KEK and insisted on the importance of an investment in accelerator R&D. R. Briggs (SAIC) reviewed the history of the development of induction accelerators from the first generation of ASTRON to the recent ATA/ETA at LLNL and LBNL, and gave an outline of recent applications in energy science and high-energy physics such as a TBA driver, a heavy ion inertial fusion driver, a neutron spallation source driver, and induction synchrotron. He then addressed crucial points concerning newly developed scenario, which had been discussed at this workshop. J. Barnard (VNL) gave an overview of heavy-ion fusion accelerator research in the U.S. Virtual National Lab. covering a whole aspect of the project. M. Shiho (JAERI/TIT) mainly introduced the achievements of R&D work developed in Japan. G. Caporaso (LLNL) reviewed an on-going research program on pulsed power technology at LLNL. J. Kishiro (KEK)

presented the concept of the induction synchrotron and an outline of the POP experiment of super-bunch acceleration at the KEK 12-GeV PS. H. Takahashi (BNL) discussed his idea of super-bunch acceleration in the FFAG scheme. K. Takayama (KEK) described the recent concept of a hadron collider promising a luminosity of more than 10^{35} /sec/cm^2 with super-bunch collision and initiated crucial beam-dynamical issues, such as the relationship between parasitic beam-beam effects and crossing geometry, and the coherent instability of super-bunch, which were given in greater detail following the talks of Y. Shimosaki, F. Zimmermann, T. Toyama. R. Yamada (FNAL) showed an example of a super-bunch collider as a possible candidate for a realistic size VLHC with detailed parameters.

K. Yamamoto (Osaka City Univ./CDF) introduced the present status of the Tevatron collider experiment: Run II and the expected physics goals in the near term. M. Sakuda (KEK) summarized the highlights of the K2K 3 year run as well as the physics of neutrino oscillations and mentioned the neutrino-oscillation experiment of the Joint Project that is expected to start in 2007. D. Michael (Caltech) gave a physics outline of neutrino oscillations, and introduced the present status of MiniBoone and NuMI/MINOS at Femilab. He then commented that an investment in proton intensity must be considered as an integral part of both the current and future neutrino programs at Fermilab. T. Kondo (KEK/ATLAS) reviewed the construction status of the LHC accelerator and described details of the ATLAS detectors. In discussing the possible upgrade plans of LHC, he remarked on the fact that most present detector components can not survive under a 10 times higher luminosity, and concluded his talk with the statement " Energy frontier physicists always welcome higher luminosities, but want higher energies more favorably in general. But if high luminosity is the only way to explore the energy frontier physics, experimentalists will surely challenge and encounter any difficulties along the way."

The second day was devoted to discussing the key devices of induction cavity and its driver. K. Ogura (Hitachi Metal) widely reported on a promising nano-crystalline magnetic material, FINEMET; the subjects were among manufacturing process, its magnetic property and a variety of applications, including hadron accelerator RF and induction devices. On behalf of A. Molvik (LLNL) and A. Falten (LBNL), W. Waldron (VNL) reported on a data-base for the magnetic characteristics of SiFe, METGLAS, FINEMET, assuming their full-swing operation, and discussed their advantages and disadvantages. C. Ohomori (KEK) clearly reviewed the essential characteristics of an RF cavity (MA cavity) employing FINMET and their performance in actual accelerators, including the barrier bucket application. K. Torikai (KEK/Kyusyu Univ.) reported on R&D work concerning a high rep-rate induction cavity for the POP experiment of super-bunch acceleration at KEK, in which a newly developed thinner FINMET tape is used. M. Watanabe (RIKEN) presented a systematic study at TIT on the magnetic characteristics for possible candidates of the core material, and discussed an essential feature of beam loading in the induction accelerating cavity with a small-scale experimental demonstration. Y. Saito (KEK) reviewed the electrical insulation problem in the vacuum of high-energy accelerators from a general point of view, which covered from the microscopic surface mechanism of breakdowns to experimental observations.

I. Oomura (Toshiba) first reviewed the historical development of semi-conducting power devices and reported on the details of the characteristics and performance of the SiC-MOSFET, which is expected as the next-generation switching element for modulators. N. Shimizu (NGK) focused his discussion on the SI-Thyristor, which has demonstrated quite attractive performance as a switching element for a modulator, and insisted on the possibility of its industrial application. W. Waldron (VNL) described a RTA injector pulsed power system consisting of thyratron-switched PFN's, a DARHT-2 PFN in the Marx configuration, and a solid-state modulator for controlling the acceleration wave form in the Heavy Ion Fusion Project, which are characterized by a high output voltage and a low rep-rate or burstmode operation. E. G. Cook (LLNL) introduced the solid-state modulator R&D at LLNL, which covered an inductive adder pulser, a fast kicker pulser, a fast kicker pulser for a proton ring accelerator and an NLC klystron modulator. K. Koseki (KEK) reported on a modulator under development for the POP experiment at KEK, which was operated at a rep-rate of 1 MHz with a resistive load of 300 Ω. K. Fukuda (AIST) introduced an outline of ultra-low-loss Power Devices Technology Japanese National project (1998-2002), where few types of SiC-MOSFET are under development, promising low on-resistance and high breakdown voltage. M. Akemoto (KEK) and H. Sato (KEK) reported on the satisfying performance of a klystron modulator and kicker power-supply using SI-Thyristors instead of the Thyratron, respectively. On behalf of J. Watson (LLNL), G. Caporaso discussed a particular subject for the amplitude control of solid-state modulators for precision fast kicker applications, where the kicker amplitude is modulated in a narrow pulse width through the beam's position feedback system. V. Vogel (KEK) presented ambitious R&D work concerning a solid-state linear induction modulator for the JLC using IGBT, which can drive 4 klystrons.

On the afternoon of the second day we held (three) four poster exhibitions. M. Leitner presented the development of super-conducting magnets for heavy-ion fusion. T. Kikuchi (TIT) demonstrated a system study on a beam buncher using a compact recirculator for beam physics issues of intense heavy ion beams. In addition, two demonstrations were given by Hitachi Metal and NGK: one was a large FINEMET bobin, which was going to be shipped to Fermilab and the other was a SI-Thyristor, which had been employed for the kicker modulator at KEK.

The third day was devoted to discussions on the beam dynamics in linear machines and circular machines. W. Chou (FNAL) reported several possible plans using barrier RF stacking to increase the Tevatron luminosity and the neutrino flux in NUMI, where the goals and methods were described and the specifications of the required hardware including the HTS fast switch were discussed. J. Marriner (FNAL) commented on barrier buckets based on their experience on longitudinal beam handling with a barrier bucket in the Recycler Ring, insisting on the importance of the barrier waveform and particular requirements on the feedback system. Y. Shimosaki (KEK) manifested the relationship between the crossing geometry and the parasitic beam-beam effects of super-bunch collision, and demonstrated how one can control the beam-beam tune spreads by choosing the crossing angle. F. Zimmermann (CERN) described the super-bunch upgrade plan of the LHC and its specific beam-physics issues; in addition he insisted on the advantageous features of the super-bunch scheme such as the mitigated e-P instability and the relatively small heat-load on the cold bore. T. Toyama

(KEK) focused his argument on the head-tail instability of a super-bunch, and demonstrated particular features of the instability based on simulation work.

A. Takagi (KEK) reported on a successful demonstration of a heavy-ion beam chopper using induction acceleration at HIMAC. T. Kikuchi (TIT) reported on crucial problems during the final longitudinal compression stage of the heavy ion fusion driver, such as an emittance dilution or collective effects. In the second presentation, Kikuchi presented a careful study on beam halo formation excited by a parametric coupling between the betatron oscillation of an individual particle and beam core oscillation originating from rapidly increasing space-charge forces during the bunching process. J. Barnard (LLNL) gave an outline of integrated beam-physics experiments for the Heavy Ion Inertial Fusion Accelerator at LBNL, consisting of a 10 MeV linear induction accelerator, a bend/drift compression line and a final focusing system, followed by a plasma neutralization chamber. In addition, M. A. Leitner (LBNL) described the features of the hardware design, a cost estimation, and expected schedule for the above-mentioned integrated beam experiment. Y. Chen (LLNL) focused her discussion mainly on beam-target interactions, that is, backstreaming ion effects, which are specific in x-ray radiography applications.

The workshop sessions were summarized on the late afternoon of the third day by the convener of each working group. They summarized the highlights at related sessions and remaining issues for each application, which must be overcome in the near future. The workshop may be concluded with the following five remarks:

–
– Two big trends of a high-gradient/low-duty and low-gradient/high-duty induction acceleration became notable. Demonstrations of the integrated beam-physics experiment at VNL and the POP experiment of super-bunch acceleration at KEK are remarkably expected.
– The rapid development of the solid-state devices is notable. Their capability has been well demonstrated. Use of new devices, such as SiC-MOSFET in a solid-state modulator is waited.
– Although a low-loss magnetic material with a large swing-amplitude is always desired, our experiences on the use of FINEMET in actual cavities have sufficiently accumulated.
– Beam physics during the bunch compression will provide an useful information to understand the halo formation and emittance blow-up mechanism, which are common to space-charge dominated beams.
– The concept of super-bunch acceleration in an induction synchrotron and collider may initiate new accelerator physics, while the beam handling experiment with the barrier bucket has manifested important aspects of the long-bunch capture.

A conference document will be published as a KEK report.

The organization of the workshop was excellent and participants agreed to have the next meeting within a few years. Credit is given to the Local Organizing Committee (J. Kishiro, K. Nigorikawa, E. Nakamura and Y. Shimosaki), the Program Committee (K. Horioka, E. Hotta, J. Barnard, J. Wei, W. Chou, Y. Chen, R. Garoby and F.

Zimmermann), the International Advisory Committee (W. Barletta, G. Caporaso, J. Marriner, J. Nishizawa, Y. Kamiya, T. Katayama, I. Hofmann, B. Autin, F. Ruggiero and T. Kondo), and the Workshop secretary (A. Shiraishi).

6.4 18th Russian Particle Accelerator Conference

Evgeny Syresin, JINR

syresin@nusun.jinr.ru

The 18th Russian Particle Accelerator Conference (RUPAC-2002) took place on October 1–4, 2002 in the town of Obninsk (Kaluga Region), about a hundred kilometres southwest of Moscow. This traditional biannual conference was hosted by the Physics and Power Engineering Institute (Obninsk) under the auspices of the Russian Academy of Sciences, two Federal Ministries — for Atomic Energy and for Industry, Science and Technology and local municipal authorities of Obninsk.

The Conference was attended by about 230 accelerator scientists and engineers from the leading accelerator centres of Russia — JINR, ITEP, IHEP, BINP, RRC "Kurchatov Institute", the Ukrainian and Aphasia research institutes and the foreign accelerator centres — CERN, FNAL, RHIC, GANIL, DESY, FZ (Juelich).

The last two years since the former Conference have witnessed a certain progress in the home accelerator centres. The major tendency in Russian accelerator physics revealed at the RUPAC is realisation of a few new long-term projects. This activity offers a sign of optimism towards a progress in the accelerator science in this country.

Several reports presented at the RUPAC dealt with the accelerator activity at JINR (Dubna, Moscow Region). A. Malakhov spoke about the latest experiments at NUCLOTRON with the extracted ion beams. The NUCLOTRON booster project is under discussion now at the Laboratory of High Energy. Its realisation would allow for a several-orders-of-magnitude increase in the intensity of the NUCLOTRON beams.

A report by Yu. Oganessian was devoted to the DRIBS Project at the Laboratory of Nuclear Reactions. The two cyclotrons, U-400 and U-400M, were combined within the ISOL scheme to produce rare exotic nuclei like ^{6}He, ^{8}He and ^{5}H with energy of 10–20 MeV/u. In the next stage, a microtron will be installed in the existing ISOL scheme to ensure synthesis of ultra-high-weight elements with $Z = 114$ and $Z = 116$ discovered at JINR.

I. Meshkov presented a report on the DELSY Project — the 3-rd generation synchrotron radiation (SR) source at JINR.

A. Sidorin spoke about the final construction stage of the low-energy positron storage ring LEPTA and about the first experiments on formation of positronium fluxes with a small energy spread and low emittance. He discussed the specifics of the positron cooling and particle dynamics under strong coupling between vertical and horizontal degrees of freedom in the LEPTA storage ring. The JINR positronium programme is attractive for CERN, where about 50,000 anti-hydrogen atoms were produced in the ATRAP and ATHENA experiments.

P. Roussel-Chomas presented the joint GANIL–JINR report on individual injection, storage and cooling of rare radioactive ions in a storage ring. The proposed

new injection scheme for rare radioactive isotopes would yield a storage rate of 1000 ions/s at an intensity of the radioactive ions at exit from fragment separator as high as a few thousand ions per second. The individual injection scheme reduces intensity of the primary ion beam by 6–7 orders of magnitude as compared to the multi-turn injection at same storage rate.

Many interesting reports were presented by the BINP (Novosibirsk). E. Levichev spoke about the VEPP–2000 electron–positron collider project based on the concept of round beams. Such beams can noticeably increase beam–beam parameter attainable and luminosity of the colliding beams.

The first stage of the fourth-generation synchrotron radiation source MARS equipped with the energy recuperation scheme has been completed at BINP this year. In the infrared region, the planned MARS brilliance will be three orders magnitude higher than the best brilliance of the existing SR sources.

There is a fair progress in the terawatt accelerator TWAC for inertial fusion studies at ITEP (Moscow). B. Sharkov reported on the first carbon beams being stored in the booster, extracted to the storage ring, and accelerated to energy of 0.7 GeV/n.

S. Ivanov, Yu. Fedotov and A. Afonin of IHEP (Protvino) reported on the current status of the IHEP 70 GeV proton synchrotron, efforts to upgrade its slow-extraction system and recent successes in employing bent crystal to deflect and extract proton beams. This year, the U 70 accelerator meets the 35^{th} anniversary of commissioning. In despite its age, it is still a reliable machine that services the experimental physics program at IHEP.

Russian accelerator physicists now participate in many international collaborations. L. Evans, the Deputy-Director of CERN, reported on the status of the LHC Project paying a due attention to involvement of the Russian accelerator centres such as BINP, JINR and IHEP.

DESY Director D. Trines informed about the status of the TESLA collider and participation of the Russian institutes in the Project. M. Yurkov spoke about the latest results obtained with the DESY TTF Free Electron Laser where the brilliance of the synchrotron radiation is eight orders of magnitude higher than that of the best SR sources.

The working seminar on electron cooling took place during and parallel to the RUPAC. Participants from Russia, Germany and France took their chance to discuss the recent progress in electron cooling.

V. Parkhomchuk of BINP (Novosibirsk) spoke about tendencies in the next-generation electron coolers. Significant results were obtained at BINP that built two electron coolers for the Lanshou ion storage complex in China. The main features of these coolers are: an electron gun with a variable beam profile, a new technology to produce magnetic field in the cooler, and an electrostatic bending deflector.

J. Stein informed about experience gained at the COSY electron cooler and about the joint COSY–JINR studies of the cooled ion beam stability in COSY. The ion beam stability in the AD (CERN) and the JINR test bench were discussed in the report of I. Meshkov.

A. Smirnov informed about recent results in the numerical simulations of the crystalline ion beam in the storage rings with the BETACOOL code.

To conclude, the major tendencies in the field exposed at the RUPAC-2002 are realisation of new accelerator projects in Russia (DRIBS and DELSY at JINR, MARS and VEPP-2000 at BINP, TWAC at ITEP) and involvement in the long-term

international collaboration in accelerator physics and engineering between the Russian institutes and the world leading research centres like CERN, FNAL, DESY, KEK and many others.

7 Forthcoming Beam Dynamics Events

7.1 ICFA Advanced Beam Dynamics Workshops

7.1.1 28th: Quantum Aspects of Beam Dynamics 2003

The Joint 28th ICFA Advanced Beam Dynamics & Advanced Novel Accelerators Workshop ON QUANTUM ASPECTS OF BEAM PHYSICS - and Other Critical Issues of Beams in Physics and Astrophysics – will be held on January 7-11, 2003 Hiroshima University, Higashi-Hiroshima, Japan. Information is available at

http://home.hiroshima-u.ac.jp/ogata/qabp/home.html

7.1.2 29th: Beam Halo Dynamics, Diagnostics, and Collimation (HALO'03) (in conjunction with 3rd workshop on Beam-beam Interactions)

The 29th ICFA Advanced Beam Dynamics & Advanced Novel Accelerators Workshop on beam halo dynamics, diagnostics, and collimation will be held on May 19–23, 2003 at the Gurney's Inn, located at the eastern end of Long Island, New York. The 3rd Workshop on Beam-beam Interactions will be organized in parallel with the HALO'03 Workshop. Information is available at

http://www.sns.bnl.gov/HALO03

http://www.rhichome.bnl.gov/AP/BeamBeam/Workshop03

7.1.3 30th: Beam Dynamics Issues for High Luminosity e+e- Factories: "e+e-Factories 2003"

Topics: This workshop will cover many issues with e+e- colliders including electron-cloud effects, beam-beam interaction, high beam-loading of RF systems, bunch-by-bunch feedbacks, potential future accelerators, interaction regions, impedances, instabilities, operation and status of present colliders. The context is to advance the luminosity of present colliders and discuss options for future even higher luminosity machines.

This workshop would be a continuation of the series of workshops held in Frascati in 1997, KEK in 1999, and Cornell in 2001.

Location and Date:
The workshop will be located at SLAC on October 14-17, 2003(Tuesday-Friday).

For information contact John Seeman (seeman@slac.stanford.edu), Maura Chatwell, or Regina Matter.

7.1.4 The 12th ICFA Mini-Workshop on high intensity and high brightness hadron beams - Space charge simulations

The 12th ICFA Beam Dynamics Mini-Workshop, devoted to Space Charge Simulation and sponsored by the Rutherford Appleton Laboratory, will be held at Trinity College, Oxford, England from April 2nd-4th 2003.Full details (including an on-line registration form) are available at

http://www.isis.rl.ac.uk/AcceleratorTheory/workshop/workshop.htm

or by emailing a member of the Organising Committee:

Chris Prior c.prior@rl.ac.uk ,

Giulia Bellodi g.bellodi@rl.ac.uk ,

Frank Gerigk f.gerigk@rl.ac.uk

7.2 Other Workshop and Conferences

7.2.1 NuFact03 5th International Workshop on Neutrino Factories and Superbeams Columbia University New York City 5-11 June 2003

NuFact03 is the fifth annual Neutrino Factory workshop. This series of annual meetings is devoted to discussing the full physics potential of the NeutrinoFactory, as well as the design and feasibility of the accelerator complex and the various detectors. The meeting will also review and discuss the prospects for neutrino superbeams and beta beams, and the associated physics programs. The NuFact03 workshop starts on Thursday June 5,2003 and ends at mid-day on Wednesday June 11, 2003. In conjunction with this workshop there will also be a summer school for students and others, the second Neutrino Factory Summer Institute, which will take place in Shelter Island, New York from May 27, 2003 to June 4, 2003. For more information refer to

http://home.fnal.gov/~dharris/nufact03_school.html

Recent developments in particle accelerators make it possible to conceive ofintense neutrino beams based on the decay of a beam of stored muons: a Neutrino Factory. A Neutrino Factory complex requires a proton accelerator capable of delivering a MW multi-GeV beam, which can also be used to generate very intense conventional neutrino beams: Neutrino Superbeams. Neutrino Superbeams and Neutrino Factory beams may enable the full neutrino mixing matrix to be precisely determined, including the measurement of CP violation in the lepton sector and a determination of the pattern of neutrino masses. A Neutrino Factory would also support an extensive program of non-oscillation neutrino physics and experiments that require a very intense muon source. Implementing a Neutrino Factory facility would be an important step towards a muon collider, perhaps the route of choice to multi-TeV lepton-anti-lepton collisions. The successful operation of such a facility, therefore, may very well represent the birth of a new approach for the study of fundamental particles and their interactions.

The purpose of the meeting is to review recent developments in Neutrino Factory and Superbeam design, the associated R&D program, and the evolving physics program that motivates Neutrino Factories and Superbeams.

Scientific Program

The NuFact03 workshop consists of a mixture of plenary and parallel, working group, sessions. Possible topics for plenary presentations include:

Status of neutrino oscillations
Solar neutrino experiments
Atmospheric neutrino experiments
Status and potential of long-baseline experiments
Short-baseline oscillation physics
Neutrino scattering and muon physics
Neutrino superbeams

Status of Neutrino Factory studies in Europe, the US and Japan
Muon cooling
High proton intensity sources and possible targets
Implications of neutrino mass
Leptogenesis
Rare muon decays

There will be three working groups:
i. Machine
ii. Neutrino oscillation: physics and detector
iii. Neutrino scattering and muon physics: physics and detector

Workshop Site

The workshop will be held in the Physics Department of Columbia University in New York City.

Registration

Details of how to register for NuFact03 will be posted on the NuFact03 web-site (http://www.cap.bnl.gov/nufact03/) around January 1, 2003.

Correspondence

Questions concerning the workshop can be addressed to:

Kathleen Tuohy, NuFact03
Physics Department, Bldg. 901A
Brookhaven National Laboratory
Upton, New York 11973

e-mail: tuohy@bnl.gov
Tel: 631-344-3845
FAX: 631-344-3248

7.2.2 COOL03 International Workshop on Beam Cooling and Related Topics, 19-22 May, 2003 in Japan

The International Workshop on Beam Cooling and Related Topics, COOL03, will take place from May 19 to 22, 2003 at the foot of Mt. Fuji in Japan. The focus of the workshop will be new developments in the physics and engineering of beam cooling. Also included are recent and updated issues in closely related strategies for obtaining high brilliance particle beams and in ion trap. The workshop follows the series of beam cooling workshops which have been held every two years. The last one was at Physikzentrum Bad Honnef (Germany) in May 2001. For this time, it will be held under

the sponsorship of the Institute of Physical and Chemical Research (RIKEN) as RIKEN Conference.
The subjects to be discussed are as follows;

I. General topics
- Highlights of beam cooling at rings in operation, under construction and proposed
- Cooling methods
- Role of cooling in particle/nuclear/atomic physics

II. Electron cooling
- Low energy
- Intermediate energy and high energy

III. Stochastic cooling
- Antiprotons
- Ions (fast cooling)
- Combination with e-cooling

IV. Muon cooling
- Principle of ionization cooling
- Proposed experimental tests
- Role in muon-factory designs

V. Laser cooling and other novel cooling methods

VI. Limits to cooling, beam ordering
- Conditions for beam ordering
- Experimental results(chains/3-D crystal)
- Application

VII. Other topics
- Diagnostic methods
- Cooling effects by inelastic atomic intra-beam scattering
- Ion trap
- Others

Up-to-date information about the workshop is available on the COOL03 web site at
http://www.riken.go.jp/lab-www/beamphys/cool03/index.html

If you have any questions, please contact;
Takeshi Katayama (RIKEN/Univ. of Tokyo), chair of the workshop,
katayama@postman.riken.go.jp, or
Tadashi Koseki (RIKEN), scientific secretary of the workshop, cool03@riken.go.jp .

8 Announcements of the Beam Dynamics Panel

8.1 ICFA Beam Dynamics Newsletter

8.1.1 Aim of the Newsletter

The ICFA Beam Dynamics Newsletter is intended as a channel for describing unsolved problems and highlighting important ongoing works, and not as a substitute for journal articles and conference proceedings which usually describe completed work. It is published by the ICFA Beam Dynamics Panel, one of whose missions is to encourage international collaboration in beam dynamics.

Normally it is published every April, August and December. The deadlines are 15 March, 15 July and 15 November, respectively.

8.1.2 Categories of Articles

The categories of articles in the newsletter are the following:

1. Announcements from the panel.
2. Reports of Beam Dynamics Activity of a group.
3. Reports on workshops, meetings and other events related to Beam Dynamics.
4. Announcements of future Beam Dynamics-related international workshops and meetings.
5. Those who want to use newsletter to announce their workshops are welcome to do so. Articles should typically fit within half a page and include descriptions of the subject, date, place, Web site and other contact information.
6. Review of Beam Dynamics Problems: this is a place to bring attention to unsolved problems and should not be used to report completed work. Clear and short highlights on the problem are encouraged.
7. Letters to the editor: a forum open to everyone. Anybody can express his/her opinion on the beam dynamics and related activities, by sending it to one of the editors. The editors reserve the right to reject contributions they judge to be inappropriate, although they have rarely had cause to do so.
8. Editorial.

The editors may request an article following a recommendation by panel members. However anyone who wishes to submit an article is strongly encouraged to contact any Beam Dynamics Panel member before starting to write.

8.1.3 How to Prepare a Manuscript

Before starting to write, authors should download *the latest* model article file, in Microsoft Word format, from the Beam Dynamics Panel home page

http://wwwslap.cern.ch/icfa/

It will be much easier to guarantee acceptance of the article if the latest model is used and the instructions included in it are respected. These model files and instructions are expected to evolve with time so please make sure always to use the latest versions.

The final Microsoft Word file should be sent to one of the editors, preferably the issue editor, by email.

The editors regret that LaTeX files can no longer be accepted: a majority of contributors now prefer Word and we simply do not have the resources to make the conversions that would be needed. Contributions received in LaTeX will now be returned to the authors for re-formatting.

In cases where an article is composed entirely of straightforward prose (no equations, figures, tables, special symbols, etc.) contributions received in the form of plain text files may be accepted at the discretion of the issue editor.

Each article should include the title, authors' names, affiliations and e-mail addresses.

8.1.4 Distribution

A complete archive of issues of this newsletter from 1995 to the latest issue is available at

http://wwwslap.cern.ch/icfa/

This is now intended as the primary method of distribution of the newsletter.

Readers are encouraged to sign-up for to electronic mailing list to ensure that they will hear immediately when a new issue is published.

The Panel's Web site provides access to the Newsletters, information about Future and Past Workshops, and other information useful to accelerator physicists. There are links to pages of information of local interest for each of the three ICFA areas.

Printed copies of the ICFA Beam Dynamics Newsletters are also distributed (generally some time after the Web edition appears) through the following distributors:

Weiren Chou	chou@fnal.gov	North and South Americas
Helmut Mais	mais@mail.desy.de	Europe* and Africa
Susumu Kamada	Susumu.Kamada@kek.jp	Asia** and Pacific

* Including former Soviet Union.
** For Mainland China, Chuang Zhang (zhangc@bepc3.ihep.ac.cn) takes care of the distribution with Ms. Su Ping, Secretariat of PASC, P.O.Box 918, Beijing 100039, China.

To keep costs down (remember that the Panel has no budget of its own) readers are encouraged to use the Web as much as possible. In particular, if you receive a paper copy that you no longer require, please inform the appropriate distributor.

8.1.5 Regular Correspondents

The Beam Dynamics Newsletter particularly encourages contributions from smaller institutions and countries where the accelerator physics community is small. Since it is impossible for the editors and panel members to survey all beam dynamics activity world-wide, we have some *Regular Correspondents*. They are expected to find interesting activities and appropriate persons to report them and/or report them by themselves. We hope that we will have a "compact and complete" list covering all over the world eventually. The present *Regular Correspondents* are as follows

Liu Lin	liu@ns.lnls.br	LNLS Brazil
S. Krishnagopal	skrishna@cat.ernet.in	CAT India
Ian C. Hsu	ichsu@ins.nthu.edu.tw	SRRC Taiwan

We are calling for more volunteers as *Regular Correspondents*.

8.2 ICFA Beam Dynamics Panel Members

Caterina Biscari	caterina.biscari@lnf.infn.it	LNF-INFN, Via E. Fermi 40, Frascati, Italy
Swapan Chattopadhyay	swapan@jlab.org	Jefferson Lab, 12000 Jefferson Avenue, Newport News, VA 23606, USA
Pisin Chen	chen@slac.stanford.edu	SLAC, P.O. Box 4349, MS26, Stanford, CA 94309, USA
Weiren Chou	chou@fnal.gov	FERMILAB, MS 220, P.O.Box 500, Batavia, IL60510, USA
Yoshihiro Funakoshi	yoshihiro.funakoshi@kek.jp	KEK, Oho, Tsukuba, IBARAKI 305-0801, Japan.
Kohji Hirata	hirata@soken.ac.jp	Sokendai, the Graduate Univ. for Advanced Studies, Shonan Village, Hayama, Miura, Kanagawa, 240-0193, Japan
Sergei Ivanov	ivanov_s@mx.ihep.su	Institute for High Energy Physics, Protvino, Moscow Region, 142281 Russia
John M. Jowett	John.Jowett@cern.ch	CERN, CH-1211 Geneva 23, Switzerland
Kwang-Je Kim	kwangje@aps.anl.gov	Argonne Nat. Lab., Advanced Photon Source, Accelerator Systems Division, 9700 S. Cass Avenue, Bldg 401/C4265, Argonne, IL 60439
Alessandra Lombardi	Alessandra.Lombardi@cern.ch	CERN, CH-1211 Geneva 23, Switzerland
Helmut Mais	mais@mail.desy.de	DESY, Notkestrasse, 85 D-2000, Hamburg 52, Germany
Olivier Napoly	Olivier.Napoly@cea.fr	DAPNIA-SEA, CEA Saclay, 91191 Gif/Yvette CEDEX, France
David Rice	dhr1@cornell.edu	Cornell University, 271 Wilson Lab, Ithaca, NY 14853-8001, USA
Yuri Shatunov	Yu.M.Shatunov@inp.nsk.su	Acad. Lavrentiev prospect 11, 630090 Novosibirsk, Russia
Jie Wei	wei1@bnl.gov	BNL, Bldg. 911, Upton, NY 11973-5000, USA
Chuang Zhang	zhangc@mail.ihep.ac.cn	IHEP, CAS, BEPC National Laboratory, P.O. Box 918, 9-1, Beijing 100039, China

The views expressed in this newsletter do not necessarily coincide with those of the editors. The individual authors are responsible for their text.

9 Appendix

SIMULATION CODES USED FOR SLOW EXTRACTION DESIGN AND ANALYSIS (compiled at the 10th ICFA Miniworkshop)

Code Name	type	Institution	support	who?	contact	source code ?	compiler	platforms	libs	parallel ?	dimensions
SLEX	Hamiltonian integrator	TRIUMF	limited	S. Koscielniak	shane@triumf.ca	yes	F77 ANSI	Linux	CERNLIB GPLOT	no	H,L
retrack	element by element	BNL	limited	K.Brown	kbrown@bnl.gov	yes	C++	any unix	none	no	H,V
bnlmad	element map/tracking	BNL	limited	K.Brown	kbrown@bnl.gov	yes	F77/C	any unix	OpenGL	no	H,V,L
CERN MAD	element map/tracking	CERN	limted		Frank.Schmidt@cern.ch	yes	F77	most	CERN LIB	no	H,V,L
CATCH	tracking	IHEP	full	V. Biryukov	rfliller@bnl.gov	yes	F77 ANSI	any unix	no	no	H,V,dp/p
AGILE	general purpose	cern	limited	P. Bryant	philip.bryant@cern.ch	no	Turbo Pascal	windows	?	no	H,V,dp/p
slowex	element by element	cern	no	C.Steinbach	marco.pullia@cern.ch	yes	Qbasic	dos	?	no	H,dp
mirko	general purpose	GSI	yes	B.Franczak	b.franczak@gsi.de	no	F90	vms/windows	none	no	H,V,dp/p
evol	rotate & kick	BNL	yes	S.Peggs	peggs@bnl.gov	yes	F77 ANSI	unix	none	no	H,V.dp
Tomi	tracking/matrix	KEK	limited	M.Tomizawa	masahito.tomizawa@kek.jp	yes	F77	vms	no	no	H,V,dp/p
plato	library *	CERN	limited	M.Giovannozzi	massimo.giovannozzi@cern.ch	yes	F77 ANSI	any unix	CERNLIB	mpi	H,V
beam	ags specific	BNL	limited	N.Tsoupas	tsoupas@bnl.gov	yes	F77	unix	none	no	H,V,dp/p
extra	element by element	TERA	limited	M.Pullia	marco.pullia@cern.ch	yes	ansi C	unix		no	H,V,dp/p
SAD	tracker	KEK	limited	Oide		no	F77	Tru64		no	

* element by element tracking, normal forms, post processing tracking data

** thick elements replaced by thin elements

Code Name	order of map *	space charge/collective	original application	documentation/ language	lattice input ?	single turn map ?	time variation/ dependances	which physics ?	element support	gui or text based ?	scattering/halo	Micado SVD ?	Correction	Run time, Speed	Known Deficiencies
SLEX	2nd	no	KAON/KOPIO	yes	no	NA	yes	1/3 int	S hits	text	NA	no	no	*	see documentation
retrack	NA	no	BAF/KOPIO	yes/English	yes		yes	multiturn extraction	C,F,S,T	text	no	no	no	***	dp/p
bnlmad	3rd	limited		some/English	yes	yes	limited	any	C,F,T,M,CM,G	text	limited	Micado	yes	**	can't do lots of particles
CERN MAD	3rd	no		English	yes	yes	no	any	C,F,T,M,CM,G	text	limited	Micado	yes	**	can't do lots of particles
CATCH	NA	no	crystals @ IHEP	yes/English	NA	NA	no	channeling scattering	crystal.	text	scattering	NA	NA	**	Can be very slow
AGILE	nth	yes	CAS	yes, english	yes	no	yes	any	C,F,S	text	scattering	simplex	yes	*	slow for tracking
slowex	2nd	no	PS Extraction	limited, english	yes	no	no	1/3 int	S	text	no	no	no	****	limited in scope
mirko	nth	linear	Beam line design	yes,german	yes	NA	yes	any	C,F,M,CM	text	no	no	yes	****	documentation
evol	BB,10pole	no	SPS Beam-Beam	yes, english	yes	no	yes	nonlinear	M.T.BB	text	no	no	no	****	very specialized
Tomi	nth	no	JHF	no	no	no	yes	general slow extraction	TM,S	text	no	no	no	**	input interface
plato	nth	no	DA	yes	via mad	yes	no	any	C,TM**	text	no	no	limited	**	
beam	nth	no	AGS	no	NA	no	no	AGS	NA	text	no	no	yes	***	for BNL AGS only
extra	any	no	PIMMS	no, english	yes	no	yes	1/3 int	C,S	text	no	no	no	**	many
SAD		no	TRISTAN	yes/English	yes		yes			text	no	no		**	

* Maximum order of element map

Element Key:

C = Collimators
F = Foils
M = Standard Magnet Types
S = Septa
T = Time Variation of Element strengths
G = General Matrices
TM = Thick lens elements
CM = Constraint Matching algorithms

Speeds:

* Slow
**
***
**** very fast

STATUS OF INSTRUMENTATION (compiled at the 11th ICFA Miniworkshop)

	Profile	**Emittance**	**BPM**	**Beam Loss**	**Current**	**Mean Energy and Phase**	**Energy / phase Spread**	**Misc**
Planned Linacs								
SNS Linac	Wire (low energy)	Slit & Collector[2]	Shorted strip, RF IQ receiver[4]	Ion Chamber5	Toroid[7]	phase from BPMs		
	Laser wire[1] (Superconducting region)	Beam Shape Monitor[3]		Liquid Scintillator[6]				
				Neutron detector				
RIA	Wire	Low energy: Slit/Collector	Shorted strip	Neutron detectors and medium and high energies	All energies: BCM, low and medium energies - Faraday cup	Phase:Resonant Pickup[1] at low and medium energy, Shorted strip everywhere	Bunch shape: all energies: wire/sec electron[2] at low energy SBD/GasProp.[3]	
		medium & high energy: wire/rms[4]				Energy:all energies-TOF, at low energy SBD/GasProp.[3]		
FNAL P Driver	Moveable single plane grids (48 wires, 0.5-1.0-1.5 mm spacing)[1]		Single plane stripline, 0.5 mm resolution[1]	Argon Ion chambers[1]	BCT			
	slow single wire scanners							
	Ioniz. Type MCP Ampl., 48 strips 1.5 mm apart[1]							
J-PARC (JKJ)	Wire Scanner	Slit & Collector[2]	Stripline[1]	Ion Chamber[3]	Toroids(slow)[4]	Beam phase monitor[6]	Momentum analyzer (future plan)	

					Toroids(fast)[5]			
Existing Linacs								
ISIS Linac	Wire scanners (low rep. rate only) in LEBT between preinjector and injector and in HEBT between injector and synchrotron[1]	Slit-and-collector in LEBT between preinjector and injector	Wire scanners (low rep. rate only) in LEBT between preinjector and injector and in HEBT between injector and synchrotron	Argon-filled ionisation chambers running alongside Tanks 2, 3, 4 and alongside HEBT beam line	Toroidal current transformers, three between preinjector and injector, three between tanks, five in HEBT	1. In HEBT straight before debuncher, fast toroids, time-of-flight measurement of beam bunches using 1 GHz 'scope 2. After debuncher, phase detection at 202.5 MHz on signals from capacitive pick-ups (see Note 2) 3. See Note 3	1. No energy spread measurement before debuncher 2a. After debuncher, by bending magnet and wire scanner (low rep. rate only) 2b. After debuncher, by monitoring time evolution of chopped beam in synchrotron	DT condition by monitoring X-ray dose rates from tanks[4]
INR (Moscow) Linac	Wire scanner, harp	Injection line - slit/collector, higher energies - rms with 3 to 5 wire scanners	Strip line, TM_{110} cavity[1]	Photomultiplier without scintillator, ionization chamber	Current transformer, wall current monitor for short pulses	Absolute and relative energy-time of flight with two current harmonic monitors, phase - current harmonic monitor	Magnnetic spectrometer/bunch shape monitor	Residual gas monitor[2], collector combined with energy degrador for phase scan
LANSCE Linac and transport lines	Wire	Slit and collector[4]	Stripline w/ 50 ohm termination	Ion Chamber[12]	Toroid			Secondary emission current monitors
	Harp	rms with multiple profiles[5]	Capacitive (ring extraction line)	Liquid Scintillator	Faraday cups			Guard rings

								Absorber collectors[10]
LEDA Injector	Video using either viewscreens or background gas fluorescence	Off-line emittance measuring unit, measures part of r-r' space	None	None	Toroid (DC and AC)[7]	Power Supply potential		Potential on ring (Electron Trap) provides improved accuracy input toroidal current measurment.
					arc current			
LEDA Halo Line	Wire scanner/Halo scraper[2]	rms fits from 4 profiles with~π/2 phase advance between profiles	Micro-stripline w/ 50 ohm termination[3]	Ion Chamber[5]	Toroid (AC)	Cylindrical Capacitive, 50 ohm termination[4]		
		rms from single profile scanning upstream magnet		CsI Scintillator[6]	Wall current	Resistive wall current		
LEDA HEBT	Wire scanner	rms from single profile scanning upstream magnet	Stripline w/ 50 ohm termination[3]	Ion Chamber	Toroid (AC)			Beam Stop Power
	Background gas fluorescence using injected nitrogen.[1]		Capacitive (ring, ring extraction line)	CsI Scintillator				
GSI Linac	Harp, IPM, fluoresence[1]	slit-grid, pepper-pot[2]	capacitive pick-up, 2 GHz bandwidth		Toroid (AC)[3]	capacitive pick-up[4]	particle-detector[5], bunch shape monitor[6]	
IPNS Linac								
Source and 750 kV column		slit scanner, test stand only		CT[1]	CT			
50 MeV Linac				CT, LM[2]	CT			
50 MeV Line	WS[3], Scintillator[4], SFC[5]	ESEM[6], WS[7]	terminated strip-lines	liquid scintillator/PMT, CT	CT	ESEM	ESEM	

CERN Linac		Slit & secondary emission grid[2]	Magnetic pick-ups	CT difference[1]	CT			
BNL Linac		Slit-collector, WS	striplines	scintillators	Toroid, Faraday cup, FCT	TOF (not used)		

Additional Notes:

SNS: H- linac, 52 mA
DTL structure from 2.5 to 86 MeV,
CCL structure from 86 to 185 MeV
SC from 370 to 1 GeV (beta = 0.61 and 0.81 families)

1) A prototype will also be in the lower energy MEBT. Highly desirable for superconducting region to minimuze risk of particle contamination of cavities.
2) Transverse measurements. Temporary devices will be available during commissioning of lower energy MEBT and DTL systems
3) Longitudinal measurement.
4) Dual plane, 4 stripline design. position + relative phase ,402 + 805 MHz, direct IF digitizer @ 40 M Samples/sec
5) Volume detector (N) (~ 10 kHz,)
6) Photo multiplier, > 1 MHz response, MPS input.
7) Fast current transformer, 15-50 mA

RIA: low energy:< 9.3 MeV/u, medium energy: < 80 MeV/u, high energy > 80 MeV/u
For the RIB Linac of RIA, diagnostics sensitive to beam intensities from 102 to 1011 particles per second are needed.
Secondary electron/position sensitive micro-channel plate detector, surface barrier detectors,
gas counters for detecting individual ions will be important.
1) Superconducting Resonator used as Phase Monitor
2) RF deflection of secondary electrons
3)Solid State Diode Detector or Gas Counter to verify beam purity.
4) Low-duty factor operation for these diagnostics using a beam chopper..

FNAL P driver 400 MeV Line
1) Integrating over injection
2) B163Hz - 20 MHz, injection turn resolution, 0.1%

J-PARC (JKJ) 1) Fast response.
2) Measured in the MEBT at 3 MeV

3) Argon gas
4) Beam current range 0.1 - 100 mA
5) Frequency response: 20MHz - 3 GHz, rise time: 500 psec
6) Using fast toriods. Energy is measured by TOF in principle, detecting a phase difference between RF components of the signals from two fast toroids at separated positions.

ISIS: ISIS linac is 70 MeV 202.5 MHz H– injector for ISIS 800 MeV synchrotron
Four tanks: 665 keV input energy from Cockcroft-Walton preinjector – 10 MeV, 10 – 30 MeV, 30 – 50 MeV, 50 – 70 MeV
Debuncher cavity in HEBT between injector and synchrotron
At present linac runs with 20 mA pulses, ~200 μs long, at 50 pps
In 2003, RFQ (already running on test stand) will replace Cockcroft-Walton, and will lead to 30 mA pulses within linac

1) Two "beam diluters" (each essentially just a pepper pot lid) are provided in LEBT between preinjector and injector to attenuate beam to 40% or 10% (or 4%) while setting up

2) Useful for monitoring variation of energy during pulse
3) "Threshold foils", viz blocks of graphite which just stop 30, 50 and 70 MeV protons are provided shortly after the end of the linac for rough energy identification

4) Excessive X-ray dose rate is symptom of excessive electron emission from drift tube surfaces within tank. High numbers of electrons inside tank lead to charge being deposited in RF window at rate higher than charge can leak away, and lead to window breakdown
5) On RFQ test stand, input and output beam emittances measured using slit-and-collector devices, output beam energy spectrum measured using novel gas scattering spectrometer (and, shortly, using magnetic spectrometer), output beam bunch width measured using coaxial target

INR Linac •Energy = 500 MeV
•Current 15 mA
•200 μs, 50 Hz
•Up to 150 μA average
1) Now out of use. Both monitors and electronics were designed and fabricated improperly.
2)Big noise due to emission from the accelerating cavities. Is planned to be installed in the injection line.

LANSCE: 1) Nitrogen at 1 std. atm. Same type of ion chambers also used in personnel protection system.
2) Used for fast, ns time scales. Saturates on PSR extraction losses.
3) Fast, but less sensitive, so does not saturate on PSR extraction losses.
4) Slit and collector method used up to 100 MeV.
5) Used at 800 MeV.
6) Primary BPM system for ring, but only works well for injected beam with 201 MHz structure.
7) Only have a couple of these in the ring.
8) No profile measurements in ring, but measure profile immediately after extraction. Can deduce ring profile at any time by extracting early.
9) Have both fast and slow toroids.
10) Used after each DTL tank.
11) ANL-style, with LANL-developed high-bandwidth electronics at detector
12) Also use ion chambers for personnel protection (separate electronics from loss monitors)

LEDA: 1.) Background gas or luminescent monitor tested and compared with traditional wire scanner. Reported in BIW2000.
2.) Integrated wire scanner with halo scraper, typical 100000:1 range, charge detection method, stepper motor actuation.

3.) Dual plane, 4 micro-stripline design. Position processor, 350-MHz, Log-ratio technique + on-line calibration, +/- 0.1 dB over >75 dB range, digitizer @ 1 M Sample/sec.
4.) Uses capacitive and resisive wall current monitors. < 0. 1s degrees at 350-MHz, 200+ kHz BW, > 45 dB dynamic range, full 2p measurment range.
5.) Standard volume detector. Operated from 10s kHz to few Hz.
6.) PM tube and CsI scintillator allowed for >10^7 dynamic range.
7.) DCCT from Bergoz with few 0.1 Hz to 100 Hz BW, ACCT from Bergoz with few Hz to near 1 MHz BW. Both capable of performing transmission measurements with range of few 0.1s mA to >100mA range.

IPNS 50 MeV H- linac
1) Pearson Coil and home-built, 100 mV/mA amplified, <20 MHz BW, full power
2) Loss Monitors--External Radiation Monitors (ERMs)
3) Wire Scanners, horiz. and vert., low power, reduced bandwidth
4) plastic scintillator and video camera (reduced bunch, low power)
5) Segmented Faraday Cup (reduced bunch, low power)
6) Energy Spread and Energy Monitor, terminated BPMs (longitudinal, full power)
7) stepping and stationary wire (temporal macropulse, low power, low BW)

GSI Linac all ions, up to 10 mA, pulse length 0.1 - 5 msec, frequency 36/108 MHz up to 18 MeV/u
1) Harp: dynamic shortening of pulse length, IPM: ion detection, no MCP, Fluoresence: equiped with Chevron MCP image intensifier
2) slit-grid: dynamic shortening of pulse length, pepper pot: Al2O3 viewing screen
3) GSI design, droop 0.5% for 5 ms, 0.1 microA resolution used for dynamic pulse shortening
4) using TOF, resolution > 1.e-4
5) attenuation by Rutherford scattering, used fast diamod and 50 Ohm MCP detectros, coincidence technique yield phase and energy of single particles
6) Uses secondary electrons from residual gas, prototype development

CERN Linac 1) Watchdog program monitors 2 consecutive pulses
2)Transverse and longitudinal emittances for single pulse

BNL Linac H- beam
•Energy = 200 MeV
•Current 35mA
•500 µs, 7.5 Hz
•Up to 150 µA avg. for BLIP
•Polarized proton 300 µA, 65% Polarization

Planned Rings	**Profile**	**Emittance**	**BPM**	**Beam Loss**	**Current**	**Misc**	**Tune**
SNS Ring	Wire (low intensity) IPM (high intensity) Luminescent[1] (proposed) Harp		Open strip[2]	Ion Chamber[3] Liquid Scintillator[4]	Toroid[5]	e-detecors[6] beam-in-gap[7]	
J-PARC (JKJ) 3GeV Synchrotron	IPM SEM[2]		Diagonal cut ESM[3] Stripline[4]	Ion Chamber Scintillator	Toroids[5] Wall current monitor	e-detectors beam-in-gap (proposed)	
J-PARC (JKJ) 50 GeV MR	gas sheet PM[1] SEM[2]		Diagonal cut ESM[3] Stripline[4]	Ion Chamber Scintillator	Toroids[5] Wall current monitor	e-detectors beam-in-gap (proposed)	
FNAL P Driver	Ionization type, MCP, 64 strips 1mm apart, L=3m[4]		Single plane elliptic electrostatic PU[1]	Ar filled ion chambers[5]	Fast BCT[2] DCT[3]	100kHz - 0.6 GHz wall current monitor fast stiplines - 1m long, 50 Ohm for wide band diagnostics transverse dampers - 1m long	Single plane elliptic electrostatic PU[6]

CERN LHC	wire (lin. low intensity)[5] IPM (all intensities)[3] luminescent[4]	synchroton light[7]	button[8] few strip[9]	Ion Chamber[11] ASEM[10,12]	Toroid	quadrupolar BPM[14]	
Existing Rings:							
CERN Rings:							
BOOSTER, PS	wire rotative[1]		electrodes	ASEM[10]	Toroid	quadrupolar BPM[13]	
transfer l.	SEM grids		electrodes	ASEM[10] ion chambers[11]			
SPS Ring	wire (lin. low int., rot. high int.)[2] IPM (all intensities)[3] luminescent[4]	synchroton light[6]	electrodes	ion chamber[11]	Toroid	e-cloud strip det.	
transfer l.	OTR screens		buttons	Ion chambers[11]			
ISIS Synchrotron	residual gas monitor[1] single wire 'halo' monitor[2] multi wire single turn[3]	emittance determined from profile monitors	single plane split induction electrodes[5]	Argon filed coaxial cables	Toroid[6]	Thermocouples[7] Beam Chopper[8] Beta Kicker[9]	

FNAL Booster	one horizontal and one vertical IPM with turn-by-turn data acquisition	see devices under "Profile" for transverse emittance	4-electrode stripline type pickups (~50)	"Tevatron" style ion chambers in tunnel (~60)	AC toroid with Hereward feedback	"Time-of-Flight" relative energy monitor in 400MeV injection line	Pinger for horizontal tune measurement (vertical pinger temporarily? appropriated for extraction gap creation)
	slow single-wire scanners at injection point	wall current monitor for longitudinal emittance	AM-PM electronics operating at fundamental RF frequency (38-53 Mhz)[1]	Uncalibrated plastic scintillator / phototube devices at selected locations to see fast losses[2]	DCCT	~ 6GHz bandwidth wall current monitor for longitudinal instability diagnostics, mountain range displays, and bunch length detector	
		Multi-wire harp type profile monitors in injection and extraction lines	AM-PM electronics operating at injected bunch frequency (200MHz) on just a few BPM locations	Interlocked rad. detectors (chipmunks) outside tunnel provide useful "average" beam loss information (~50)	Wall current monitor for bunch-by-bunch intensity information	Wall current monitor for low level RF system phase feedback	
DESY Rings							
DESYIII	fast[5] wire scanners (up to 220 mA)		inductive pick-up[7]	Scintillator[8]	Toroid[10]	"stepping wire" (in preparation)[2]	
	IPM[1] (first prototype was tested many years ago)					3 resistive wall monitors[13]	
PETRAp	fast[5] wire (up to 160mA)		capacitive pickup (button) (for e and p)[12]	Long segmented Ion Chamber (planed)	Toroid[9,10,11]	"stepping wire" (in preparation)[2]	
	IPM[1] (sensitive, correct beam width at small bunch currents only)					2 resistive wall monitors[13]	

HERAp	OTR Screen (proposed, for injection[6]) IPM[1] (sensitive, correct beam width at small bunch currents only) fast[5] wire (up to 160mA)		Directional coupler Pickup (Stripline)[12]	PIN diode BLMs (counting mode)[3]	Toroid[9,10,11]	BLMs at scrapers[2,4] "stepping wire" (in preparation)[2] fast wall current pick-up for bunch length measurement	
LANSCE Ring	None in ring[8]	rms from profiles of extracted beam	Stripline w/ 50 ohm termination[6] Capacitive[7]	Ion Chamber[1] Liquid Scintillator[2] Vacuum photo diode[3]	Toroid[9] Wall current	e-detectors[11] Pinger e -sweeper	
GSI Synchrotron	IPM[1] HARP[2]	IPM[1] transverse Schottky[3]	capacitive pick up[4]	plastic scintillator[5]	Toroid AC [6] Toroid DC[7]	longitudinal Schottky[8], capacitive pickup[9] tomography[10]	Tune: exciter + pickup (BTF)[11], transverse Schottky
IPNS	IPM[1] (horiz.), RWM[2] (long.), CT[3] (long.)		PIE[4] electrodes	PMT/scintillators, CT	CT	RFA (electrons)	PIE electrodes
IPNS Ring	SSEMs[5], SWIC/PAS[6]	SSEMs, SWIC/PAS	SSEMs, SWIC	ICs[7]	CTs[8]		
PTS Transfer Line							
BNL Rings							

RHIC	Transverse: IPM, Luminesence Longitudinal: WCM	Transverse: Schottky, Luminesence Longitudinal WCM, Schottky	shorted stripline, 25 cm long, single + dual phase	ion chambers (TeV Style)	DCCT, WCM	Buttons	coherent:Kicked tune, incoherent: Schotttky+ PLL
AGS							

Additional Notes:

SNS : 248m storage ring
< 1.3 GeV P
up to 1.44x 1014 ppp (1 msec storage)

1) gas ionization system
2) Dual plane, 4 stripline design. position + relative phase , 65M samples/sec
3) Volume detector (N) (~ 10 kHz,)
4) Photo multiplier, > 1 MHz response, MPS input.
5) Fast current transformer, 15 mA - 100 A
6) Related to e-P instability - need 100 MHz response
7) To measure residual beam in the extraction gap, < 1.e-4 of nominal beam intensity

J-PARC (JKJ) 1) Under R&D for high intensity beam.
2) Using metalized thin films for high intensity is under R&D. Planned to install in inj. / ext. beam transport lines.
3) For COD measurement / single pass
4) Fast response.
5) Wideband frequency is covered by several toroids.

FNAL P driver 16 GeV Synchrotron
1) 100 mm length, Turn-by-turn measurements, ± 1.0 mm
2) 1.5 kHz-20 MHz, 5 V/A, 245 mm ID, Turn-by-turn measurements, 0.1% error
3) 245 mm ID, Resolution 10 mA, 500 Hz drift 5mA/24 h
4) turn-by-turn time resolution
5) V=0.11 cc, Time resolution 0.1 ms
6) , 100 mm length FEE, Resolution of 0.01 tune units,kick of a few tenths of a mm

LHC / CERN Rings: 1) 20 m/s
2) 0.6 and 6 m/s
3) e-detection, commisioning phase, intensity dependence observed in the SPS
4) commisioning phase, backgrond problem in the SPS
5) total allowed beam intensity 1 E13, in last weeks lower threshold observed in the SPS, under investigation
6) light from the edge of a bending magnet

7) light from a undulator at 450 GeV and at 7 TeV from a the edge of a bending magnet
8) mounted on the quad mag, cold
9) near IP and some special
10) Aluminium Cathode Electron Multiplier
11) 1 liter N2 at 1 atmosphere
12) few units for the observation of fast losses
13) radial magnetic field detection, no common mode sigbal, bunch lendth 200 ns
14) strip line

ISIS Ring 163m, 70-0800 MeV RCS, 50 Hz. 2x1013 ppp, Harmonic 2 RF System
1) Single detector stepped over beam width.
2) halo position determined by measured beam loss on adjacent BLM.
3) used for 1st turn orbit setup with a beam stop.
4) Scintilators used for single turn injection and extraction beam diagnostics
5) 200 MHz bandwidth, switching gain devices for use with high intensity and chopped beams. Used for transverse measurements and summed for longitudinal measurements

6) Resolution range 1x1010 to 4x1013 protons
7) Thermocouples placed on dipole vacuum chambers downstream of beam collector systems to prevent dipole damage
8) electrostatic chopper in jection line controls injection pulse length from <1 turn to full intensity (160 turns)
9) Fast h and v kicker magnets (rise time ~ 1us , duration ~ 0.5 ms) perturbs orbit for transverse lattice measurements.

FNAL Booster Ring: multi-turn H- charge exchange injection at 400MeV with 200MHz bunch structure, typically 12 turns
200MHz structure washes out in few turns, then beam is semi-adibatically captured in Booster harmonic 84 buckets (38 MHZ at 400MeV)
accelerate to 8 GeV in 33 millisec (15 Hz resonant magnet circuit)
RF harmonic = 84; frequency 38-53 Mhz
typical injected intensity 5E11 to 7.5E12
typical high intensity injection-to-extraction efficiency 70%
1) blind from injection until RF capture (~25-30 turns)
2)sub-microsecond timescale

DESY : 1) gas ionization monitor system
2) For tail measurements
3) 10 MHz response, counting mode
4) PMTs and PIN diodes
5) up to 1 m/s, upgrade planed
6) for max. 10 bunches only, to measure the quadrupole moment
7) 30 kHz-250 MHz Bandwidth
8) Photomultiplier, > 10 MHz response.
9) DCCT slow current transformer typ PCT or M-PCT, 0-200 mA, res: 0.5 mA, CD - 100kHz
10) AC Fast current transformer, 30 kHz - 20 MHz, Cal: 1011 p/V, res: <<10mA, meas. precise transport efficiency
11) difference of 9) and 10) = coasting beam
12) Broadband readout (<96 ns)
13) for bunch length, timing and feedback; 2 MHz - 1 GHz bandwidth

LANSCE Ring:
1) Nitrogen at 1 std. atm. Same type of ion chambers also used in personnel protection system.

2) Used for fast, ns time scales. Saturates on PSR extraction losses.
3) Fast, but less sensitive, so does not saturate on PSR extraction losses.
4) Slit and collector method used up to 100 MeV.
5) Used at 800 MeV.
6) Primary BPM system for ring, but only works well for injected beam with 201 MHz structure.
7) Only have a couple of these in the ring.
8) No profile measurements in ring, but measure profile immediately after extraction. Can deduce ring profile at any time by extracting early.
9) Have both fast and slow toroids.
10) Used after each DTL tank.
11) ANL-style, with LANL-developed high-bandwidth electronics at detector
12) Also use ion chambers for personnel protection (separate electronics from loss monitors)

GSI Synchrotron - all ions, space charge limit < 1012, ions (charge dependent) up to 12 GeV/u, fast and slow extraction, electron cooling possible, 218 m circumference

1) MCP + wire array readouut, ion deflection (new development: B field and electron detection, MCP + phosphor + CCD)
2) First turn diagnostic
3) for debunched beam, capacitive pick up plates
4)show box type, high impedance pre-amp, 100 MHz bandwdth
5) counting mode, max. rate ~ 5 MHz
6) for injection, 1 Mhzbandwidth passive transformer, 0.1 microA resolution
7) DC bandwidth, 50 kHz, 1 microA resolution
8) for momentum spread of DC beam
9) bunch shape observation bandwidth 100 MHz (high impedance) bandwidth 1 GHz (50 Ohm)
10) phase shape reconstruction using capacitive pickup
11) frequency sweep or while noise excitation

IPNS Ring 450 MeV RCS, 30 Hz
1) Position and Profile System (PAPS)--only weak magnetic field (3-4 G, ave.) present; residual from combined-function magnets (full power, 5 kHz)

2) Resistive Wall Monitor (full power, wide-band)
3) Pearson Coils (full power, <20 MHz)
4) split-can pair, horizontal and vertical (full power, < 50 MHz)
5) Segmented Secondary Emission Monitors (full bunch, low power)
6) Segmented Wire Ionization Chamber, Au-coated, W wire, 2 mil (0.03 mil Au) / Position And Size monitor (package 2 m in front of target, full power)
7) Ionization chambers
8) Pearson coils and Bergoz MPCT (full power, reduced BW)